Micelles and bicelles as membrane mimics for membrane protein investigations

Ashton Tirrell Brock

Columbia, South Carolina

B.S. Chemistry, Winthrop University, 2011

A Dissertation presented to the Graduate Faculty

of the University of Virginia in Candidacy for the Degree of

Doctor of Philosophy

Department of Chemistry

University of Virginia

May, 2016

"Call it a clan, call it a network, call it a tribe, call it a family. Whatever you call it, whoever you are, you need one."

– Jane Howard (1935-1996) US journalist, writer

"Nothing will work unless you do."

– Maya Angelou (1928-2014) US poet, author, civil rights activist

Abstract

Membrane proteins have essential cellular functions in transport, signaling, energy conversion and catalysis. These ubiquitous proteins comprise approximately 30% of the genome, and with their roles in intra- and extracellular communication, membrane proteins are the target of over 60% of the therapeutic drugs on the market. While membrane protein research is imperative, there is significantly less known about the function, stability, and structure of these proteins as compared to soluble proteins.

Membrane protein research is challenged by the native environment of these proteins: the lipid bilayer. Bilayer mimics such as detergent micelles and lipid-detergent bicelles are often used to isolate membrane proteins. Utilizing these mimics requires an extensive screening process to identify the appropriate amphiphilic environment for biophysical characterization, functional assays, and high-resolution structure determination of membrane proteins. To enable rational mimic selection, the goal of this research is to investigate the structural properties of micelles and bicelles to determine how their physical characteristics can forward membrane protein research.

Often considered more membrane-like than micelles, the "ideal" bicelle is composed of a lipid bilayer encapsulated by a detergent rim. Because of the propensity for detergents to form ellipsoid micelles in aqueous environments, the feasibility of distinctly separated lipid and detergent domains suggested by the "ideal" bicelle model is questioned, especially in respect to detergent-rich bicelles. To investigate the viability of the "ideal" bicelle, the structure and composition of detergent-rich bicelles was elucidated with small angle X-ray and neutron scattering. Small angle scattering results suggest that detergent-rich bicelles form ellipsoid structures similar to mixed micelles, with higher

degrees of mixing between lipid and detergent components than suggested by the “ideal” model. As lipid concentration is increased, the aggregate transitions from a mixed micelle to bicelle structure. This research emphasizes the importance in understanding the structures of the mimics used for membrane protein research; the size and shape of these ellipsoidal detergent-rich bicelles can have a significant impact on mimic selection.

The influence of detergent micelles on protein function was also investigated. Understanding the key physical detergent properties that impact protein activity will also guide membrane mimic selection. The activity of several membrane proteins is currently being assayed in varying detergent micelles to correlate trends between the micelle and active, stable protein. Functional results from two membrane enzymes, outer membrane phospholipase A1 (OMPLA) and lipoprotein signal peptidase A (LspA) suggest that the detergent head group charge and size has a major effect on protein activity, and the carbon tails of these detergents have minor impacts on detergent binding and catalysis. Identifying similar trends with other protein-detergent complexes will guide the selection of the appropriate detergent to use for membrane protein research, and ameliorate arduous detergent screening.

Table of Contents

List of Figures

List of Tables

Chapter 1: Membrane proteins in research

All functions of living organisms are made possible by the actions of proteins. Highly abundant and extraordinarily diverse in cells, these biomolecules perform essential cellular processes to sustain life. Fundamentally, proteins are polymers of 20 or more amino acids. The amino acid sequence, or primary structure, of these proteins is dictated from a DNA sequence, representing the "Central Dogma" of molecular biology – DNA is transcribed to RNA, which is translated to protein.[1] Once translated from the ribosome, these proteins adopt one or more three-dimensional conformations in which their functional roles are performed.

In 1953, Sanger and Thompson determined the complete amino acid sequence of bovine insulin, writing: [2,3]

> "It is certain that proteins are extremely complex molecules but they are no longer completely beyond the reach of the chemist, so that we may expect to see in the near future considerable advances in our knowledge of the chemistry of these substances which are the essence of living matter"

The substantial progress in the field of protein chemistry that Sanger predicted was exemplified with the publishing of the first high-resolution, three-dimensional protein structure of myoglobin in 1960 via X-ray crystallography.[4] Following these discoveries, over 24,000 unique protein structures have been deposited in the RCSB Protein Data Bank. Despite this increasing wealth of information, there is more to learn about the diverse structures and functions of proteins.

1.1 Membrane protein background

Proteins can be divided into two classes: soluble and membrane proteins. Soluble proteins fold with hydrophobic residues excluded from the aqueous solvent, within the inner core. Unlike their soluble counterparts, membrane proteins have both hydrophobic and hydrophilic domains on their surface. Because exposure to the aqueous solvent is unfavorable for these nonpolar residues, membrane proteins fold within the cellular membrane such that the hydrophobic residues interact with the hydrocarbon core while the polar residues remain in the exterior of the membrane. The cellular membrane satisfies the hydrophilic and hydrophobic protein surface requirements, and stabilizes the functional fold of membrane proteins.

The membrane is an environment consisting of lipids organized in a two-layered planar structure with polar head groups facing the aqueous space and nonpolar tails on the interior. Native bilayers are 40 to 50 Å thick, with the hydrophobic region spanning ~ 30 Å and a head group shell of 10 Å or less. The assembly and composition of the bilayer is discussed extensively in Section 1.3. Because of the hydrophobicity of the membrane, it is unfavorable for polar and charged residues to interact with the interior of the bilayer. Hydrophobic residues interact with the bilayer hydrocarbon core, stabilizing the protein's fold via van der Waals interactions with the bilayer hydrophobic tails.[5]

The trends of protein primary structure and fold in bilayers were expanded several researchers including Wimley and White, who determined the preference for specific amino acid partitioning into the membrane.[6] This research monitored the difference in free energy of a membrane peptide, WL-X-LL, as it was altered at the X position for varying amino acids and exposed to octanol and water. The amino acids with the highest free energy of transition were most likely present in transmembrane domain (TMD) of

the bilayer. Following establishing this relationship between amino acids and membrane partitioning, the hydrophobicity scale, a measure of how soluble an amino acid is in water, was developed. As expected, it was unfavorable for charged and polar residues to interact with the hydrocarbon core of the membrane in comparison to nonpolar amino acids. Therefore, the hydrophilic residues tend to localize near the lipid head groups or in the periplasmic or extracellular space.

Additional studies analyzed the frequency and position of amino acids of several membrane proteins. Typically, leucine is the most prevalent residue in membrane protein sequences, followed by isoleucine, valine, alanine, phenylalanine, and glycine.[7] Lysine and aspartate are the least prevalent amino acids.[7] Basic residues are more populated within the intracellular side of the protein, resulting in the positive-inside rule that often used for identifying the topology of membrane helices.[8] Lysine and arginine, also tend to "snorkel," orienting themselves to allow an association between their long aliphatic chains with the hydrophobic bilayer core while extending beyond the core for interactions between their positive charged groups at the end of the amino acid with the lipid polar head group.[9] Aromatic residues localize near the membrane interface, enabling hydrogen bonding with lipid head groups or water molecules while maintaining nonpolar interactions with hydrocarbon lipid tails.[10-12] Membrane protein topology is often predicted using this knowledge of the localization of charged, aromatic, and nonpolar residues in a lipid bilayer environment (Figure 1.1).

While all membrane proteins share common distributions of certain amino acids, the proteins can also be divided into two subclasses by fold: α-helical bundles and β-barrels (Figure 1.2). α-helical bundles, found in every cellular membrane and the inner

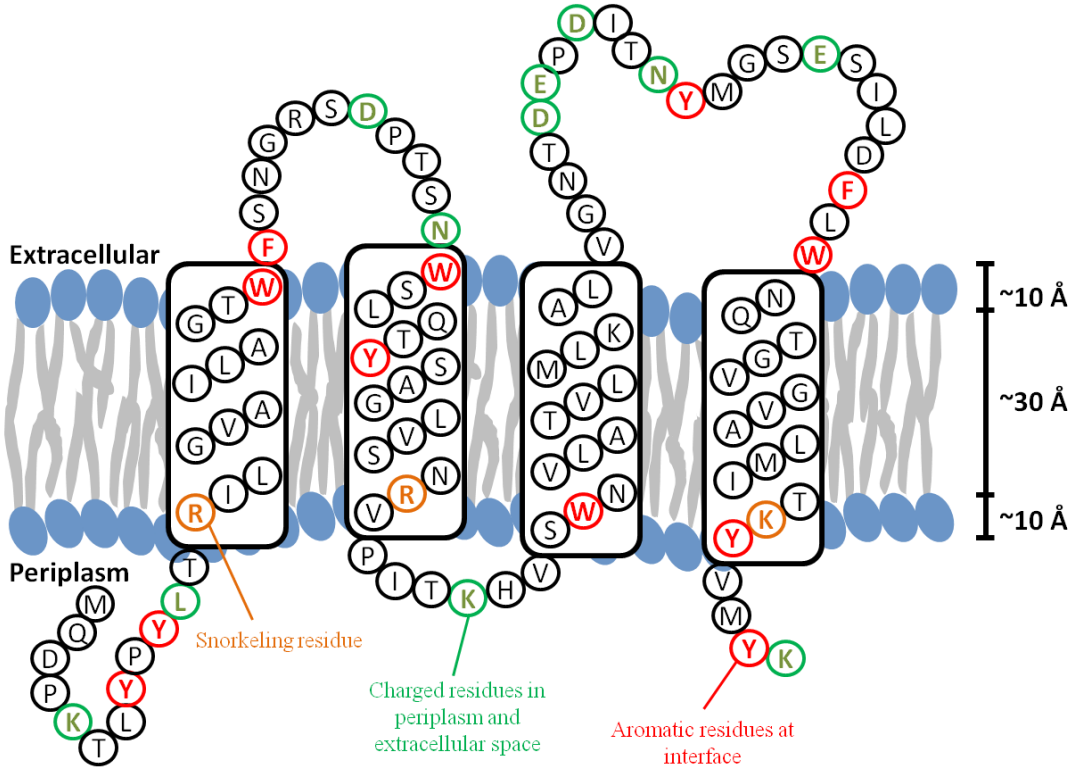

Figure 1.1 Membrane protein topology depicted with a fictional amino acid sequence. Native bilayers are 40 to 50 Å thick, with the hydrophobic region spanning ~30 Å and a head group shell thickness of 10 Å or less. Membrane proteins often have similar topology, regardless of the type of membrane or the secondary structure of the protein. This topology includes the charged and polar residues (green) in the aqueous periplasm or extracellular space, the aromatic residues (red) near the bilayer interface, the snorkeling residues (orange) and the interior of the bilayer containing mostly hydrophobic residues (black).

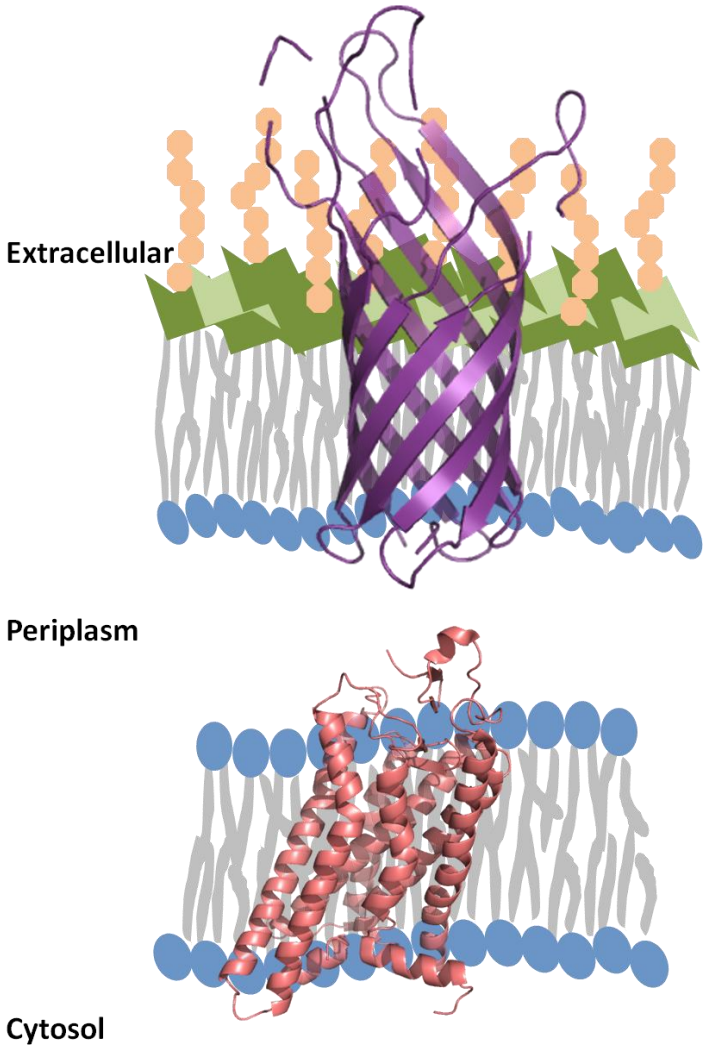

Figure 1.2. Examples of membrane protein tertiary structures. α-helical bundles and β-barrels, such as rhodopsin (pink) and OmpA (purple), located in the inner and outer membrane, respectively, are the protein structures found in cellular membranes. These structures can be monotopic or polytopic, attached to one side of the membrane or spanning the entire membrane one or more times.

membrane of bacteria and organelles, are composed of membrane spanning α-helices.[13] Depending on the entry point, slope, and straightness, the length of the transmembrane helices varies from 20 to 40 residues, with typically 3.6 residues per turn.[14] β-barrels are only found in Gram-negative outer membranes, and in the outer membrane of mitochondria and chloroplasts.[15] Several antiparallel β-strands form a closed cylinder via hydrogen bonds within the interior, making the rigid, stable β-barrel. Typically, β-barrels have a periplasmic domain with tight turns and an extracellular side with longer loops.[16] β-barrels span the membrane with up to 22 β-strands of 9 to 11 residues each and a tilt of 20-45° with respect to the membrane.[13]

Most bacterial α-helical and β-barrel proteins are both targeted and inserted into the membrane through a translocon. Ribosomes making α-helical bundles typically bind cotranslationally with the SecYEG translocon in the inner membrane. The α-helical protein is then translated directly into the membrane, moving laterally from the SecYEG translocon channel.[10] β-barrels are transferred to the SecYEG translocon via SecB, and then posttranslationally translocated through the SecYEG and inner membrane with the aid of the SecA ATPase. β-barrel proteins are then chaperoned through the periplasmic space and inserted into the outer membrane via the Bam (β-barrel assembly machinery) complex.[10] Once at their final destination in the inner and outer membranes, these membrane proteins participate in their cellular roles.

1.2 Significance of membrane proteins

Membrane proteins are essential to the cell with functions in transporting, signaling, energy conversion, and catalysis. As such, these proteins are ubiquitous; approximately 30% of the genome encodes for membrane proteins.[17] These proteins have

significant pharmaceutical implications because of their role in intra- and extracellular communication. Membrane proteins are the target of approximately 60% of all of the FDA-approved drugs on the market, ranging from allergy medicine responding to membrane receptors to diuretics that interact with membrane transporters.[18-19] Despite their significance to physiology and medicinal research, there is considerably less information about membrane proteins than soluble proteins. Of the 24,693 unique protein structures deposited in the Protein Data Bank, only 584 (~2%) are membrane proteins.[20] Progress in membrane protein characterization is complicated by low protein expression and lack of *in situ* biophysical techniques, but the most problematic challenge is the membrane protein native environment, the lipid bilayer.

1.3 The native lipid bilayer

Membrane proteins are embedded in the lipid bilayer. This vast, heterogeneous, dynamic native membrane provides the stability and electrostatic interactions necessary for stable, properly folded, and active membrane proteins. The native lipid bilayer is not a feasible environment for most biophysical techniques used to study membrane proteins. Standard techniques such as nuclear magnetic resonance (NMR), X-ray crystallography, small angle scattering (SAS) require a highly homogenous environment, which is the opposite of a physiological lipid membrane. Researchers are challenged to solubilize membrane proteins while preserving its stability and functional fold for accurate structural or physical characterization of membrane proteins.

1.3.1 Lipid bilayer assembly

Biological membranes are mainly composed of amphipathic glycerophospholipids and membrane proteins. Each lipid has a hydrophilic polar head group and two

hydrophobic nonpolar acyl carbon tails. The assembly of lipid bilayers, monolayers, and other phases are driven by the hydrophobic effect.[21] Water molecules self-associate via hydrogen bonding. Insertion of nonpolar molecules, such as lipids, into an aqueous environment distorts these interactions, and forces water molecules to reorder around the nonpolar entity. There may or may not be a loss of hydrogen bonds during this reordering of water molecules, affecting the enthalpy. However, the cage, or clathrate, that water forms around the nonpolar molecule is greatly ordered, resulting in a substantial loss of entropy. The water molecules lower this entropic cost by sequestering the nonpolar molecules into larger aggregates, reducing the total surface area of exposed nonpolar material and decreasing the amount of water molecules in clathrates, increasing entropy.[21] Van der Waals forces between lipid acyl tails further stabilize the nonpolar aggregate.[21] This nonpolar, lipid aggregate surrounded by water maximizes the polar-polar water interactions and nonpolar-nonpolar acyl tail interactions, while minimizing unfavorable polar-nonpolar interaction between water and the hydrocarbons.

1.3.2 The fluid mosaic model

The fluid mosaic model was proposed by Singer and Nicholson in 1972 after much debate about the lipid membrane structure and composition (Figure 1.3).[22] The first principle established by the model is that the lipid aggregate is a bilayer, as opposed to the monolayers previously expected.[23] Lipids have an overall cylindrical shape and aggregation of these molecules results in a bilayer: a two-layered planar structure with hydrophilic head groups facing the aqueous space and hydrophobic tails on the interior. Bilayer thickness depends on the number of carbons in the phospholipid acyl chains.

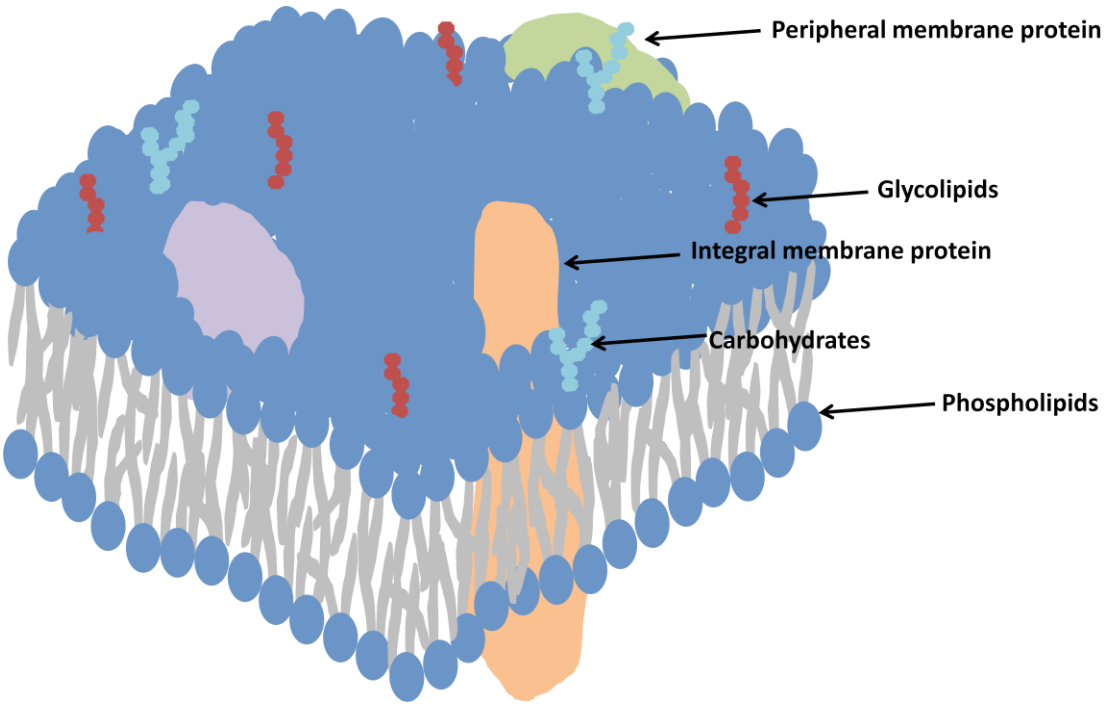

Figure 1.3. Diagram of the fluid mosaic model. The heterogeneous bilayer contains integral and peripheral membrane proteins embedded in a phospholipid bilayer. This environment also contains cholesterol, glycolipids, and carbohydrates.

Bilayers are composed of not only glycerophospholipids, but also membrane proteins, sphingolipids, sterols, glycolipids, and lipopolysaccharide. Membrane proteins scattered across the bilayer surface with other membrane contents create the "mosaic" effect of the membrane. The bilayer composition can range from 80% lipid and 20% protein (myelin) to 25% lipid and 75% protein (mitochondrial inner membrane).[24] There are several different types of lipids in the bilayer including zwitterionic phosphatidylethanolamine (PE) and phosphatidylcholine (PC), as well as anionic phosphatidylserine (PS), phosphatidylinositol (PI), and phosphatidylglycerol (PG). The dominant sterol molecule in bacterial membranes is cholesterol.[24] A nonuniform distribution of these contents disrupts the tight packing between glycerophospholipids and contributes greatly to the degree of membrane fluidity.

Another aspect of the fluid mosaic model is the mobility of the membrane components. Lipids can move rotationally, laterally, and transversely. Lateral and transverse diffusion affect the bilayer asymmetry while rotational motion (a single lipid rotating around its axis) does not. Lateral diffusion (microsecond timescale) occurs when neighboring lipids switch places within a monolayer.[25] Transverse diffusion is a slower process (minutes to days), where a lipid from one side, or leaflet, of the bilayer "flip-flops" with a lipid on the other leaflet.[25]

The membrane also undergoes phase changes and shifts from a gel to liquid state. Lipid acyl chains are highly ordered and tightly packed in the gel phase, contrary to the liquid phase where there is rotational freedom. Several factors impact membrane fluidity including temperature, alkyl chain saturation, and membrane composition. Like most molecules, the thermal energy from a high temperature (23 to 75°C, depending on lipid

tail length) causes an increase in lipid motion, resulting in a more liquid state.[26] The degree of saturation of the acyl chains affects how closely they can interact via van der Waals forces. A cis-double bond introduces a kink in the carbon tails, which affects how closely they can associate, decreasing melting temperature (Tm). Changes in the membrane composition affect membrane fluidity in several ways. An increase in acyl chain length allows more van der Waals interactions between each lipid, increasing Tm.[26] Cholesterol regulates fluidity for both gel and liquid states. The large molecule stabilizes and increases the rigidity of the membrane, ordering the lipids at higher temperatures.[27] The sterol also separates the phospholipids, partitions into the densely packed lipids, and reduces lipid ordering.[28]

1.3.3. The bacterial inner membrane

Gram-negative bacterial cells contain both an inner and outer membrane, separated by the periplasmic space. Unlike eukaryotic cells that contain intracellular organelles such as the endoplasmic reticulum and mitochondria that perform a number of essential membrane-associated cellular processes, bacteria lack organelles, and consequently, all of these essential functions occur at the bacterial inner membrane (IM). Energy production, protein secretion, lipid biosynthesis, transport, and cellular signaling events all take place within the inner membrane.[29] The IM is a phospholipid bilayer; in *E. coli*, the primary phospholipids present are PE and PG, but there are lesser amounts of PS and cardiolipin.[29]

1.3.4. The bacterial outer membrane

The outer membrane provides resistance to toxic host molecules and a permeability barrier between the cell and the extracellular environment.[30] The bilayer is

highly asymmetric, with the inner leaflet consisting of glyerophospholipids (70-80% PE and 20-30% PG lipids) and cardiolipin while the outer leaflet is primarily composed of LPS (Figure 1.4).[31]

LPS contains three parts: the hydrophobic anchor, Lipid A, the core oligosaccharide, and the O-antigen polysaccharide. Lipid A interacts with phospholipids of the inner leaflet via van der Waals forces, forming the 30 Å thick bilayer. Unlike phospholipids in the inner leaflet, all carbon chains of lipid A are saturated.[32] The lipid A core is modified with several phosphate groups that contribute to the overall negative charge of the moiety. The O-antigen is a repetitive glycan polymer that interacts with the extracellular space.[32] The O-antigen composition is bacterial strain-specific, but can also vary within one bacterial strain.[32] Modifications to LPS have an impact on the host cell's immune response, which will be mentioned below in Section 1.4.2. with PagP function.[32]

1.4 Functions of membrane proteins

Membrane proteins participate in a variety of functions; the three primary classes are transporters, receptors, and enzymes. Transport across the membrane can occur in several ways. Active transport proteins move a molecule or ion against a concentration gradient. These proteins require one of two primary sources of energy for this function: energy from the hydrolysis of ATP (primary active transport) or energy provided when a molecule moving with the concentration gradient is coupled to the transport of a molecule moving against the gradient (secondary active transport). A well-characterized active transport protein is the Na+/K+ pump.[33] The pump transports two K+ ions into and three Na+ ions out of the cell with every ATP hydrolyzed. Lactose permease from *E. coli* is a secondary active transporter, specifically a symport protein which uses the proton

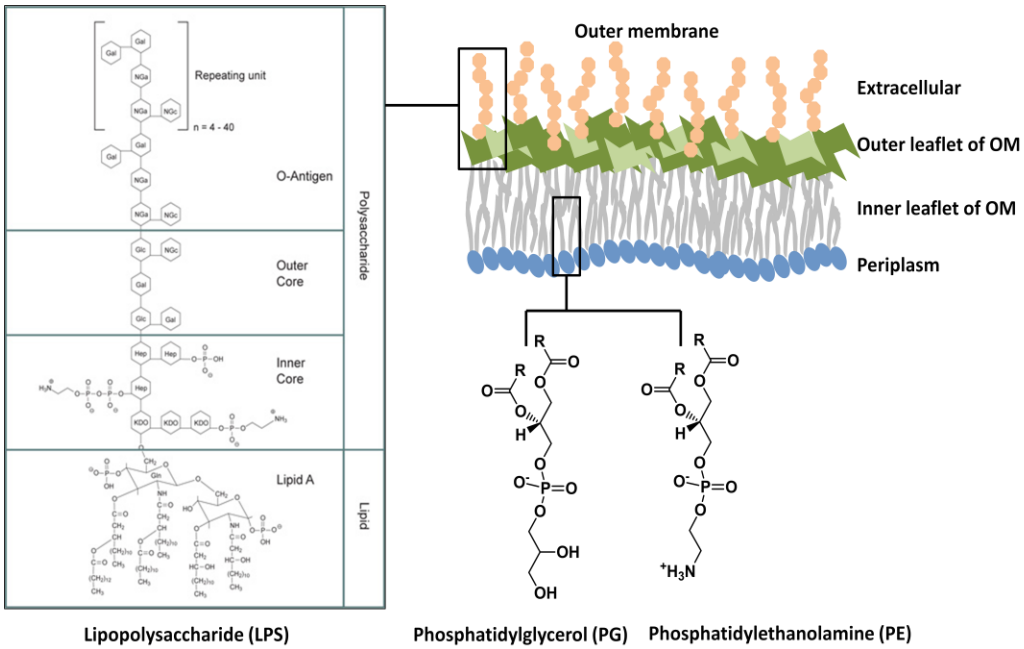

Figure 1.4. Composition of the outer membrane. The outer membrane has an inner leaflet on the periplasmic face and an outer leaflet that faces the extracellular space. The inner leaflet contains mostly PG and PE lipids. The outer leaflet contains LPS, which contains lipid A, the core oligosaccharide composed of 3-deoxy-α-D-mannooctulosonic acid (KDO) and heptulose (Hep), and the O-antigen polysaccharide comprised of galactosamine (NGa) and glucosamine (NGc).

gradient across the membrane to transport both lactose and H+ across the membrane.[34] In contrast to the active transporters, porins, such as PhoE, the phosphophorin, are passive transporters, moving molecules and ions down the concentration gradient across the membrane. Membrane receptors span the plasma membrane and transduce signals in response to ligand interaction. G-protein coupled receptors (GPCRs) are a classic example of membrane receptors; GPCRs bind ions, nucleotides, hormones, neurotransmitters, and even photons.[35] Upon ligand binding, the GPCR changes conformation, activating G-proteins and triggering the cell to complete specific functions.

Membrane enzymes are involved in the catalytic functions of the cell. They participate in transport, signaling, and in the electron transport chain and other redox reactions. Examples are diacylglycerol kinase, an enzyme involved in replenishing phophatidic acid in the cell and formate dehydrogenase, a single TMD membrane enzyme that catalyzes the oxidation of formate to carbon dioxide.[36,37] Part of this dissertation will focus on the function and activity of four bacterial membrane enzymes: outer membrane phospholipase A (OMPLA), the PhoPQ-activated gene protein (PagP), the temperature-regulated protease OmpT, and lipoprotein signal peptidase A (LspA).

1.4.1. OMPLA structure and function

OMPLA is the first outer membrane β-barrel enzyme to be functionally characterized.[38] The *E. coli pldA* gene codes for a mature OMPLA protein of 269 amino acids, preceded by a signal sequence of 20 residues for protein translocation across the inner membrane.[39] The 31 kDa β-barrel protein is comprised of 12 β-strands, and its structure was determined in 1999 via X-ray crystallography.[40] OMPLA belongs to a family of lipid-hydrolyzing enzymes, but does not share sequence similarity with the

other soluble proteins in the group.[36] OMPLA is inactive as a monomer, but active as a reversible dimer (Figure 1.5A). The dimer has calcium-dependent phospholipase A1 and A2 abilities, cleaving the acyl chain from either carbon 1 or carbon 2 of phospholipids into lysophospholipids (Figure 1.6).[41,42] OMPLA dimerization and calcium-dependent activity is a response to perturbations of the integrity of the outer membrane. Typically, the outer leaflet of the outer membrane is composed of only lipopolysaccaride (LPS), a large lipid and polysaccharide molecule, while the inner leaflet contains phospholipids. Events such as heat shock, EDTA treatment, and phage-induced lysis negatively affect this normal lipid asymmetry.[38] These disruptions in the membrane integrity cause phospholipids that normally remain on the inner leaflet of the outer membrane to move to the outer leaflet, accessing the active site of OMPLA, triggering dimerization, and resulting in calcium-dependent phospholipase cleavage.

OMPLA has implications in several biological processes. The constitutive expression of OMPLA suggests that it is a housekeeping enzyme, responding to any perturbations to the outer membrane integrity in the cell.[41] OMPLA cleavage of phospholipids results in an accumulation of lysophospholipids in the outer membrane. These amphiphilic molecules often perturb membranes, destabilize blood cell membranes, and contribute to increased hemolysis.[43] Phospholipases also play a role in the virulence of several pathogenic bacteria. Three bacteria, *Proteus mirabilis*, *Helicobacter pylori*, and *Staphylococcus saprophyticus*, produce urease, a potent virulence factor necessary for the pathogens to colonize the gastric mucosa.[44,45] Phospholipases degrade the gastric membrane, allowing for the release of ureases into the

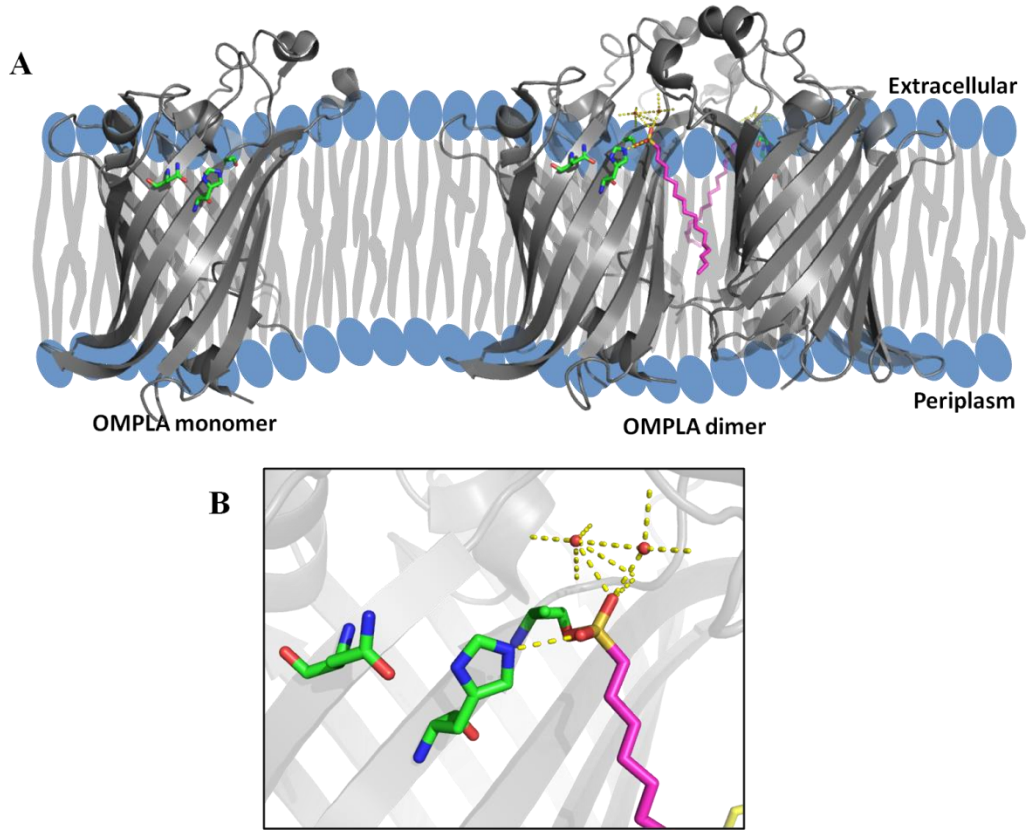

Figure 1.5. Structure of OMPLA. A) OMPLA (PDB ID: 1qd6) is monomeric in its inactive form and forms a homodimer (right) when active. B) The OMPLA active site residues Ser144, His142, and Asn156 bind two phospholipid substrates (magenta) between the dimer interface. These residues perform calcium dependent hydrolysis of the phospholipids with the aid of two catalytic water molecules (red). Following substrate cleavage, the OMPLA dimer disassociates.

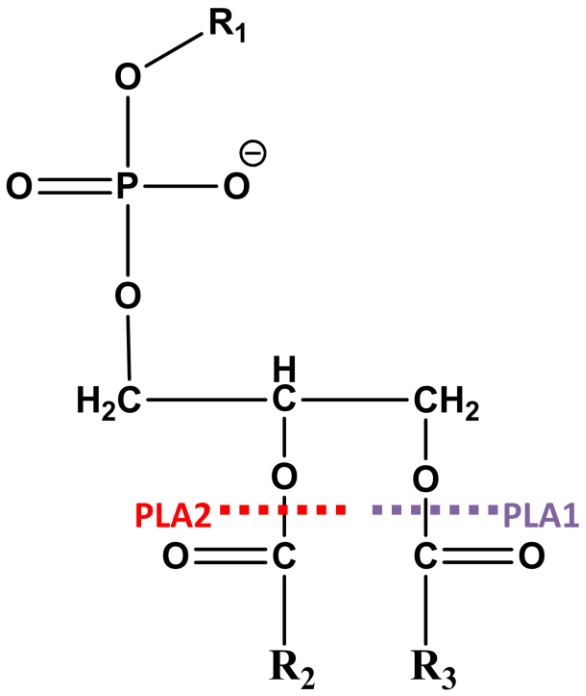

Figure 1.6. Phospholipid cleavage sites for OMPLA cleavage. Phospholipase A1 cleaves the acyl chain from carbon 1 of the phospholipid (purple) and phospholipase A2 cleaves the acyl chain from carbon 2 (red).

host. Bacterial ureases aid in the colonization of the host by neutralizing gastric acid and providing ammonia for pathogenic bacterial protein synthesis.[46] High amounts of urease in the stomach are associated with hepatic encephalopathy, peptic ulcers, and infection stones.[47]

Bacteriocin-release proteins (BRP) also use OMPLA to secrete colicins through the outer membrane. The BRP signal peptide, which is not degraded after processing, accumulates in the cytoplasmic membrane.[48] Over expression of BRP accumulates these peptides in the membrane which in turn, activates the OMPLA dimer, permeabilizes the cell membrane, and allows colicin release.[49] The release of colicins kills other bacteria of the same species, providing a competitive advantage for nutrient bacteria.[50]

There are several structural components vital for OMPLA dimerization, substrate binding, and activity. Monomeric and dimeric OMPLA do not exhibit structural differences, and both contain a catalytic triad of Ser144, His142, and Asn156 at the interface of the membrane (Figure 1.5B).[40] The Ser144 and His142 have been identified by chemical modification and site-directed mutagenesis as essential active site residues, resembling traditional serine hydrolases, while the Asn-156 is less conserved.[51-53] The OMPLA dimer is formed via the association of the flat barrel side of each monomer, creating the substrate binding pockets: two clefts along the hydrophobic subunit interface that run down from the two active sites.[40] Therefore, the OMPLA monomer is inactive because of the lack of substrate binding pockets, not due to the absence of the catalytic residues. Because of the relatively large binding pockets, a broad range of substrates can interact with the dimer. This includes substrates of with different head groups, multiple acyl chains, and of various acyl chain lengths.[54]

Reversible dimerization is activated primarily by the binding of the substrate to the OMPLA catalytic residues. Upon dimerization, the two substrate acyl chain fit into the clefts created by the monomers and serine hydrolysis of the phospholipid occurs. Calcium contributes marginally to the dimerization process, but is essential to enzymatic activity.[42] Each monomer has two Ca^{2+} binding sites, one with high affinity (K_D 36 μM) and one with lower affinity (K_D 358 μM).[55] In monomeric OMPLA, one calcium binding site is 10 Å away from the active site. After dimerization, a second calcium binding site, also known as the catalytic calcium site, is formed at the dimer interface. The calcium is ligated by Ser-152 and polarizes the two water molecules, creating the oxyanion hole necessary for serine hydrolysis.[41] In summary, there are 3 factors that contribute to the activity of the enzyme: 1) formation of substrate binding pocket, 2) the oxyanion stabilization provided by the catalytic calcium, and 3) physical interaction between the active site and the substrate.[36]

1.4.2. PagP structure and function

The PhoPQ-activated gene protein, PagP, is an outer membrane palmitoyltransferase that plays a role in the PhoPQ regulatory system. PagP was discovered while studying Salmonella and the role of the PhoPQ two-component signal transduction pathway in the virulence of pathogenic Gram-negative bacteria.[56] Upon invasion of pathogenic bacteria, the pathogen must withstand the host's defense system: antimicrobial peptides and macrophage phagosomes. The PhoPQ system regulates bacterial resistance to the host's defensive mechanism.[57] During pathogenic invasion, the host stimulates PhoQ, the sensor kinase, causing it to autophosphorylate. This phosphorylation subsequently transphosphorylates PhoP, the response regulator. Once

phosphorylated, PhoP binds DNA and activates the expression of *pags* (PhoP activated genes). These gene products allow the pathogenic bacteria to survive inside the host.[58] Among the *pags* is *pagP*, encoding the PagP membrane enzyme.

PagP participates in the PhoPQ virulence system by modifying lipid A on the outer leaflet of the outer membrane. PagP catalyzes the transfer of a palmitate chain from the sn-1 position of a phospholipid to the hydroxyl group of the N-linked R-3-hydroxymyristate chain on the proximal glucosamine unit of lipid A (Figure 1.7).[56] Modification of lipid A interferes with outer membrane signaling and attenuates its ability to activate the host's immune response.[59] Therefore, the nature and efficacy of the host immune response to bacterial infection are dependent on the structural component of lipid A, which in turn is determined by PagP.[60]

PagP is expressed in several Gram-negative bacteria, including *Salmonella*, *Legionella*, *Bordetella*, and *Yersinia*; however, this project focuses on *E. coli* PagP.[60] The PagP structure was determined by both solution NMR and X-ray crystallography in 2002 and 2004, respectively (Figure 1.8).[56,61] The monomeric protein is 19 kDa, with 141 residues forming the 8-stranded antiparallel β-barrel, preceded by a 19-residue short amphipathic N-terminal helix on the periplasmic side of the membrane.[56] The helix anchors the protein to the membrane, and can facilitate enzymatic activity even under external stress.[59] The barrel has a distinct 25° tilt in respect to the membrane, and is composed of shorter β-strands than typical outer membrane β-barrels. Although the

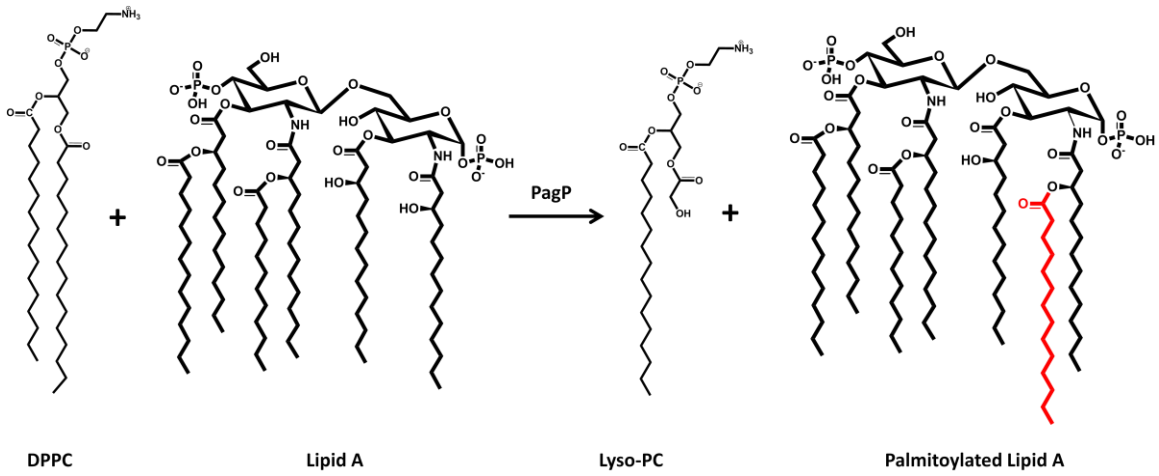

Figure 1.7. PagP palmitoylation of Lipid A. PagP transfers a palmitate chain from a phospholipid to the hydroxyl group of the N-linked R-3-hydromyristate chain on the proximal glucosamine unit of lipid A (red).

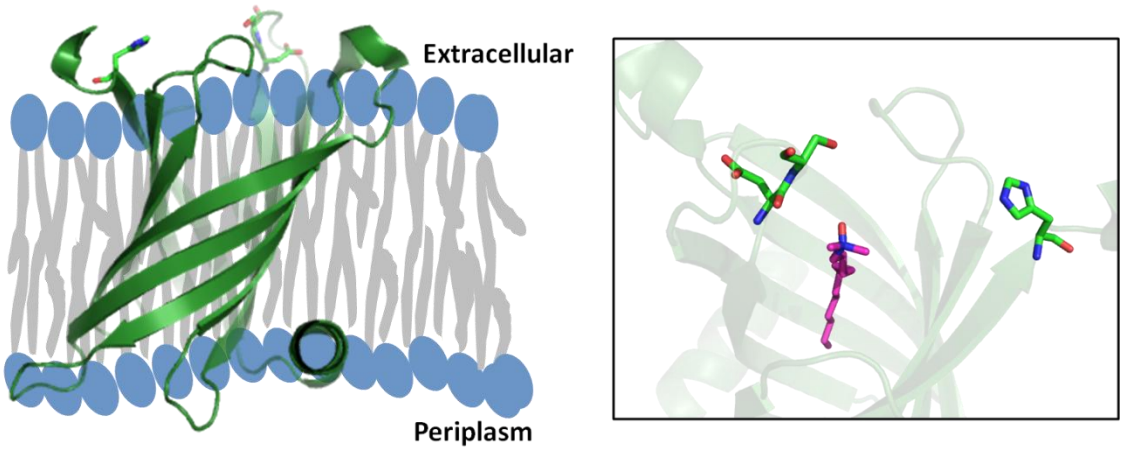

Figure 1.8. Structure of PagP. PagP is an 8-stranded β-barrel protein with a 25° tilt. PagP active site residues include Ser77, His33, and Asp76 at the bilayer interface. The protein was determined in LDAO, FC12, and OG detergents. This figure depicts an LDAO (magenta) in the PagP binding cavity.

catalytic mechanism remains to be elucidated, the tilt of the barrel places the possible catalytic residues, His33, Asp76, and Ser77, on the extracellular interface of the membrane, around a high concentration of lipid A (Figure 1.8).[56]

PagP has a cavity on the inside of the barrel to interact with the phospholipid palmitate donor and lipid A acceptor. The binding pocket is lined with hydrophobic residues and extends approximately halfway into the barrel. The extracellular surface of this cavity contains the three putative active site residues. This binding cavity serves as a "hydrocarbon ruler," and transfers, specifically, only 16-carbon palmitate chains from phospholipids to lipid A.[61] This highly precise ruler is dependent on a conserved Gly-88 at the bottom of the cavity, which, if substituted, can result in a broader specificity.[62] Weakened hydrogen bonds at the two laterally positioned faces of PagP form two faces within the protein responsible for the entry and exit of phospholipid and lipid A.[63]

PagP can adopt its native fold in multiple detergents, including LDAO, FC12, DDM, OG, and Cyclofos7.[61,62] The cavity can also be bound by detergents; both LDAO and FC12 detergents have shown an inhibitory effect of PagP palmitoylation. Both detergents have similar properties as the phospholipids and can fit into the interior of PagP, while other detergents with larger head groups and carbon tails, such as DDM and Cyclofos-7, do not have the same effect.[61]

While the PagP barrel remains rigid, the outer loops, especially loop 1 (L1), are highly mobile (nanoseconds).[64] PagP dynamics and conformations were elucidated by studying the structure of the protein in FC12, OG, and Cyclofos7 micelles. NMR relaxation experiments suggest that PagP exists in an exchange between two states that differ significantly in mobility and L1 loop structure.[64] The relaxed (R) state is more

mobile, potentially for substrate access, while the tense (T) state is rigid, possibly for catalysis. The detergents play a role in these conformations. The R state conformers for FC12, OG, and Cyclofos7 PagP protein-detergent complexes (PDC) are similar, but the T states of the three have distinctly different chemical shifts, suggesting a complete rearrangement of L1.[64] These differences emphasize the necessity to study these membrane proteins in several environments for a complete understanding of protein structure, function, and dynamics.

1.4.3. OmpT structure and function

OmpT, the temperature-regulated outer membrane protein, is a part of the omptin family of proteins found in Gram-negative bacteria. Most omptins are bacterial virulence factors and function as aspartic proteases.[65] Bacterial proteases can affect the immune response by degrading the host's antibodies and antimicrobial peptides, impairing the fibrin clots that prevent bacterial migration through invasion of the host's epithelial and phagocytic cells.[66] Specifically, the function of OmpT in *E. coli* is to cleave the antimicrobial peptide, proteamine, which is excreted by epithelial cells of the urinary tract.[67] With this purpose, OmpT is associated with complicated urinary tract disease.[68]

OmpT of *E. coli* is the most characterized member of the omptin family. The structure of the 297 residue enzyme was determined via X-ray crystallography in 2001 (Figure 1.9).[69] The enzyme is a vase-shaped 10-stranded antiparallel β-barrel that extends about 40 Å above the lipid bilayer with extracellular loops extending near the outer edge of LPS.[62] Extension of the barrel and active site into the extracellular space allows OmpT to access the substrate peptides for cleavage.

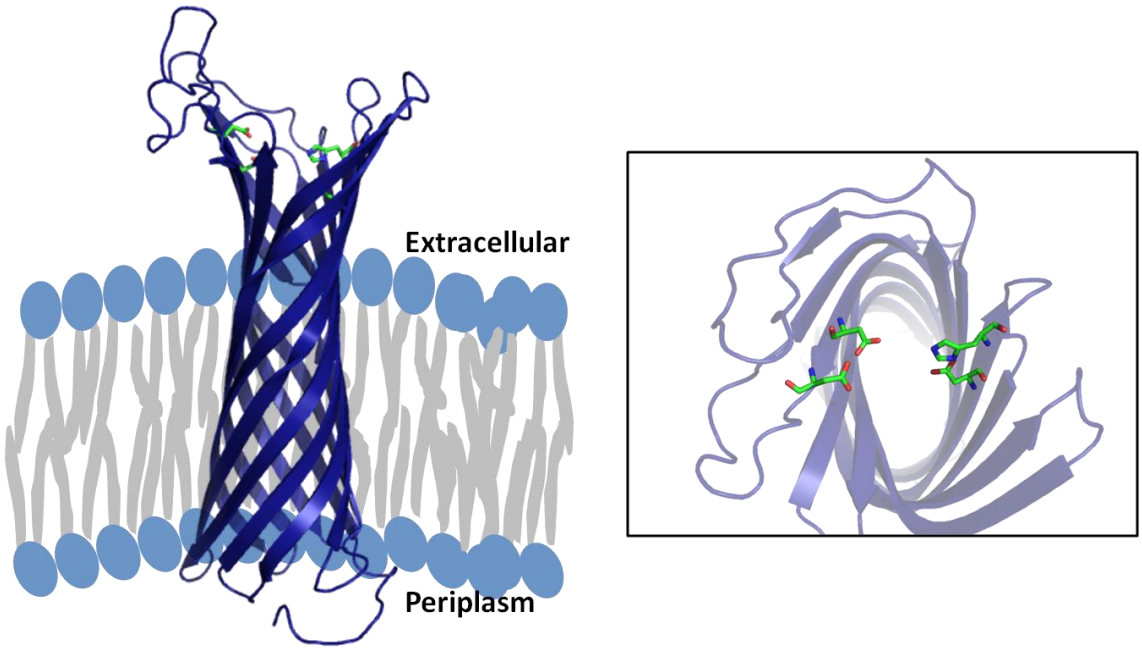

Figure 1.9. Structure of OmpT. The OmpT β-barrel extends into the extracellular space, into the LPS in the outer membrane. OmpT has two catalytic pairings in the extracellular space, Asp210/His212, and Asp83/Asp85.

OmpT degrades antimicrobials by cleaving the bond between two basic amino acids within peptides. The active site of OmpT lies extracellularly in a groove at the top of the barrel with two catalytic pairings, Asp210/His212 and Asp83/Asp85 (Figure 1.9). Based on crystal structure analysis, OmpT shares the catalytic residues of both serine and aspartate proteases, and is formally classified as an aspartate protease.[69] His212 and Asp83 are bridged by a water molecule that acts as a nucleophile in place of the absent catalytic serine, and attacks the peptide carbonyl of the substrate.[70] Asp83 and Asp85 stabilizes the oxyanion intermediate of the peptide cleavage reaction.[65]

Several additional factors play a role in OmpT activity. Electrostatic interactions impact OmpT cleavage specificity and affinity for the substrate. OmpT is highly selective toward basic peptides due to the negative environment near the active site on the extracellular membrane surface.[69] Increased ionic strength, high pH, and acidic amino acids near the active site can decrease OmpT-substrate affinity.[69] OmpT activity is also dependent on LPS, as LPS association may ensure OmpT is only active when inserted into the outer membrane.[69] LPS extends far beyond the surface of the OmpT active site, which can shield other proteins from being degraded by the enzyme. Only cationic peptides small enough to penetrate the LPS layer of the outer membrane will be targeted by OmpT.[38]

1.4.4. LspA structure and function

LspA is an α-helical membrane protein that spans the inner membrane of Gram-negative and Gram-positive bacteria.[71] The *E. coli lsp* gene codes for a mature LspA protein of 164 amino acids.[72] The 21 kDa protein is comprised of four transmembrane helices, containing five conserved domains (Figure 1.10).

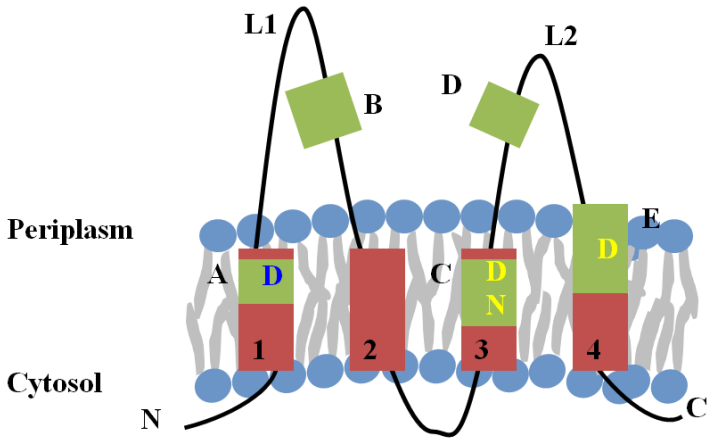

Figure 1.10. LspA topology. LspA is comprised of four transmembrane helices (red) with 5 conserved regions (green, A-E). Catalytic residues (yellow) are in conserved regions C and E while an important aspartate for protein folding (blue) is in conserved region A.

The first conserved region, A, is located in TMD 1 and has a sequence of dxxtk (uppercase represents strictly conserved residues and lowercase depicts mostly conserved amino acids). The *B. subtilis* Asp-14 in this region is critical for protein structure; mutations of this residue results in misfolding and degradation of LspA by proteases within the cell.[73] Region B is located in the periplasmic loop 1, and has the motif NxGaaf. The third conserved region, C, contains the sequence iiggaxlgNxxDr, and is located partially within TMD3. Region D contains the triplet vvd in the periplasmic loop 2 and region E has the consensus sequence FNxAD, in or near the periplasmic space.[71] These domains play vital roles in the function of the α-helical protein.

LspA is a type II signal peptidase involved in protein secretion, specifically cleaving signal peptides from prolipoproteins as they are exported by the Sec pathway through the bacterial inner membrane.[71] Signal peptides play an indispensible role in protein insertion. Some proteins are translated with short (5 to 30 residue) signal peptides, or signal sequences, at the N-terminus. These peptides are responsible for directing the newly synthesized protein to the correct cellular compartment and facilitating co-translational or post-translational translocation through the inner membrane. Co-translational translocation occurs during protein translation; once the signal peptide emerges from the ribosome, it is recognized by the signal-recognition particle (SRP) which halts further translation.[74] The SRP directs the signal peptide-ribosome-mRNA complex to the SRP receptor at the surface of the inner membrane where the signal peptide is inserted into the translocon, the ribosome is docked onto the cytoplasmic face of the translocon, and the protein synthesis into the periplasm or inner membrane resumes.[75] Post-translational translocation is initiated after protein synthesis is

completed. The signal peptide is recognized by the SecB chaperone protein which transfers the protein to the SecA ATPase that pumps the protein through the translocon.[75] Once the protein is in its targeted destination, the signal peptides have carried out their function, and they are cleaved by signal peptidases such as LspA (Figure 1.11).[71]

Signal peptides cleaved by LspA generally do not share sequence homology, but they do have three conserved domains: a positively charged N-terminus (N) region, a central hydrophobic domain (H-region), and the C-terminal domain that contains the consensus LspA cleavage sequence, Leu-X-X-Cys (Figure 1.12).[71] LspA functions as aspartate protease to hydrolyze the linkage between signal peptides and mature protein. Asn99 and Asp102 in the conserved region C and Asp129 in region E of *B. subtilis* are critical for activity, with both aspartate residues proposed to compose the catalytic residues at the active site.[76]

In vitro LspA activity has been studied with several methods. The cleavage of radioactively labeled preproteins by LspA has been monitored with SDS-PAGE and autoradiography as they are synthesized using an *E. coli* wheat germ transcription system.[77] Synthetic signal peptide cleavage via LspA has also been measured with fluorescence and HPLC.[78] LspA activity is inhibited by globomycin, a cyclic peptide antibiotic. Globomycin acts as a substrate analog to signal peptides, binding LspA and interfering with the processing and translocation of prolipoproteins.[79] The inhibition of LspA leads to an accumulation of prolipoprotein in the inner membrane and inhibits bacterial growth, making globomycin an attractive drug.[79]

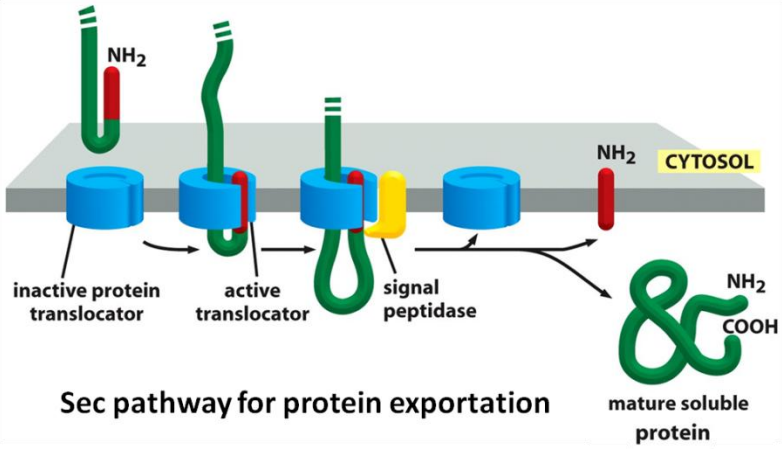

Figure 1.11. Simple Sec pathway diagram for protein exportation. Signal peptides (red) target the protein translocon (blue) in the inner membrane. Upon binding to the translocon, the proprotein is transported across the membrane. Signal peptidases (yellow) cleave the signal peptide from the proprotein after the protein has translocated into the periplasm.

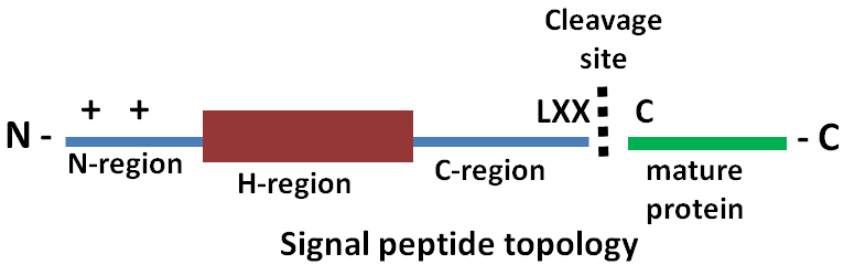

Figure 1.12. Topology of the LspA signal peptide substrate. Typical signal peptides have a positive charged N-terminus (N-region, red) followed by a hydrophobic domain (H-region) and C-terminal region (C-region) that contains the canonical signal peptidase cleavage sequence (L-X-X-C). Cleavage of the peptide from the prolipoprotein results in mature protein.

1.5. Thesis objectives

The native lipid bilayer presents a challenge for the biophysical characterization of membrane proteins. Conducting experiments on membrane proteins require purifying the protein from the lipid environment, yet when removed from the amphiphilic environment, the proteins often aggregate in aqueous buffers. To maintain the integrity of the protein for future experiments, researchers almost always use membrane mimics to isolate, purify, and/or reconstitute the proteins. During protein purification, the membrane protein embeds into the membrane mimic, and the new environment can provide the same stabilization as the bilayer. Although necessary for membrane protein research, these mimics often perturb the stability and functional fold of the protein. Therefore, when conducting research on a membrane protein *in vitro*, there is a generous amount of time and money spent on finding a suitable membrane mimic for a stable and active protein. The aim of this work is two-fold: 1) determine the micelle properties important for stabilizing membrane protein activity *in vitro* by monitoring the function of four membrane enzymes (OMPLA, PagP, OmpT, and LspA) folded into varying detergents, and 2) characterize the physical structure of bicelles. This research will provide guiding principles for membrane mimics selection for use in future membrane protein research.

1.6. References

1. Crick, F. 1970. Central dogma of molecular biology. Nature 227:561-563.

2. Sanger, F. and E. Thompson. 1953. The amino-acid sequence in the glycyl chain of insulin. Biochem J 53: 353-366.

3. Sanger, F. 1952. The Arrangement of Amino Acids in Proteins. Adv Protein Chem 7: 1-67.

4. Kendrew, J, R. Dickerson, E. Strandberg, R. Hart, D. Davies, D. Phillips, and V. Shore. 1960. Structure of myoglobin: A three-dimensional fourier synthesis at 2 Å resolution. Nature 185: 422-427.

5. White, S. and W. Wimley. 1999. Membrane protein folding and stability: physical principles. Annu Rev Biophys Biomol Struct 28: 319-365.

6. Wimley, W. and S. White. 1996. Experimentally determined hydrophobicity scale for proteins at membrane interfaces. Nat Struct Mol Biol 3: 842-848.

7. Chamberlain, A., Y. Lee, S. Kim, and J. Bowie. 2004. Snorkeling preferences foster an amino acid composition bias in transmembrane helices. J Mol Biol 339: 471 – 479.

8. Sipos, L. and G. von Heijne. 1993. Predicting the topology of eukaryotic membrane proteins. Eur J Biochem 213: 1333-1340.

9. Garrett, L. and C. Grisham. 2008. Biochemistry. 4th ed. Belmont: Brooks Cole.

10. Ippolito, J., R. Alexander, and D. Christianson. 1990. Hydrogen bond stereochemistry in protein structure and function. J Mol Biol 215: 457-471.

11. de Planque, M., J. Boots, D. Rijkers, R. Liskamp, D. Greathouse, and J. Killian. 2002. The effects of hydrophobic mismatch between phosphatidylcholine bilayers and

transmembrane α-helical peptides depend on the nature of interfacially exposed aromatic and charged residues. Biochem 41: 8396-8404.

12. Shank, L., J, Broughman, W. Takeguchi, G. Cook, A. Robbins, L. Hahn, G. Radke, T. Iwamoto, B. Schultz, and J. Tomich. 2006. Redesigning channel-forming peptides. Biophys J 90: 2138-2150.

13. Elofsson, A. and G. von Heijne. 2007. Membrane protein structure: prediction versus reality. Annu Rev Biochem 76: 125-140.

14. Papaloukas, C., E. Granseth, H. Viklund, and A. Eloffson. 2008. Estimating the length of transmembrane helices using Z-coordinate predictions. Protein Sci 17: 271-278.

15. Dalbey, R., P. Wang, and A. Kuhn. 2011. Assembly of Bacterial Inner Membrane Proteins. Annu Rev Biochem 80: 161-187

16. Wimley, W. 2003. The versatile β-barrel membrane protein. Curr Opin Struct Biol 13: 404-411.

17. Almen, M., K. Nordstrom, R. Fredriksson, and H. Schioth. 2009. Mapping the human membrane proteome: a majority of the human membrane proteins can be classified according to function and evolutionary origin. BMC Biol 7: 1-14.

18. Yildirim, M., K. Goh, M. Cusick, A. Barabasi, and M. Vidal. 2007. Drug-target network. Nat Biotechnol 25: 1119-1126.

19. Rask-Andersen, M., M. Almen, and H. Schioth. 2011. Trends in the exploitation of novel drug targets. Nat Rev Drug Discov 10: 579-590.

20. Berman, H., J. Westbrook, Z. Feng, G. Gilliland, T. Bhat, I. Shindyalov, P. Bourne. 2000. The protein data bank. Nucl Acid Res 28: 235-242.

21. Tanford, C. 1991. The hydrophobic effect: formation of micelles and biological membranes. Krieger Publishing Company, Malabar, FL.

22. Singer, S. and G. Nicolson. 1972. The fluid mosaic model of the structure of cell membranes. Sci 175: 720-731.

23. Gorter, E. and F. Grendel. 1925. On biomolecular layers of lipoids on the chromocytes of the blood. J Exp Med 41: 439-443.

24. Cooper, G. 2000. The cell: a molecular approach. Sinauer Associates: Sunderland, MA.

25. Hong, C., P. Tieleman, and Y. Wang. 2014. Microsecond molecular dynamics simulations of lipid mixing. Langmuir 30: 11993-12001.

26. Gennis, R. 1989. Biomembranes: molecular structure and function. Springer: New York, NY.

27. Lindblom, G. and G. Oradd. 2009. Lipid lateral diffusion and membrane heterogeneity. Biochim Biophys Acta 1788: 234-244.

28. Heimburg, T. 2007. Thermal biophysics of membranes. Wiley-VCH: Weinhem, DEU.

29. Silhavy, T., D. Kahne, and S. Walker. 2010. The bacterial cell envelope. Cold Spring Harb Perspect Biol: 1-17.

30. Nikaido, H. and M. Vaara. 1985. Molecular basis of bacterial outer membrane permeability. Microbiol Rev 49: 1-32.

31. Caligur, V., R. Gates, G. Lipscomb, L. Masterson, M. Tyson, E. Rathbone, I. Wright, A. Electricwala, and R. Wohlgemuth. 2016. Glycobiology analysis manual. Sigma-Aldrich Life Science, St. Louis, MO.

32. Lerouge, I. and J. Vanderleyden. 2002. O-antigen structural variation: mechanisms and possible roles in animal/plant-microbe interactions. FEMS Microbiol Rev 26: 17-47.

33. Morth, J., B. Pedersen, M. Buch-Pedersen, J. Andersen, B. Vilsen, M. Palmgren, and P. Nissen. 2011. A structural overview of the plasma membrane Na+, K+ - ATPase and H+-ATPase ion pumps. Nature Rev Mol Cell Biol 12: 60-70.

34. Abramson, J., S. Iwata, and H. Kaback. 2004. Lactose permease as a paradigm for membrane transport proteins. Mol Membr Biol 21: 227-236.

35. Ji, T., M. Grossmann, and I. Ji. 1998. G-protein coupled receptors: Diversity of receptor-ligand interactions. J. Biol Chem 273: 17299-17302.

36. Luckey, M. 2008. Membrane Structural Biology with Biochemical and Biophysical Foundations. Cambridge University Press, New York, NY.

37. Tishkov, V. and V. Popov. 2004. Catalytic mechanism and application of formate dehydrogenase. Biochem Mosc 69: 1252-1267.

38. Bishop, R. 2008. Structural biology membrane-intrinsic β-barrel enzymes: sentinels of the bacterial outer membrane. Biochim Biophys Acta 1778: 1881-1896.

39. Dekker, N., K. Merck, J. Tommassen, and H. Verheij. 1995. *In vitro* folding of *Escherichia coli* outer membrane phospholipase A. Eur J Biochem 232: 214-219.

40. Snijder, H., I. Ubarretxena-Belandia, M. Blaauw, H. Verheij, M. Egmond, N. Dekker, and B. Dijkstra. 1999. Structural evidence for dimerization-regulated activation of an integral membrane phospholipase. Nature 410: 717-721.

41. Dekker, N. 2000. Outer membrane phospholipase A: known structure, unknown biological function. Mol Microbiol 35: 711-717.

42. Stanley, A., P. Chuawong, T. Hendrickson, and K. Fleming. 2006. Energetics of outer membrane phospholipase A dimerization. J Mol Biol 358: 120-131.

43. Schmiel, D., E. Wagar, L. Karamanou, D. Weeks, and V. Miller. 1998. Phospholipase A of *Yersinia enterocolitica* contributes to pathogenesis in a mouse model. Infect Immun 66: 3941-3951.

44. Berstad, A.E., K. Berstad, and A. Berstad. 2002. pH-activated phospholipase A2: an important mucosal barrier breaker in peptic ulcer disease. Scand J Gastroenterol 37: 177-189.

45. Mobley, H, G Mendz, and S Hazell. 2001. *Helicobacter pylori*: physiology and genetics. ASM Press, Washington, DC.

46. Mobley, H. 1996. The role of Helicobacter pylori urease in the pathogenesis of gastritis and peptic ulceration. Aliment Pharmacol Ther 10: 57 – 64.

47. Mobley, H, and R Hausinger. 1989. Microbial ureases: significance, regulation, and molecular characterization. Microbiol rev 53: 85-108.

48. Van der Wal, F., G. Koningstein, C. ten Hagen, B. Oudega, and J. Luirink. 1998. Optimization of bacteriocin release protein (BRP)-mediated protein release by *Escherichia coli*: random mutagenesis of the pCloDF13-derived BRP gene to uncouple lethality and quasi-lysis from protein release. Appl Environ Microbiol 64: 392-398.

49. Dekker, N., J. Tommassen, and H. Verheij. 1999. Bacteriocin release protein triggers dimerization of outer membrane phospholipase A *in vivo*. J Bacteriol 181: 3281-3283.

50. Mader, A., B. von Bronk, B. Ewald, S. Kesel, K. Schnetz, E. Frey, and M. Opitz. 2015. Amount of colicin release in *Escherichia coli* is regulated by lysis gene expression of the colicin E2 operon. PLoS One 10: 1-17.

51. Brok, R., I. Belandia, N. Dekker, J. Tommassen, and H. Verheij. 1996. *Escherichia coli* outer membrane phospholipase A: role of two serines in enzymatic activity. Biochem 35: 7787-7793.

52. Brok, R., N. Dekker, N. Gerrits, H. Verheij, and J. Tommassen. 1995. A conserved histidine residue of *Escherichia coli* outer membrane phospholipase A is important for activity. Eur J Biochem 234: 934-938.

53. Kingma, R., M. Fragiathaki, H. Snijder, B. Dijkstra, H. Verheij, N. Dekker, and M. Egmond. 2000. Unusual catalytic triad of *Escherichia coli* outer membrane phospholipase A. Biochem 39: 10017-10022.

54. Stanley, A., A. Treubrodt, P. Chuawong, T. Hendrickson, and K. Fleming. 2007. Lipid chain specificity by outer membrane phospholipase A. J Mol Biol 366: 461-468.

55. Ubarretxena-Belandia, I., J. Boots, and N. Dekker. 1998. Role of cofactor calcium in the activation of outer membrane phospholipase A. Biochem 37: 16011-16018.

56. Hwang, P., W. Choy, E. Lo, L. Chen, J. Forman-Kay, C. Raetz, G. Prive, R. Bishop, and L. Kay. 2002. Solution structure and dynamics of the outer membrane enzyme PagP by NMR. PNAS 99: 13560-13565.

57. Groisman, E., C. Parra-Lopez, M. Salcedo, C. Lipps, and F. Heffron. 1992. Resistance to host antimicrobial peptides is necessary for *Salmonella* virulence. Proc Natl Acad Sci 89: 11939-11943.

58. Vescovi, E., F. Soncini, and E. Groisman. 1996. Mg2+ as an extracellular signal: environmental regulation of *Salmonella* virulence. Cell 84: 165-174.

59. Huysmans, G., S. Radford, D. Brockwell, and S. Baldwin. 2007. The N-terminal helix is a post-assembly clamp in the bacterial outer membrane protein PagP. J Mol Biol 373: 529-540.

60. Ramasubramanian, B. and R. Mahalakshmi. 2015. Residue-dependent thermodynamic cost and barrel plasticity balances activity in the PhoPQ-activated enzyme PagP of *Salmonella typhimurium*. Biochem 54: 5712-5722.

61. Ahn, V., E. Lo, C. Engel, L. Chen, P. Hwang, and L. Kay. 2004. A hydrocarbon rule measures palmitate in the enzymatic acylation of endotoxin. EMBO J 23: 2931-2941.

62. Khan, M., J. Moktar, P. Mott, M. Vu, A. McKie, T. Pinter, F. Hof, and R. Bishop. 2010. Inscribing the perimeter of the PagP hydrocarbon ruler by site-specific chemical alkylation. Biochem 49: 9046-9057.

63. Khan, M. and R. Bishop. 2009. Molecular mechanism for lateral lipid diffusion between the outer membrane external leaflet and a β-barrel hydrocarbon ruler. Biochem 48: 9745-9756.

64. Hwang, P. and L. Kay. 2005. Solution structure and dynamics of integral membrane proteins by NMR: a case study involving the enzyme PagP. Methods Enzymol 394: 335-350.

65. Hritonenko, V. and C. Stathopoulos. 2007. Omptin proteins: an expanding family of outer membrane proteases in Gram-negative *Enterobacteriaceae*. Mol Memb Biol 24: 395-406.

66. Haiko, J., M. Suomalainen, T. Ojala, K. Lahteenmaki, and T. Korhonen. 2009. Breaking barriers – attack on innate immune defenses by omptin surface proteases of enterobacterial pathogens. Innate Immune 15: 67-80.

67. Stumpe, S., R. Schmid, D. Stephens, G. Georgiou, and E. Bakker. 1998. Identification of OmpT as the protease that hydrolyzes the antimicrobial peptide proteamine before it enters growing cells of *Escherichia coli*. J Bacteriol 180: 4002-4006.

68. Webb, R. and M. Lundigran. 1996. *OmpT* in *Escherichia coli* correlates with severity of disease in urinary tract infections. Med Microbiol Lett 5: 8-14.

69. Vandeputte-Rutten, L., R. Kramer, J. Kroon, N. Dekker, M. Egmond, and P. Gros. 2001. Crystal structure of the outer membrane protease OmpT from *Escherichia coli* suggests a novel catalytic site. EMBO J 20: 5033-5039.

70. Baaden, M. and M. Sansom. 2004. OmpT: molecular dynamics simulations on an outer membrane enzyme. Biophys J 87: 2942-2953.

71. Paetzel, M., A. Karla, N. Strynadka, and R. Dalbey. 2002. Signal peptidases. Chem Rev 102: 4549-4579.

72. Yu, F., H. Yamada, K. Daishima, and S. Mizushima. 1984. Nucleotide sequence of the lspA gene, the structural gene for lipoprotein signal peptidase of *Escherichia coli*. FEBS Lett 173: 264-268.

73. Tjalsma, H., G. Zanen, G. Venema, S. Bron, and J. van Dijl. 1999. The potential active site of the lipoprotein-specific (type II) signal peptidase of *Bacillus subtilis*. J Biol Chem 274: 28191-28197.

74. Walter, P., I. Ibrahimi, and G. Blobel. 1981. Translocation of proteins across the endoplasmic reticulum I. Signal recognition protein (SRP) binds to *in vitro*-assembled polysomes synthesizing secretory protein. J Cell Biol 91: 545-550.

75. Gilmore, R., G. Blobel, and P. Walter. 1982. Protein translocation across the endoplasmic reticulum I. Detection in the microsomal membrane of a receptor for the signal recognition particle. J Cell Biol 95: 463-469.

76. Tjalsma, H., G. Zanen, G. Venema, S. Bron, and J. van Dijl. 1999. The potential active site of the lipoprotein-specific (type II) signal peptidase of *Bacillus subtilis*. J Biol Chem 274: 28191-28197.

77. Zwizinski, C. and W. Wickner. 1980. Purification and characterization of leader (signal) peptidase from *Escherichia coli*. J Biol Chem 255: 7973-7977.

78. Zhong, W. and S. Benkovic. 1998. Development of an internally quenched fluorescent substrate for *Escherichia coli* leader peptidase. Anal Biochem 155: 66-73.

79. Dev, I., R. Harvey, and P. Ray. 1984. Inhibition of prolipoprotein signal peptidase by globomycin. J BIol Chem 260: 5891-5894.

Chapter 2: Membrane mimics

2.1. Detergent micelles

2.1.1. Self-association of detergent monomers

Detergents are amphiphilic surfactants. They typically consist of a nonpolar, hydrophobic alkyl chain covalently linked to a polar, hydrophilic head group, making their amphiphilic nature very similar to lipids. There are over 100 synthetic detergents that are used for membrane protein research. The larger head group surface area to tail volume ratio gives detergent monomers an overall conical shape. Although this conical shape prevents bilayer formation, detergents self-associate to form micelles that can be small spheres, ellipsoids, or long cylindrical rod-like structures.[1]

Micelle formation occurs above a defined concentration of total detergent monomers in solution, called the critical micelle concentration (CMC).[2] Below the CMC, detergents exist as individual monomers. Above the CMC, the monomer concentration remains unchanged while the concentration of micelles increases (Figure 2.1).[1] The CMC is different for every detergent and is dependent on the degree of hydrophobicity of the detergent. Detergents with longer alkyl tails are more hydrophobic, and have smaller CMCs. Conversely, less hydrophobic detergents with shorter nonpolar tails have higher CMCs. Increasing a detergent monomer nonpolar tail by 2 methyl groups results in a decrease in CMC by an order of magnitude.[1]

Micelle formation requires an attractive force between hydrocarbon tails. The van der Waals forces between alkyl tails favor interaction and aggregation of the detergent monomers while head group repulsions prevent giant micelle formation.[1] The number of

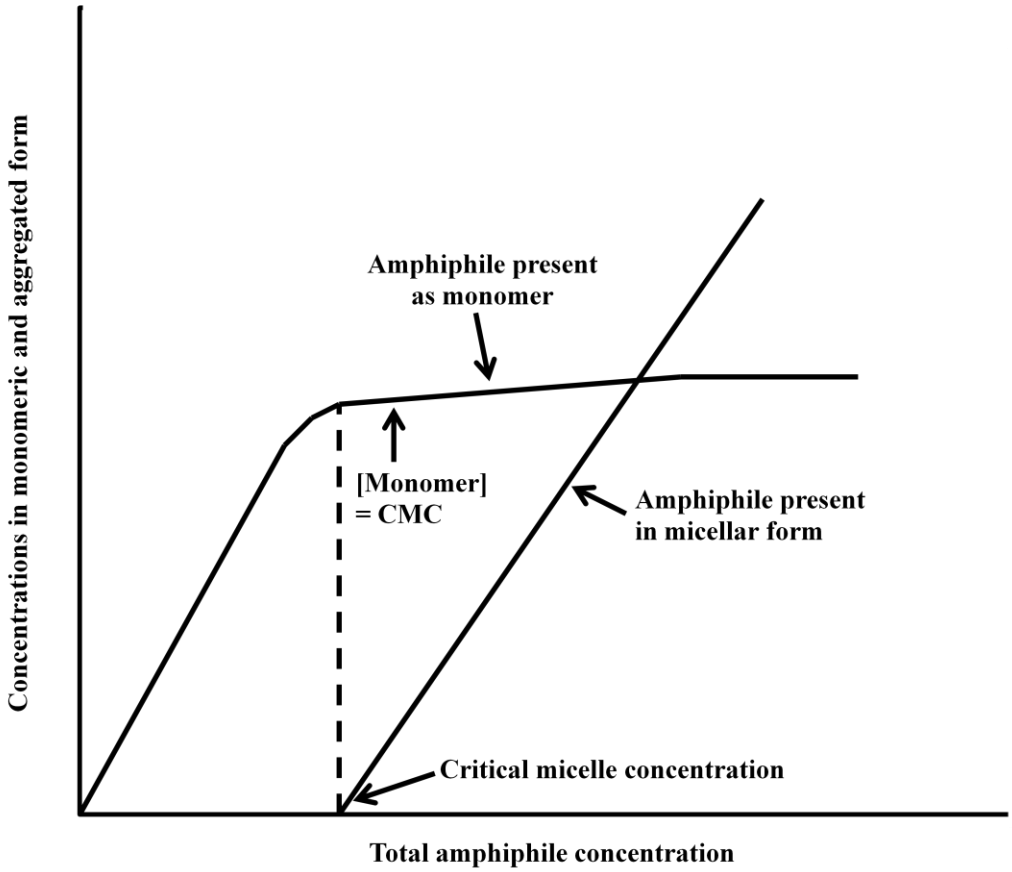

Figure 2.1. The relationship between monomeric concentration and total concentration of amphiphiles in solution. The monomeric detergent concentration increases until it reaches the CMC. Above CMC, the addition of more detergent contributes solely to the concentration of micelles.

detergent monomer within one micelle is called the aggregation number (N). Micelles formed by amphiphiles with shorter tails, such as FC8, are small (N = 35). As carbons are added onto the tail, there is more space to accommodate more monomers into the aggregate, making larger micelles (FC14, N = 110).

There are distinct trends and geometric considerations for the dimensions of detergent micelles. As earlier alluded, the CMC and N are dependent on the length of the alkyl tail. An addition of two carbons onto the tail of a detergent will decrease the CMC by an order of magnitude and increase N by approximately 20 monomers.[1] The volume (V) of the hydrocarbon core is determined using Tanford's formula:[1]

$$V = 27.4 + 26.9*n_c \quad [1]$$

where n_c is the number of alkyl chain carbons, V is in cubic Angstroms, and the constants are derived from the densities of liquid hydrocarbons and Traube's formula for calculating molecular volume from each volume constant of the constituent elements of molecular solutions. Because there is no hole in the interior of the micelle, the maximum extension of the hydrophobic chain (L_{max}) into the core can be derived using the distance of 2.53 Å between alternate carbon atoms of a fully extended chain with the addition of the van der Waals radius of the terminal methyl group (2.1 Å). L_{max} is represented with this formula:[1]

$$L_{max} = 1.5 + 1.265*n_c \quad [2]$$

2.1.2. General detergent micelle categories

Detergents have a variety of head groups and carbon tails whose properties affect the membrane protein differently. These detergents are categorized by these traits, and will be briefly discussed in this section, followed by an in-depth discussion of the

properties of each of these detergent micelles. Figure 2.2. depicts the structures of these detergents.

Phosphocholine (FC) detergents have a negatively charged phosphate and a positively charged choline group in the polar head, resulting in a zwitterionic charge. Phosphocholine detergent alkyl tail lengths vary between 8 and 16 carbons. FC12 (often called DPC) is one of the most used phosphocholine detergents. The FC12 nomenclature derives from the phosphocholine, or foscholine, head group and its 12 carbon alkyl tail.

Cyclofos detergents have a zwitterionic phosphocholine head group with a bulky cyclohexyl hydrocarbon ring at the end of the tail. These detergents are available with 1 to 7 alkyl carbon tail lengths. Anzergents, also called zwittergents, have polar heads that consist of a sulfate and choline group. Anzergent 310, 312, 314, 316, and 318, with the corresponding tail lengths of 10 to 18, are produced by Anatrace.

Glucoside and maltoside detergents have a sugar head group that is covalently bonded to the hydrophobic alkyl tail. Glucoside detergents have glucose head groups while maltoside head groups are derived from maltose. Both types of detergents are available with a broad range of carbon tail lengths (6 to 12 for glucosides and 6 to 16 for maltosides). Cymal detergents also have the maltose head group, but contain a cyclic ring at the end of its hydrocarbon tail. Cymal is available with 1 to 7 carbon tail lengths.

Steroid-like detergents include CHAPS, Big CHAPS, and CHAPSO. They all have a tetracyclic nonpolar tail with a structure similar to the cholesterol that is present in native membranes. With their large size, these detergents normally form micelles composed of only a few detergent monomers.[4]

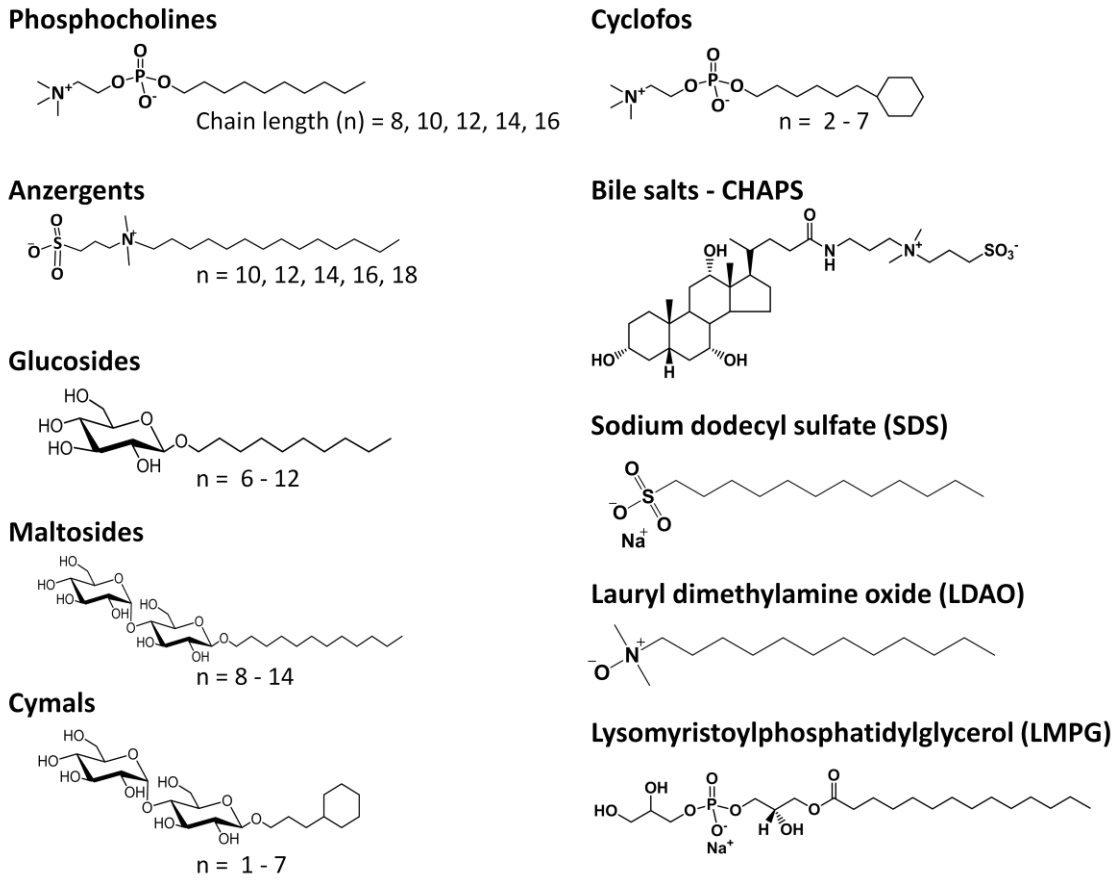

Figure 2.2. Common detergent monomer structures. Detergents are categorized based on head group type, and have varying alkyl tail lengths (n).

There are other extensively used detergents that have not been utilized for the work completed in this thesis. This includes a highly denaturing anionic detergent, sodium dodecyl sulfate, other zwitterionic detergents, such as lauryl dimethylamine oxide, and a variety of polyethylene detergents.[5,6] Each detergent is different; therefore, each detergent micelle has its own properties that affect the membrane protein differently.

2.1.3. Micelle properties

Micelle properties are derived from the characteristics of individual detergent monomers, and have a significant effect on membrane proteins. Micelle properties not only include CMC and N, but also the shape, size, radius of gyration (R_g), shell thickness, hydrophobic thickness, surface area, volume, and charge. Small angle X-ray scattering (SAXS) has been used to determine multiple properties of various detergent micelles.[7] Core-shell ellipsoid fitting of the SAXS data provided the core and shell volumes as well as the core axial dimensions (a and b) and the head group shell thickness, t, of the micelles (Figure 2.3).[7] Table 2.1. depicts the specific properties of detergent micelles that will be discussed in this section.[7]

2.1.3.1. Effects of head group

In detergent micelles, the polar head group forms a uniform hydrophilic shell around the micelle hydrocarbon core. Detergents have a variety of head groups with different structures, thicknesses, and charges that directly impacts the surface area and shape of the micelle head group shell.

SAXS analysis of FC10, FC12, and FC14 detergents indicate that the phosphocholine head groups shell has a thickness of approximately 3 Å.[7] The Anzergent

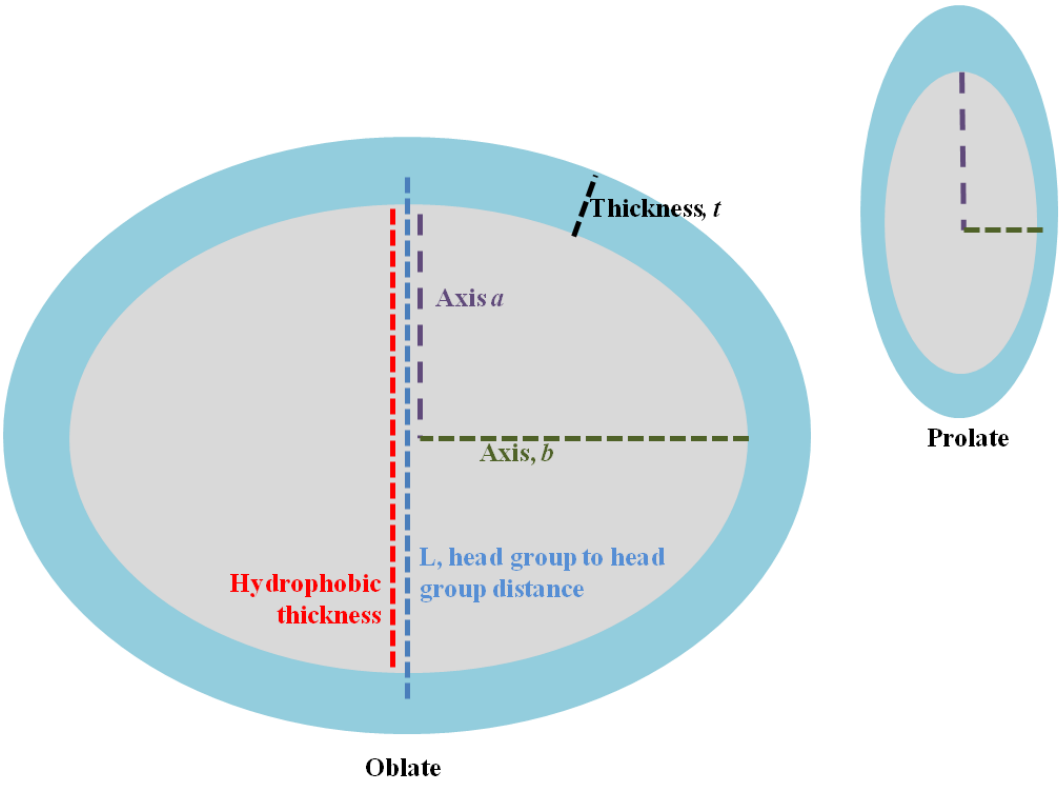

Figure 2.3. Ellipsoidal model of a micelle. Micelles have a core-shell ellipsoidal model. The ratio between minor and major axes, *a* and *b*, dictates the prolate or oblate micelle shape. Micelle properties such as the head group shell thickness, radius of gyration, hydrophobic thickness, and head group to head group distance are depicted.

Detergent	CMC (mM)	N	Shell thickness (Å)	Charge	Shape	Tail lengths (Å)[b]	Rg (Å)	L (Å)	Volume (Å^3)[c]
FC10	11	39-45	2.7-3.0	zwitterionic	prolate	14.2	25.9	27.6-28.2	494
FC12	1.5	68-80	2.7-3.0	zwitterionic	prolate	16.7	34.5	33.9-34.5	548
FC14	0.12	88-91	2.7-3.0	zwitterionic	prolate	19.2	50.2	41.4-42.0	602
OG	18-20	27-100[a]	2.9-3.5	nonionic	oblate	11.6	29.6	26.9-27.5	419
NG	6.5	133[a]	2.9-3.5	nonionic	oblate	12.9	34.2	29.6-30.2	446
DG	2.2	200-400[a]	2.9-3.5	nonionic	oblate	14.2	n.d.	32.1-32.7	472
OM	19.5	35-47	5.4-5.8	nonionic	oblate	11.6	22.0	27.9-28.5	590
DM	1.8	86-103	5.4-5.8	nonionic	oblate	14.2	26.2	33.4-34.0	644
DDM	0.17	135-149	5.4-5.8	nonionic	oblate	16.7	31.8	39.4-40.0	698
LMPG	0.16	63-69	5.3-6.1	anionic	oblate	19.2	26.9	38.7-39.3	639

Table 2.1. Properties of detergent micelles. [a]Glucoside aggregation numbers were derived from literature, [b]alkyl tail lengths were derived from Tanford's formula [2], [c]volume was predicted from Tanford's formula [3].

head groups are assumed to have a similar size; Anzergent polar heads are composed of similar groups to phosphocholine, a choline and a sulfate group. The glucose head group on glucoside detergents result in a thicker head group than the phosphocholines at ~ 3.5 Å.[7] As expected, the detergents with maltose head groups, such as maltosides and Cymals, have even larger head group shells of approximately 5.8 Å.[7]

With their respective chemical structures, the FC, Cyclofos and Anzergent detergent head groups are zwitterionic while the glucoside, maltoside and Cymal detergents have nonionic heads. The charge and size of the head group impacts the surface area and shape of the micelle. Electrostatic repulsions between the charged or larger head groups increase the surface area of the micelles, preventing tight packing of the detergent monomers and increasing the surface area.[1] An analysis of surface packing characteristics is described by this dimensionless packing parameter, P:[8]

$$P = \frac{v_c}{a_o l_c} \quad [3]$$

where v_c is the carbon chain volume, a_o is the optimal head group area, and l_c is the critical chain length, the longest effective length that the chain can be extended in the micelle. The packing parameter reflects the curvature of the micelle.[8] With identical carbon tails, a micelle with a charged or larger head group would have a larger a_o, decreasing P. A smaller packing parameter represents a highly curved micelle, while a larger P reflects a less curved aggregate.[8]

This relationship is reflected in the detergents used in this project. Iyer and Blankschtein and Dupuy et. al proposed models that predicted the ellipticity and shape of nonionic micelles based on head group packing.[9,10] Independent of tail length, oblate micelles (aspect ratio a/b < 1) are predicted for small nonionic detergents, but as the head

group size increases or electrostatic repulsions occur, prolate micelles (aspect ratio a/b > 1) may be preferred.[9] This trend was confirmed by the SAXS results on the ellipticity of glucoside, maltoside, and the negatively charged lysophosphatidylglycerol (LPG) micelles.[7] The LPG micelles have a more spherical geometry (aspect ratio a/b ~ 1) compared to the uncharged, oblate glucoside and maltoside micelles. Phosphocholines, with zwitterionic head groups, also have significant electrostatic repulsions between polar heads, forming prolate micelles.[7]

2.1.3.2. Effects of alkyl tail

Detergent monomers have a variety of carbon tail lengths, varying from approximately 9 to 24 Å.[1] These tails have a direct impact on micelle properties such as the CMC, aggregation number (N), radius of gyration (R_g), head group to head group distance (L), hydrophobic thickness, and core volume (Figure 2.3). Section 2.1.1 describes the relationships between CMC and N with the alkyl tail lengths; this section will focus on the influence of the carbon tail on these other characteristics.

As expected, the R_g, L, and hydrophobic core thickness of a micelle increase with the length of the alkyl carbon tail.[7] R_g refers to the distance from the center of mass of an object. FC10 micelles have an R_g of approximately 26 Å while FC12 and FC14 micelles have R_g values of 35 and 50 Å, respectively.[7] The R_g of glucosides and maltosides follow the same trend: OG and NG R_g values are 30 and 34 Å, while the R_g of OM, DM, and DDM micelles are 22, 26, and 32 Å, respectively.[7]

L represents the head group to head group distance. The L is the length from the ellipsoidal minor axis from the center of one head group to the center of a head group directly opposite on the micelle.[1] The carbon tail linearly impacts L; every two carbons

added to the alkyl chain of phosphocholine, glucoside, or maltoside detergents increases the L by 2.5 – 3.0 Å, 1.31 Å per carbon.[7] This distance corresponds well to Tanford's formula [2].[1] L values for FC micelles range from 28 to 42 Å depending on tail length, while glucoside micelle L values differ from 24 to 32 Å and maltoside distances vary from 28 to 40 Å.[7] The hydrophobic core thickness has similar values, subtracting the contributions from the head groups from L.

The volume also increases with carbon tail length. Using Tanford's formula for volume [1], the micelle volume can be predicted for varying micelles.[1] FC10, FC12, and FC14 micelles have volumes of 494, 548, and 602 $Å^3$, respectively.[1] OG, NG, and DG micelle volumes are estimated at 419, 446, and 472 $Å^3$.[1] The volumes of OM, DM, and DDM micelles are predicted at 590, 644, and 698 $Å^3$.[1] The volume of these micelles will be significantly increased for micelles composed of detergents with a hydrocarbon ring in the carbon tail, such as Cyclofos and Cymal detergents.

2.1.4. Solubilization, folding, and stabilization of membrane proteins in micelles

Detergents are essential to the successful purification of membrane proteins. "Solubilization" of membrane proteins in detergent refers to removing the proteins from the native lipid bilayer and placing them in a new amphiphilic environment. When removed from the native, amphiphilic environment, membrane proteins often aggregate upon contact with the aqueous solvent.[11] Therefore, extracting the proteins requires using detergent to dilute and replace the native bilayer for the micellar environment. Solubilization occurs following a sequence of events:[12] 1) detergent monomers penetrate the outer monolayer of the bilayer, 2) equilibration of the detergent monomers with the native lipids in both monolayers, 3) saturation of the bilayer with excess detergents,

resulting in dilution and permeabilization of the membrane, and 4) transition of the bilayer to micelle.[12]

β-barrel membrane proteins are often overexpressed *in vitro* into inclusion bodies, an insoluble aggregate of misfolded, membrane bound protein.[13] Solubilization of the membrane protein from inclusion bodies involves resuspending the protein in a denaturant, such as urea or guanidine hydrochloride, and rapidly diluting the resuspended protein in detergent.[13] Rapid dilution of the resuspended protein results in a folded membrane protein in detergent.[13] Some α-helical membrane proteins do not express to inclusion bodies. These α-helical proteins remain bound to the membrane after bacterial cell lysis.[14] Solubilizng these proteins require pelleting the membrane fraction with high speed centrifugation and resuspending the membrane-bound protein pellet in detergent.[14]

Although the solubilizing detergent efficiently removes membrane proteins from the bilayer, it may not be the suitable detergent for protein characterization. A membrane protein in an unsuitable detergent can result in protein destabilization, aggregation, unfolding, or misfolding. An unsuitable detergent could have a head group charge that affects the protein active site, or a hydrophobic diameter that mismatches the protein. These issues with protein-detergent complexes (PDCs) are discussed in section 2.3.

Because some effective membrane solubilizers do not necessarily stabilize a specific protein's fold, the solubilizing detergent is often exchanged for a different detergent that conserves the functional fold of the protein. This process often occurs by immobilizing the affinity tagged membrane protein to an appropriately tagged column, and washing and eluting the protein in the desired detergent.[14] Obtaining a PDC that contains properly folded and active protein is often an extensive trial-and-error process

involving excessive time and money. There also more opportunities for PDC formation; mixed micelles, micelles composed of two detergents, can be used for membrane protein research, allowing for more micelles with different properties.

2.1.5. Mixed micelles

Mixing detergents with different characteristics can yield micelles with intermediate properties, providing additional membrane mimic options for protein characterization. Ideal detergent mixing occurs when the ratio of detergent components in the micelle is equal to the ratio of total detergents in solution. Originally, ideal mixing was only expected when mixing detergents with the same head group and different alkyl chain lengths, due to the electrostatic repulsions that can occur between different head groups.[8] The first experiments completed on mixed micelles used detergents with the same head groups: first, mixing two ionic detergents, followed by tests completed by mixing two nonionic detergents.[15,16] These experiments established a relationship between ideal mixed micelles and the CMC that is currently used:[8]

$$\frac{1}{CMC_{mix}} = \frac{X_A}{CMC_A} + \frac{X_B}{CMC_B} \quad [3]$$

Where X_A and X_B are the mole fractions of each detergent in the mixture, CMC_A and CMC_B are the CMCs of the pure detergents, and CMC_{mix} is the resulting CMC of the newly formed mixed micelle.[1] From these earlier experiments, newer detergent combinations have been utilized to modulate other mixed micelle properties.[17]

Micelle hydrophobic thickness can be modulated using mixed micelles. There is a dependence of L on the alkyl chain lengths of the detergents composing the mixed micelle. As increasing amounts of a shorter tailed detergent (FC10, for example) is added to a detergent with a longer tail (DDM), a linear decrease in L is observed as the mole

fraction of the FC10 increases.[17] This trend occurs when forming mixed micelles composed of detergents with varying head group and tail length.[17] The relationship between the mixed micelle tail lengths and L is linear, enabling a modulation of hydrophobic thickness by varying the mole fractions of detergent components. Therefore, a mixed micelle composed of 50% tetradecyl-maltoside and 50% octyl-maltoside forms a micelle with an L consistent with undecyl-maltoside micelles.[17]

There are similar trends with micelle volume, size, and shape. The volume of a micelle mixture of maltosides and phosphocholines varies linearly with the mole fraction of each component.[17] Mixing a larger volume detergent micelle (DDM) with increasing amounts of a smaller volume detergent micelle (FC12) linearly decreases the core volume, ultimately becoming the volume of FC12 micelles.[17] Unsurprisingly, the overall ellipsoid size dimensions change similarly when mixing smaller and larger detergents.[17] Increasing amounts of prolate FC12 micelles added to oblate maltoside detergent micelles changes the mixed micelle shape from an oblate ellipsoid to prolate.[17] An addition of anionic lysomyristoylphosphatidylglycerol (LMPG) detergent can also alter the micelle surface charge, linearly increasing the surface potential as the mole fraction of the charged component is increased in the mixed micelle.[17] These trends with maltoside and phosphocholine detergents mixtures are useful when trying to generate a micelle with normally unattainable properties. Mixed micelles also allow a systematic tuning of micelle properties to test hypotheses about micelles and protein-detergent complexes (PDC).

2.2. Bicelles

Bicelles are model membranes composed of long-chain lipids and short-chain detergents. The "ideal" bicelle in aqueous solutions is assembled with lipids forming a planar lipid-rich bilayer and detergents coating the bilayer rim (Figure 2.4).[18] These detergents on the rim stabilize the otherwise exposed lipid hydrocarbon chains. Bicelles may better model the biological bilayer and are a useful system for biophysical studies.

Bicelles overcome challenges often encountered with membrane proteins in detergent micelles and liposomes. The bicelle interior is composed of a planar bilayer region, which is closer to the native environment than the sharp ellipsoid curvature of micelles.[19] This lack of curvature was useful when studying the HIV-1 envelope peptide. Detergent micelles were confirmed to induce significant strain on the helical peptide structure in comparison to bicelles as observed with NMR decoupling measurements.[20] In addition, the membrane protein diacylglycerol kinase retains its activity in bicelles, in contrast to micelles, possibly from changes in the more planar bilayer environment.[21]

The lipid-detergent complexes also impact protein oligomerization. Sedimentation equilibrium analytical ultracentrifugation (AUC) and fluorescence resonance energy transfer (FRET) experiments indicate that the stability of the membrane transporter EmrE dimer is increased in DLPC/DHPC bicelles as opposed to DDM micelles, but the bicelle complex has less stability than DLPC liposomes.[22] Bicelles are also significantly smaller and more stable than liposomes, enabling increased biophysical characterization techniques, such as high resolution NMR structure determination and X-ray crystallography.[20]

The first bicelles described were dimyristoylphosphatidylcholine (DMPC) lipid and CHAPSO detergent mixtures published in 1990.[23] Two years later, Sanders and

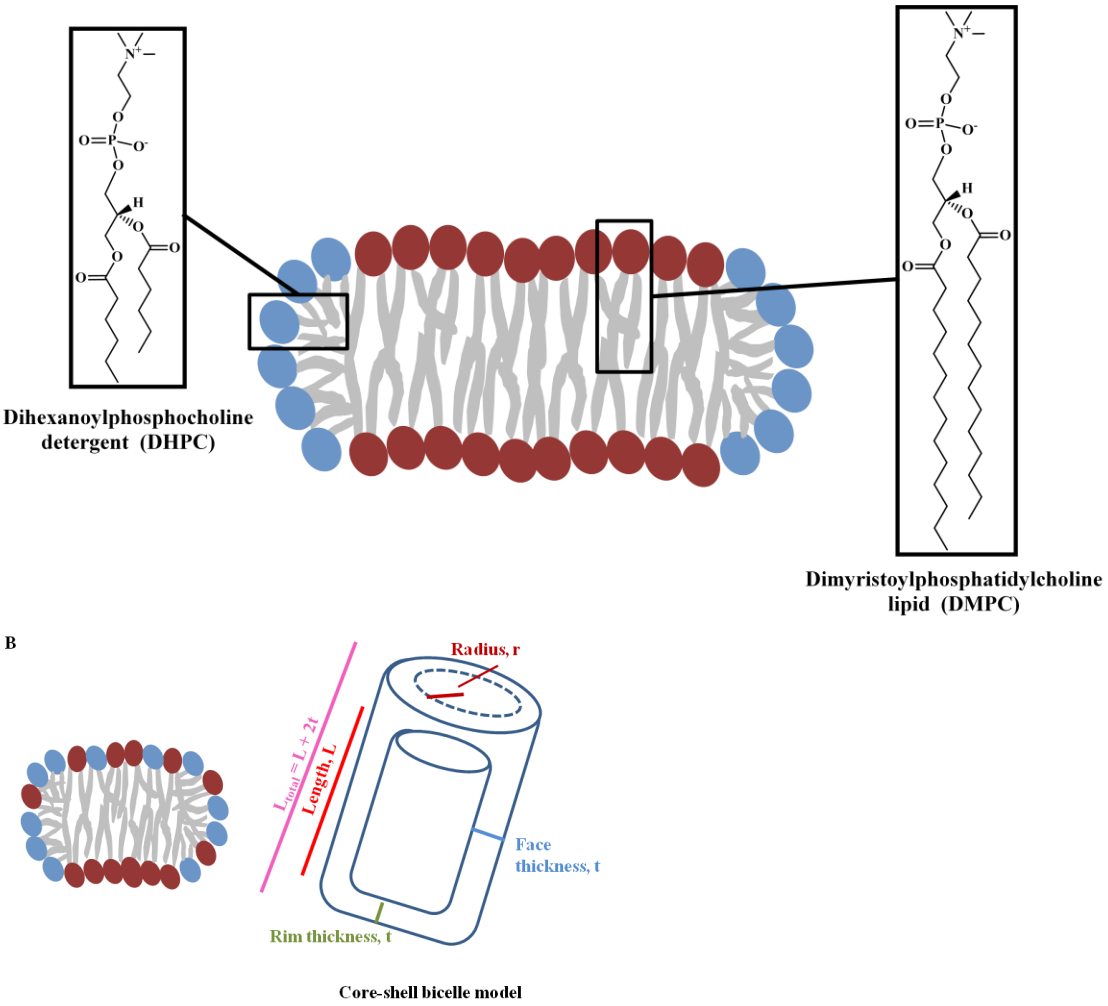

Figure 2.4. Ideal bicelle structure. A) Bicelles are planar bilayers of lipids (red) enclosed and stabilized by a detergent rim (blue). The most commonly used bicelles are composed of DMPC lipid and DHPC detergent. B) The bicelle structure depicted with mixing between detergent and lipid components and the core-shell bicelle model used to fit the aggregate.

Schwonek replaced the non-lipid CHAPSO detergent with dihexanoylphosphocholine (DHPC) detergents, making the most commonly used DMPC/DHPC bicelle.[24] Soon after, bicelles were first applied to membrane protein research.[25] This research led to several different lipid and detergent compositions and multiple applications in membrane protein research.

2.2.1. Bicelle composition

Bicelle properties are dependent upon the q-ratio, lipid and detergent mixture, total amphiphile concentration (C_L), and temperature. q is defined as the ratio of lipid and detergent concentrations:

$$q = \frac{[\text{lipid}]}{[\text{detergent}]} \quad [4]$$

q has a great impact on the size and shape of the bicelles (Figure 2.5). Lipid rich bicelles ($q > 1$) are larger structures, with a shape that is often debated.[26] These bicelles can form larger disks, perforated multi-lamellar sheets, or potentially worm-like micellar structures, and can also undergo a liquid-crystalline phase change.[26] Although lipid-rich bicelles are more commonly utilized in membrane protein research, detergent-rich bicelles are also an option for biophysical experiments. Small ($q \leq 0.5$) bicelles are ideal isotropic fast tumbling aggregates for obtaining high-resolution solution-state NMR spectra as opposed to magnetically aligned high-q bicelles.[27,28] The research in this thesis will discuss detergent-rich bicelles. These bicelles have a low q-ratio, $q \leq 1$, and are smaller discoidal structures. Several methods have been used to characterize these low-q bicelles including NMR, electron microscopy, fluorescence spectroscopy, dynamic light scattering, and small angle neutron scattering.[29,30]

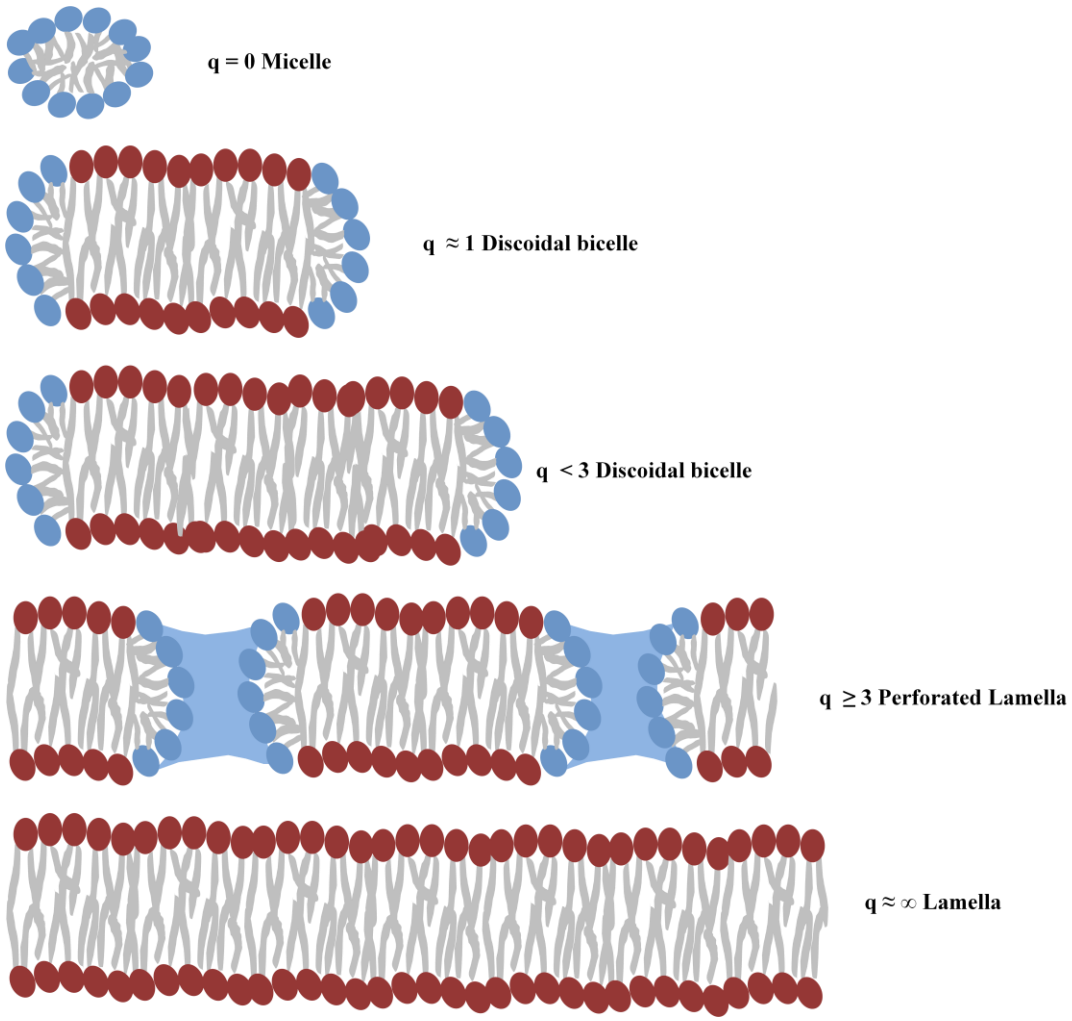

Figure 2.5. Bicelle structure dependence on q. With increasing lipid concentration, micelles transition to bicelles, perforated lamella, and bilayers.

While the most common bicelle mixture is DMPC lipid and DHPC detergent, other combinations have been successful in biophysical research. Lipids with negatively charged head groups, such as dimyristoylphosphatidylglycerol (DMPG) and dimyristoylphosphatidylserine (DMPS), have been used in bicelle mixtures with DHPC. These acidic bicelles were less stable because the negative charged DMPG and DMPS are less miscible with DHPC than the neutral DMPC lipid.[31] Unsaturated lipids such as 1-palmitoyl-2-oleyl-sn-3-glycerophosphocholine (POPC) destabilize the bicelles as expected; any degree of unsaturation will result in less packing between lipids.[32] Saturated lipids with longer hydrophobic tails such as dipalmitoylphosphatidylcholine (DPPC) successfully form bicelles, but tumble slower than other bicelle compositions, making them less useful for NMR experiments.[33]

The DHPC detergent is often replaced with CHAPS in bicelle compositions. The rigidity of the CHAPS molecule with DMPC increases bicelle stability.[34] Another detergent used in place of DHPC is Cyclofos-6. Cyclofos-6 has a smaller CMC than DHPC, and DMPC/Cyclofos-6 bicelles are stable at lower total amphiphile concentrations. With a bulky ring in the alkyl tail, Cyclofos-6 is also less likely to partition into the lipid domain of the bicelle, remaining in the rim of the structure and resulting in a more native structure to use for membrane protein research.[35]

2.3. Difficulties with protein-mimic investigations

Membrane mimics, such as micelles and bicelles, are often used for the biophysical characterization of membrane proteins; however, they are not the native bilayer and pose investigative challenges. Hydrophobic mismatch, aggregation, protein misfolding, and attenuated function are all possible consequences of an ill-fitting protein-

mimic complex. All of these negative consequences emphasize the importance of understanding the structural properties of these mimics and selecting better mimics for membrane protein experiments.

2.3.1. Challenges with protein-detergent complexes

Although detergent micelles are one of the standard tools for membrane protein reconstitution and characterization, there are several pitfalls to using detergents for membrane protein studies. Sometimes the organization of the hydrocarbon tails cannot accommodate the membrane protein, resulting in a hydrophobic mismatch.[36] There are several consequences of hydrophobic mismatch which subsequently impact protein function, including protein aggregation, backbone conformational changes, tilting, and surface orientation.[36-38]

Detergents also have a major impact on membrane enzyme kinetics. For example, enzymatic studies of a membrane rhomboid protease, GlpG, indicate that protein activity varies depending on the detergent environment.[38] GlpG has higher activity when solubilized in phosphocholine or maltoside detergents with 10 to 12 carbon lengths.[38] The function of the protein is significantly attenuated when folded in detergents with longer nonpolar tails.[38]

The substrates for membrane enzymes are often phospholipids or amphiphilic molecules with structures that are similar to detergent monomers. This can result in two issues when studying protein function in a PDC: detergent inhibition and substrate-micelle partitioning. When solubilizing and folding the membrane enzymes in micelles, a detergent can have an antagonist interaction with the enzyme. The enzyme may bind detergent monomers due to similar qualities to its substrate, inhibiting the substrate from

interacting with the active site residues. An example is the LDAO detergent monomer present in the binding cavity of PagP described in Chapter 1. PagP activity is inhibited in LDAO and similar FC12 detergents due to antagonist inhibition.[39]

Substrate partitioning into the micelle can occur when the amphiphilic substrate acts as a detergent monomer, interacting with the micelle via alkyl tail van der Waals interactions and head group repulsions. When this interaction occurs, the substrate may not reach the active site residues of the enzyme. Substrate partitioning into micelles can reduce enzymatic activity and cause false-negatives when conducting functional assays in PDCs. This concern is more pronounced when studying OMPLA, an enzyme that cleaves phospholipids. The substrate for OMPLA activity is an amphiphilic molecule similar to a phosphocholine detergent. Therefore, several procedures and controls must be conducted when assaying OMPLA activity to overcome these issues.

There are many properties of detergent monomers, micelles, and mixed micelles to note, as well as several advantages and difficulties with characterizing protein-detergent complexes. A suitable PDC to use for accurate characterization of a membrane protein would have a minimal denaturing affect on the protein, would not affect protein-substrate interactions, and the detergent would contain an appropriate hydrophobic thickness to accommodate the transmembrane domain of the protein. An ideal detergent would also enable functional studies, with minimal substrate and enzyme active site interactions. These traits are identified by systematically varying detergent properties and correlating micelle characteristics with protein function. In this study, the function of four membrane enzymes will be monitored in different micelles, and these key physical

detergent properties for active protein will be identified. Chapters 3 and 4 describe the results from this study as well as future directions to test these new hypotheses.

2.3.2. Challenges with low-q bicelle structures

Although protein-bicelle complexes are used for the biophysical characterization of membrane proteins, there are still debates on the structure of the bicelles used for these investigations.[21,26] The ideal bicelle model suggests that low-q bicelles are a disk consisting of distinctly separated lipid bilayer domain surrounded by a detergent rim.[29,40] It is widely accepted that lipid-rich bicelles are more likely to form the ideal bicelle structure; however, due to the tendency of detergents to form mixed micelles in detergent-rich conditions, low-q bicelles may have some degree of mixing of the lipid and detergent components.[26,41]

Ideal bicelle structures have been proposed and refuted in detergent-rich systems. Electron microscopy suggests ideal bicelle-like particles using detergent-rich DMPC/DHPC mixtures of $q \leq 0.5$.[29] ^{31}P NMR studies also suggest there is little mixing between the DMPC and DHPC components of q = 0.05 to 0.5 bicelles.[29] Contrary to these studies, similar ^{31}P NMR experiments indicate that at low-q, mixed micelles are likely to form.[41] Elucidating the structure and composition of detergent-rich bicelles will impact membrane protein research and guide membrane mimic selection. Membrane proteins fold and function differently in ideal bicelle systems vs. mixed micelles, and this can be exploited if using the correct mimic.

The stability and size of low-q bicelles are also dependent on the total concentration of amphiphiles (C_L) in solution and the temperature. The C_L studied in bicelles varies from below 1% to 35% (w/v).[34,42] Dynamic light scattering and cryo-

transmission electron microscopy were used to measure the size and shape of the DMPC/DHPC bicelle mixtures with C_L of 4%, 8%, and 16% (w/v) at q = 0.5 and 1.[43] In summary, low-q (0.5), low C_L bicelles (4% w/v) are smaller, 29 Å micelle-like particles in which the DMPC and DHPC are more mixed. Bicelles with a C_L of 8% and 16% are slightly larger at 32 Å. An increase in temperature resulted in an enlargement of the low-q 8% and 16% bicelles, but did not have any effect on the 4% bicelles. This same set of experiments was repeated with q = 1 bicelle mixtures with similar results. The 4% bicelles remained smaller and unchanged while the 8% C_L bicelles increased in size by 23 Å and the 16% increased by 14 Å. This led to the conclusion that detergent rich, low C_L bicelles are smaller, temperature-independent particles and less stable, larger bicelles are formed with higher C_L.[43]

These experiments demonstrated the effect of temperature and composition on the phase separation of bicelles. DMPC lipids are in an ordered gel phase below 23°C with the hydrocarbon chains closely packed while at higher temperatures the hydrocarbons are fluid and loosely packed in the liquid crystalline phase. The 8% and 16% C_L samples show temperature dependence, which indicates a bilayered structure of the DMPC within the bicelle interior that can undergo the typical DMPC lipid phase changes at low and high temperatures.[36] The 4% C_L bicelles were unaffected by temperature, suggesting that there was a higher degree of mixing between the DMPC and DHPC, preventing the gel phase at low temperatures.[36] These observations support the notion that bicelles with low C_L are closer to mixed micelles than the "ideal" bicelle that contains the separate lipid and detergent components. These results emphasize the importance of choosing the appropriate lipid and detergent mixtures when designing a suitable membrane mimic.

Currently, there are few methods that can resolve the composition and structural components of bicelles. Small-angle scattering can give structural information on these low-q bicelles, and specifically, small angle neutron scattering (SANS) can resolve the internal composition of these mimics. Molecular simulations can also generate actual low-q bicelle structures. Chapter 5 will discuss small angle scattering and MD simulations and the bicelle structural information learned from using these techniques.

2.4. References

1. Tanford, C. 1991. The hydrophobic effect: formation of micelles and biological membranes. Krieger Publishing Company, Malabar, FL.

2. Jones, M. and D. Chapman. 1995. Micelles, monolayers, and biomembranes. Wiley-Liss, Inc., New York, NY.

3. Cohn, E. and J. Edsall. 1943. Proteins, amino acids, and peptides. Reinhold: New York, New York.

4. Le Maire, M., P. Champeil, and J. Moller. 2000. Interaction of membrane proteins and lipids with solubilizing detergents. Biochim Biophys Acta 1508: 86-111.

5. Imamura, T. 2006. Encyclopedia of surface and colloid science. Taylor and Francis: New York, NY.

6. Tschesche, H. 2012. Methods in protein biochemistry. Walter de Gruyter, Berlin, Germany.

7. Oliver, R., J. Lipfert, D. Fox, R. Lo, S. Doniach, and L. Columbus. 2013. Dependence of micelle size and shape on detergent alkyl chain length and head group. PLoS ONE 8: e62488.

8. Isrealachvili, J. 1998. Intermolecular and surface forces. 2nd ed. Harcourt Brace and Company: New York, NY.

9. Iyer, J. and D. Blankschtein. 2012. Are ellipsoids feasible micelle shapes? An answer based on a molecular-thermodynamic model of nonionic surfactant micelles. J Phys Chem B 116: 6443-6454.

10. Dupuy, C., X. Auvray, C. Petipas, R. Anthore, F. Costes, et al. 1996. Small angle X-ray and neutron scattering study of the micellization of (N-alkylamino)-1-deoxylactitols in water. Langmuir 12: 3162-3172.

11. Luckey, M. 2008. Membrane protein structural biology with biochemical and biophysical foundations. Cambridge University Press, New York, NY.

12. Lichtenberg, D., H. Ahyayauch, F. Goni. 2013. The mechanism of detergent solubilization of lipid bilayers. Biophys J 105: 289-299.

13. Scopes, R. 2001. Strategies for protein purification. Curr Protoc Protein Sci Unit 1.2.

14. Lin, S. and G. Guidotti. 2009. Chapter 35 purification of membrane proteins. Methods Enzymol 463: 619-629.

15. Clint, J. 1975. Micellization of mixed nonionic surface agents. J Chem Soc Faraday Trans 71: 1327-1334.

16. Shinoda, K., T. Nakagawa, B. Tamamushi, T. Isemura. 1963. Colloidal surfactants: some physicochemical properties. Academic Press, New York, NY.

17. Oliver, R., J. Lipfert, D. Fox, R. Lo, J. Kim, S. Doniach, L. Columbus. 2014. Tuning micelle dimensions and properties with binary surfactant mixtures. Langmiur 30: 13353-13361.

18. Macdonald, R., Q. Saleem, A. Lai, and H. Morales. 2013. NMR methods for measuring lateral diffusion in membranes. Chem Phys Lipids 166: 31-44.

19. Durr, U., R. Soong, and A. Ramamoorthy. 2013. When detergent meets bilayer: birth and coming of age of lipid bicelles. Prog Nucl Magn Reson Spectrosc 69: 1-22.

20. Chou, J., J. Kaufman, S. Stahl, P. Wingfield, and A. Bax. 2002. Micelle-induced curvature in a water-insoluble HIV-1 env peptide revealed by NMR decoupling measurement in stretched polyacrylamide gel. J Am Chem Soc Comm 124: 2450-2451.

21. Sanders, C., and G. Landis. 1995. Reconstitution of membrane proteins into lipid-rich bilayered mixed micelles for NMR studies. Biochem 34: 4030-4040.

22. Dutta, S., E. Morrison, and K. Henzler-Wildman. 2014. EmrE dimerization depends on membrane environment. Biochim Biophys Acta 1838: 1817-1822.

23. Sanders, C. and J. Prestegard. 1990. Magnetically orientable phospholipid bilayers containing small amounts of a bile salt, CHAPSO. Biophys J 58: 447-460.

24. Sanders, C. and R. Schwonek. Characterization of magnetically orientable bilayers in mixtures of dihexanoylphosphocholine and dimyristoylphosphocholine by solid-state NMR. Biochem 31: 8898-8905.

25. Sanders, C., B. Hare, K. Howard, J. Prestegard. 1994. Magnetically oriented phospholipid micelles as a tool for the study of membrane associated molecules. Prog Nucl Magn Reson Spectrosc 26:421-444.

26. Gaemers, S. and A. Bax. 2001. Morphology of three lyotropic liquid crystalline biological NMR media studied by translational diffusion anisotropy. J Am Chem Soc 123: 12343-12352.

27. Vold, R., R. Prosser, and A. Deese. 1997. Isotropic solutions of phospholipid bicelles: a new membrane mimetic for high-resolution NMR studies of polypeptides. J Biomol NMR 9: 329-335.

28. Kamienska, K., C. Jameson, and W. Schilf. 2013. Nuclear magnetic resonance. Royal Society of Chemistry, London, United Kingdom.

29. Glover, K., J. Whiles, G. Wu, N. Yu, R. Deems, J. Struppe, R. Stark, E. Komives, and R. Vold. 2001. Structural evaluation of phospholipid bicelles for solution-state studies of membrane associated biomolecules. Biophys J 81: 2163-2171.

30. Luchette, P., T. Vetman, R. Prosser, R. Hancock, M. Nieh, C. Glinka, S. Krueger, and J. Katsaras. 2001. Morphology of fast-tumbling bicelles: a small angle neutron scattering and NMR study. Biochim Biophys Acta 1513: 83-94.

31. Struppe, J., J. Whiles, and A. Vold. 2000. Acidic phospholipid bicelles: a versatile model membrane system. Biophys J 78: 281-289.

32. Cho, H., J. Dominick, and M. Spence. 2010. Lipid domains in bicelles containing unsaturated lipids and cholesterol. J Phys Chem B 114: 9238-9245.

33. Lind, J., J. Nordin, and L. Maler. 2008. Lipid dynamics in fast-tumbling bicelles with varying lipid bilayer thickness: effect of model transmembrane peptides. Biochim Biophys Acta 1778: 2526-2534.

34. McKibbin, C., N. Farmer, P. Edwards, C. Villa, and P. Booth. 2009. Urea unfolding of opsin in phospholipid bilayers. Photochem Photobiol 85: 494-500.

35. Lu, Z., W. Van Horn, J. Chen, S. Mathew, R. Zent, and C. Sanders. 2012. Bicelles at low concentrations. Mol Pharm 9: 752-761.

36. Kerman, A. and V. Ananthanarayanan. 2007. Conformation of a double-membrane-spanning fragment of a G protein-coupled receptor: effects of hydrophobic environment and pH. Biochim Biophys Acta 1768: 1199-1210.

37. Killian, J. 1998. Hydrophobic mismatch between proteins and lipids in membranes. Biochim Biophys Acta 1376: 401-416.

38. Foo, A., B. Harvey, J. Metz, N. Goto. 2015. Influence of hydrophobic mismatch on the catalytic activity of *Escherichia coli* GlpG rhomboid protease. Protein Sci 24: 464-473.

39. Ahn, V., E. Lo, C. Engel, L. Chen, P. Hwang, and L. Kay. 2004. A hydrocarbon ruler measures palmitate in the enzymatic acylation of endotoxin. EMBO J 23: 2931-2941.

40. Prosser, R., J. Hwang, and R. Vold. 1998. Magnetically aligned phospholipid bilayers with positive ordering: a new model membrane system. Biophys J 74: 2405-2418.

41. Triba, M., D. Warschawski, and P. Devaux. 2005. Reinvestigation by phosphorus NMR of lipid distribution in bicelles. Biophys J 88: 1887-1901.

42. Katsaras, J. and T. Gutberlet. 2013. Lipid bilayers: structure and interactions. Springer Science and Business Media, Berlin, Germany.

43. Ye, W., L. Jesper, J. Eriksson, and L. Maler. 2014. Characterization of the morphology of fast-tumbling bicelles with varying composition. Langmuir 30: 5488-5496.

Chapter 3: The influence of detergents on the function of β-barrel enzymes

The bilayer mimic selected for membrane protein characterization effect the fold and function of the protein. Typically, initial detergent selection is based on the overall project goal. For this study, the size of the protein's transmembrane domain (TMD) as well as the detergent head group charge and size are often considered. Choosing a detergent with short alkyl tails may result in micelles that are smaller than the TMD, and likewise, selecting a detergent with longer alkyl tails may yield micelles that engulf the entire protein. Prevention of the protein aggregation that results from this hydrophobic mismatch is an initial aim for membrane protein researchers. Also, the head group charge and size will be regarded, especially if the active site residues of the protein are positioned in the head group region. These considerations are a starting point for membrane protein investigations; however, detergent selection continues to be an arduous trial-and-error process. The research in this chapter focuses on monitoring the influence of different detergents on the activity of membrane proteins. This systematic variation of detergents will emphasize key detergent properties that are essential in maintaining active membrane proteins. This chapter will focus on the function of outer membrane phospholipase A (OMPLA) in varying detergents, along with preliminary data from other membrane proteins.

3.1. Protein-detergent complex formation with OMPLA

As discussed in Chapter 2, successfully obtaining a protein-detergent complex (PDC) to characterize is a multi-step process. OMPLA was recombinantly expressed into insoluble, inactive, and unfolded protein aggregates called inclusion bodies. These inclusion bodies were isolated by lysing the cells with a high pressure homogenizer and

removing the cell debris via centrifugation. The inclusion bodies were washed several times with buffer to remove contaminants. The unfolded aggregate was resuspended in a denaturing buffer containing urea to prepare the protein for refolding.

Refolding the protein is required to obtain potentially functional and folded protein for biophysical characterization. The conditions for refolding are protein specific, and require detergent to prevent aggregation. The OMPLA refolding procedures were adapted from Burgess et. al. and optimized by varying the refolding detergent and incubation temperatures.[1] OMPLA was confirmed to refold best in pH 10 borate and decyl maltoside (DM) detergent buffer at 50°C overnight (Figure 3.1).

Successful refolding does not confirm that the protein is functional. Often, the refolding detergent is not the optimal detergent to maintain protein stability for long-term characterization. Thus, the detergent is exchanged for another, typically, via chromatography. OMPLA detergent exchange occurs by adding the refolded protein to an ion exchange column with DEAE resin. The protein is immobilized in the resin and is washed with buffer containing excess amounts of the new detergent, exchanging the detergents via dilution. OMPLA is eluted in the new PDC with high potassium chloride concentration and dialyzed to remove the high salt concentration (Figure 3.2). Generally, the next step is to study the protein with several different biophysical techniques. However, to study the influence of detergents on the activity of OMPLA, this process of recombinant expression, inclusion body isolation, refolding, and detergent exchange is repeated several times, exchanging the DM-refolded OMPLA into over 20 detergents (Figure 3.3).

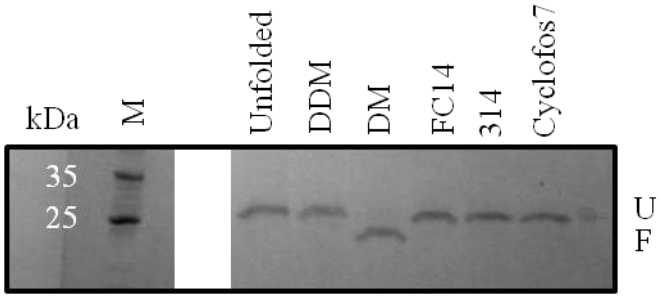

Figure 3.1. OMPLA refolding optimization in several detergents. SDS-PAGE was used to confirm OMPLA refolding in several detergents. Several lanes from samples of other proteins were removed from the gel to focus on the refolded OMPLA samples. The molecular weight marker is labeled M. Unfolded, boiled OMPLA was used for sample comparison. OMPLA was refolded overnight in pH 10 borate buffer at 50°C in dodecyl maltoside (DDM), decyl maltoside (DM), tetradecylphosphocholine (FC14), Anzergent 314 (314), Cyclofos-7, and dodecylphosphocholine (FC12) (not pictured) detergents. Folded OMPLA runs at a smaller molecular weight than unfolded OMPLA (31 kDa). DM successfully refolded OMPLA.

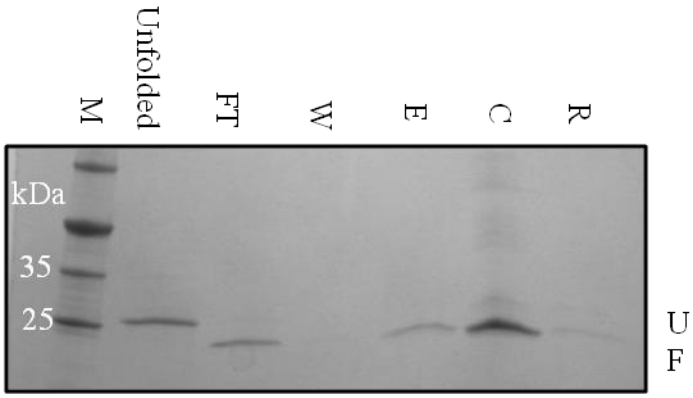

Figure 3.2. OMPLA purification and detergent exchange fractions. Refolded OMPLA was immobilized on an ion exchange column for detergent exchange into FC12 micelles. Fractions from the detergent exchange were analyzed with SDS-PAGE. The lanes of the gel correspond to unfolded, boiled OMPLA, flowthrough (FT), wash (W), elution (E), concentrated eluted protein (C), and resin (R). Folded FC12 OMPLA PDCs are confirmed in lanes 4 and 5.

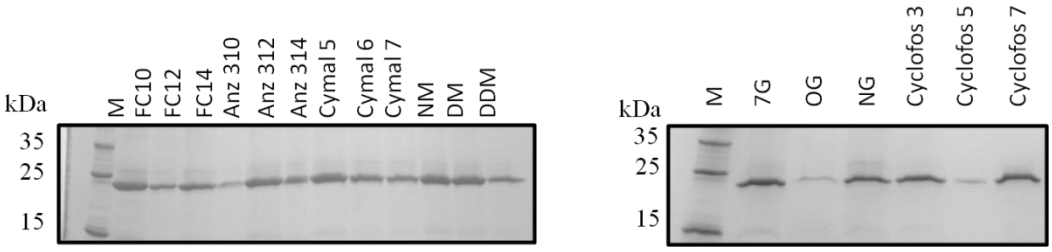

Figure 3.3. OMPLA purified in several detergents. SDS-PAGE was used to confirm the successful purification of OMPLA in 19 detergents (FC16 not pictured). Folded OMPLA runs slightly smaller than its molecular weight of 31 kDa. Anzergent 310, OG, and Cyclofos OMPLA have lower protein concentrations than the other OMPLA PDCs. With each detergent exchange conducted with the same amount of refolded OMPLA, the lower protein concentrations after purification may indicate that OMPLA forms less stable complexes in these detergents.

OMPLA exchanged into 310, OG, and Cyclofos 5 detergents were less concentrated than the other PDCs. Each detergent exchange was conducted with the same amount of refolded OMPLA; therefore, the lower protein concentrations after purification for these three PDCs may indicate that OMPLA forms less stable complexes in these detergents. After confirming OMPLA folding with SDS-PAGE, there are several other considerations that must be addressed before monitoring OMPLA activity: 1) confirmation of complete detergent exchange, 2) determination of the detergent and micelle concentration, and 3) identifying the oligomeric state of the OMPLA.

3.2. Pre-assay biophysical characterization of OMPLA

3.2.1. Detergent exchange verification and concentration determination with NMR

Monitoring detergent exchange and the micelle-to-protein ratio after membrane protein purification ensures consistent sample preparation and activity assay design. An effective technique to use for these two tasks is nuclear magnetic resonance (NMR) spectroscopy. 1-D ^{1}H NMR is often used as a first step in chemical structure determination.

NMR spectra of a detergent in a PDC before and after detergent exchange are very different depending on the detergents involved, and comparing the two can confirm the success of a detergent exchange. For example, NMR spectra for glucoside detergents have broad chemical shift peaks group between 3 and 4 ppm indicative of the hydroxyl protons on the head group. A spectrum of the phosphocholine detergents has a sharp peak at 3.2 ppm, corresponding to the hydrogens on the choline of the head group (Figure 3.4). The considerable differences between the two PDC spectra allow detergent exchange

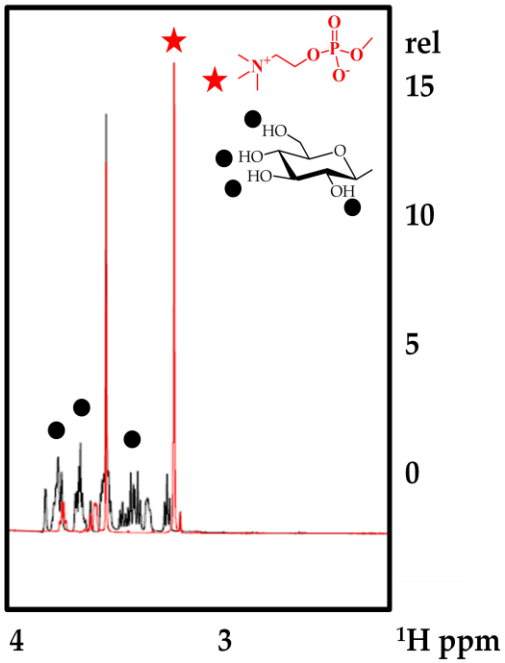

Figure 3.4. 1-D ^{1}H NMR spectra of OMPLA before and after detergent exchange. OMPLA in OG detergent (black) was exchanged with FC12 detergent (red). Proton NMR confirms successful detergent exchange. Peaks between 3 to 4 ppm indicative of the OG head group (dots) are no longer present after the detergent exchange. A sharp peak at 3.2 ppm is newly present (star), indicative of the hydrogens on the phosphocholine head group. The integral of a peak at 1.2 ppm (not shown) corresponding to methylene group on the detergent carbon tails is used for detergent concentration determination.

confirmation using NMR. ^{1}H NMR investigations of OMPLA in several steps of the purification and detergent exchange was conducted, and these spectra confirm an efficient and complete detergent exchange protocol.

The micelle-to-protein ratio is important when completing membrane protein activity assays. As described in Chapter 2, the detergent can significantly impact protein function and substrate performance. Maintaining a low (10:1 to 1:1) micelle-to-protein ratio can minimize the amount of free micelle able to impact activity assays. Also, knowing the micelle, and therefore, detergent, concentration, is important when designing activity assays with proper negative controls. 1-D ^{1}H NMR spectra enable the determination of detergent concentration. A chemical shift at 1.2 ppm is representative of the methylene tail of the detergent. Detergent concentrations are measured by comparing the methylene peak of the PDC with standard samples of known detergent concentrations. The micelle concentration is calculated from the detergent concentration with the following formula:

$$[Micelle] = \frac{[Detergent] - CMC}{Aggregation\ \#}$$

3.2.2. Determination of the OMPLA oligomerization state

An effective technique for the determination of a protein's oligomeric state is size exclusion chromatography coupled to multi angle light scattering (SECMALS). Typical column chromatography of membrane proteins is challenged by the hydrophobic nature of these proteins. Membrane proteins tend to interact with the mobile and stationary phases differently than soluble proteins, eluting at retention times that do not reflect the actual molecular weight of the protein. With SECMALS, the molecular weight of the protein is not dependent upon retention time, but light scattering, enabling a more

accurate molecular mass measurement for membrane proteins. In addition, MALS detects the detergent micelles, which can allow the determination of the size of the protein-detergent complexes.[2]

The SEC component of this technique is solely responsible for fractionating the solution into distinct peaks that can be analyzed with the detectors. Three detectors measure the protein absorbance at 280 nm (UV), the refractive index (RI), and the light scattering (LS). The UV and RI detectors provide information about the concentration of the protein while the LS detector measures the light scattering and provides a weight-average molar mass of the species. LS is proportional to the molecular mass (M_W) and the protein concentration with the following equation:[2]

$$\Delta LS = \left(\frac{I_\theta}{I_0}\right)_{solution} - \left(\frac{I_\theta}{I_0}\right)_{buffer} = K\left(\frac{dn}{dc}\right)^2 M_W C$$

where I_θ/I_0 is the ratio of the intensities of the light scattered at angle θ and the incident light.[2] ΔLS is the difference in light scattered from the protein complex and the surrounding buffer.[2] K is a constant derived from the refractive index of buffer without protein (n), the wavelength of light used (λ_0), the angle between the incident and scattered light (θ), the distance between the scattering molecule and detector (r), and Avogadro's number:[2]

$$K = \frac{2\pi^2 n^2}{\lambda_0^4 N_A}\left(\frac{1 + cos^2\theta}{r^2}\right)$$

C is the protein concentration. dn/dc is the specific refractive index of the protein, which is typically 0.187 ml/g for soluble proteins, but is unknown for membrane proteins in a PDC complex.[2] The dn/dc for membrane proteins can be determined with the following formula,

$$\left(\frac{dn}{dc}\right) = \left(\frac{dn}{dc}\right)_{protein} + \delta\left(\frac{dn}{dc}\right)_{detergent}$$

enabling an accurate calculation of the PDC molecular weight.[2] Unfortunately, the amount of detergent bound to the protein (δ) is unknown, and without knowing dn/dc of the protein, the ΔLS, and subsequently, the molecular mass of the PDC is unsolvable.[2] These difficulties in determining the PDC molecular weight is another example of the challenges with characterizing membrane proteins. To determine the dn/dc of a membrane protein, the refractive index of the protein must be measured at 690 nm wavelength at different protein concentrations in experimental buffer conditions.[3]

The OMPLA oligomerization state is of interest because the protein forms reversible dimers when active. Confirmation of the OMPLA homodimer in different detergents will give implications on the protein's activity. Currently, SECMALS has been completed with OMPLA in 7 detergents: Anzergent 312, Anzergent 314, FC12, FC14, FC16, DM, and DDM (Table 3.1). The expected 62 kDa OMPLA dimer is confirmed in Anzergent 312, FC12, and FC16 while molecular weight values for Anzergent 314, DM, and DDM OMPLA are slightly larger and FC14 OMPLA is slightly smaller. The small increase in the molecular weights of the dimer is likely due to aggregation. The SECMALS light scattering detector is highly sensitive (1 μg/mL BSA), and minimal aggregate can have a major effect on the overall molecular weight of the protein. The smaller molecular weight for FC14 OMPLA could be a result of a less stable PDC that was partially dissociated by the SEC. Figure 3.5 depicts a SECMALS chromatogram with DDM OMPLA. Although the peak is narrow and well-defined, the aggregate had a minor effect on the molecular weight measured.

	Protein Size (kDa)	Micelle size (kDa)	Micelle N	Aggregation?	Monomer?
312	60	19	58	No	No
314	77	---	---	Yes	No
FC12	69 ± 1	26 ± 0.4	75	No	No
FC14	46	---	---	Yes	No
FC16	56 ± 9	---	---	Yes	Yes
DM	92 ± 3	55 ± 15	76 – 135	No	No
DDM	106 ± 0.3	53 ± 0.4	103	No	No

Table 3.1. Molecular weights and aggregation numbers from SECMALS of OMPLA PDCs. SECMALS was conducted on 7 OMPLA PDCs. The OMPLA dimer (62 kDa) is confirmed in all of the samples, with DM and DDM PDCs eluting slightly larger and FC14 PDCs measuring slightly smaller. Large 200 kDa aggregates eluted with the 314, FC14, and FC16 samples. One FC16 sample eluted an OMPLA monomer peak (Figure 3.5). SECMALS also confirmed micelles with the expected size and aggregation number in the PDCs without the aggregates. The 312, 314, and FC14 PDCs were analyzed twice, while the other samples were examined in triplicate. These samples will be repeated for error determination and completed for all PDCs.

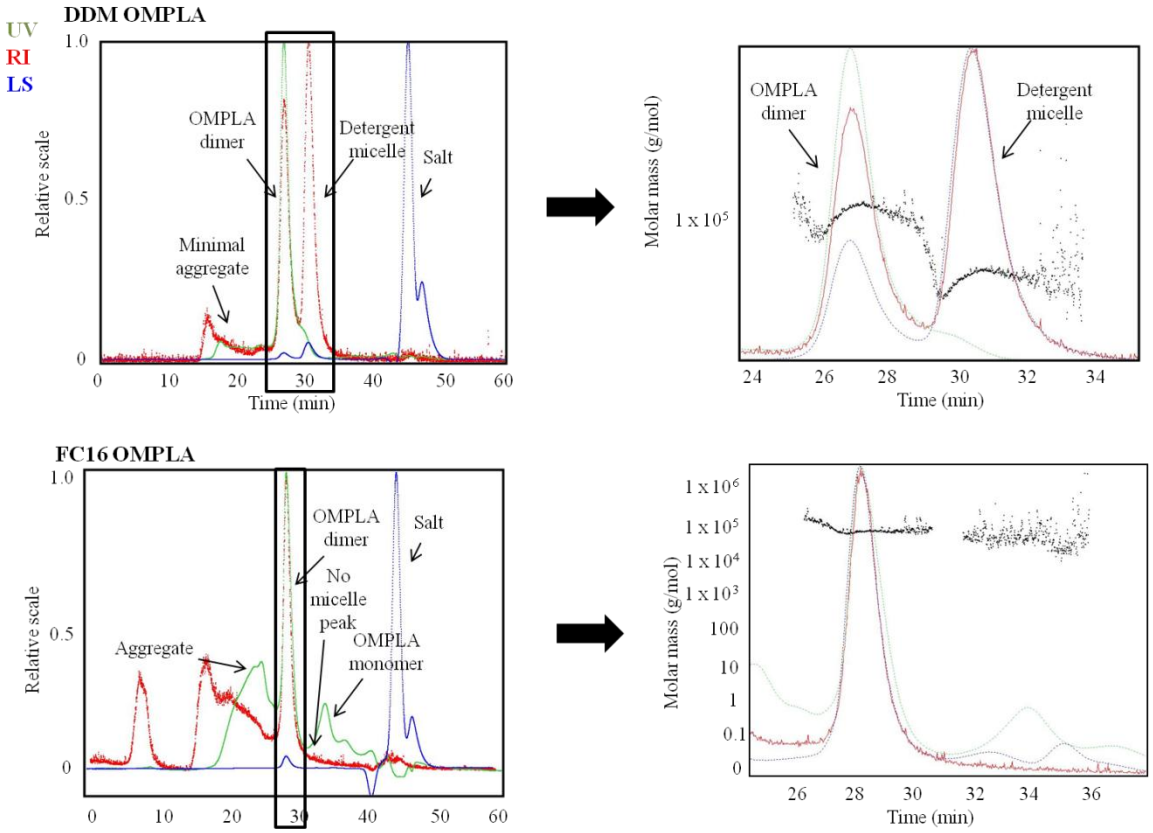

Figure 3.5. SECMALS chromatograms with DDM and FC16 OMPLA. SECMALS conducted on DDM OMPLA eluted well defined peaks for the OMPLA dimer and detergent micelle. Minimal aggregate was observed. The FC16 OMPLA SECMALS depict a large aggregate along with the OMPLA dimer and a monomer peak. A micelle peak is not observed.

The FC14, FC16, and Anzergent 314 OMPLA samples have large amounts of an approximately 200 kDa aggregate that elutes earlier in the SECMALS (Figure 3.5). These larger aggregates are potentially an effect of solubilizing OMPLA in larger micelles. FC14, FC16, and Anzergent 314 have the longest carbon tails of the detergents characterized, and thus, they form the largest micelles sampled. These large micelles have the capacity to accommodate more protein and may promote aggregation.

The FC16 OMPLA SECMALS experiments were conducted in triplicate; three separately purified OMPLA PDCs were analyzed with this method. Of the three experiments, one FC16 OMPLA sample had aggregate, dimer, and monomer present (Figure 3.5). This was the only PDC to contain OMPLA monomer present, and this may impact protein activity.

The SECMALS experiments confirm that the OMPLA PDCs are forming dimers without substrate or calcium present. OMPLA dimerization without these effector molecules has not been well-characterized in the literature. Cross-linking and equilibrium analytical ultracentrifugation experiments demonstrate that OMPLA is monomeric until the addition of substrate or calcium in dodecyl-*N*,*N*-dimethyl-1-ammonio-3-propanesulfonate (12-SB) detergent.[4,5] Only minor evidence has depicted OMPLA dimerization without the presence of calcium or substrate; glutaraldehyde cross-linking experiments conducted by Kingma et. al. depict 40% OMPLA dimer, and 60% monomer in the presence of EDTA in FC16 detergent.[6] The SECMALS confirmation of OMPLA dimers in the PDCs could be a result of detergents interacting with the OMPLA active site, triggering dimerization. This is reasonable because the detergents have similar characteristics to the phospholipid OMPLA substrate (Figure 2.2).

The empty detergent micelle size and aggregation number was also determined with SECMALS. Contrary to the UV detector at 280 nm, the light scattering instrument can monitor the detergent micelles during elution. Eluting just after the protein, the detergent micelle peaks for Anzergent 312, FC12, and DDM were at the molecular weights expected, 19, 26, and 53 kDa, respectively. The DM micelles had a molecular weight of approximately 55 kDa, slightly larger than the 43 kDa predicted. With the expected molecular weights, the aggregation numbers of these micelles were also at the projected values. The PDCs that formed large aggregates, FC14, FC16, and Anzergent 314, did not elute peaks for the detergent micelles. This is likely due to the detergents associating with the aggregates, minimizing the amount of empty micelles present for late elution. With OMPLA PDCs confirmed with two techniques, the activity of this enzyme was assayed in different micelle environments.

3.3 OMPLA activity assay design

The OMPLA activity assay monitors the calcium-dependent hydrolysis of the OMPLA substrate, 2-hexadecanoylthio-1-ethylphosphorylcholine (HEPC) (Figure 3.6).[7] After hydrolysis of HEPC via OMPLA cleavage, the free sulfur anion on HEPC interacts with another buffer component, 5,5'-dithio-bis-[2-nitrobenzoic acid] (Ellman's reagent). Ellman's reagent targets the conjugate base, cleaving itself to form a disulfide bond with the substrate.[6] This bond formation yields a stable mixed disulfide and a colored species, 2-nitro-5-thiobenzoic acid (TNB^{2-}). The increase in color change from TNB reflects OMPLA hydrolysis activity and is measured spectrophotometrically.[7]

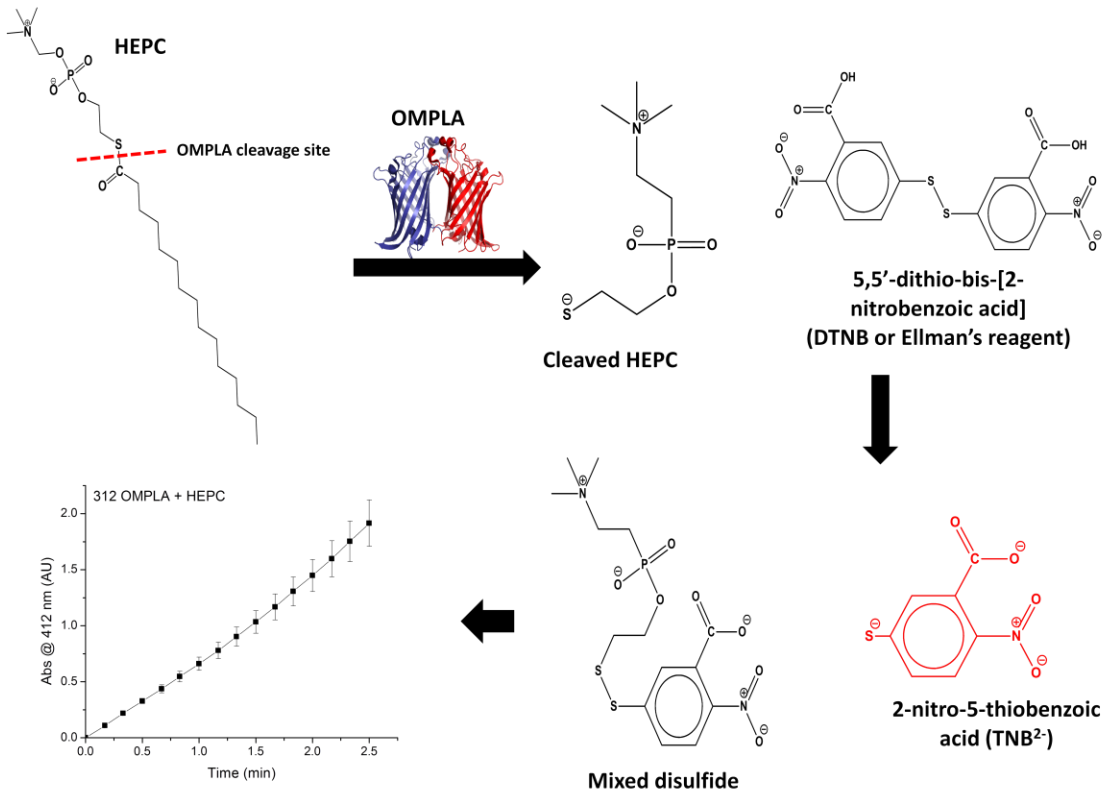

Figure 3.6. Workflow of the OMPLA activity assay. The OMPLA substrate, HEPC, is cleaved by OMPLA, yielding a free sulfur anion. Ellman's reagent targets the anion to form a mixed disulfide with the remaining HEPC molecule. This bond formation results in a colored moiety, TNB^{2-}. The increase in yellow color from TNB^{2-} production reflects OMPLA hydrolysis activity and is measured spectrophotometrically over time.

A major consideration for this assay is the HEPC substrate. This substrate is a phosphatidylcholine analog with a phosphocholine head group and 16-carbon tail. This molecule is similar to those used in the OMPLA PDCs, especially the phosphocholine detergents. With those similarities, the HEPC could likely partition into empty detergent micelles without OMPLA, not interacting with OMPLA dimer active site. Maintaining a low micelle-to-protein ratio minimizes the chances of this occurring; however, this is more challenging with detergents that have high CMCs. Substrate-micelle interactions is a problem often encountered with membrane protein research and functional assays, and is circumvented with proper controls (reaction mixture + detergent at the appropriate concentration without OMPLA + substrate) and assay design.

The assay color change is measured at 412 nm every 10 seconds for 2.5 minutes, and absorbance vs. time is plotted (Figure 3.6). The initial rate of the reaction was determined using the slope of the line between 0 and 1.5 minutes. The rate of product formation is determined using these initial rates and the molar extinction coefficient of the TNB^{2-} product. By plotting the reaction rate vs. substrate concentration, the curves were fit using the Michalis-Menten equation:

$$\nu = \frac{V_{max}[S]}{K_M + [S]}$$

where ν is the reaction rate, V_{max} is the maximum rate of reaction, [S] is the substrate concentration, and K_M is the substrate specificity (Figure 3.7). The Michaelis constant, K_M, is the substrate concentration at which the reaction is at half-maximum, and is an inverse measurement of the substrate's affinity for the enzyme. $V_{max} = k_{cat}[E]_0$, where

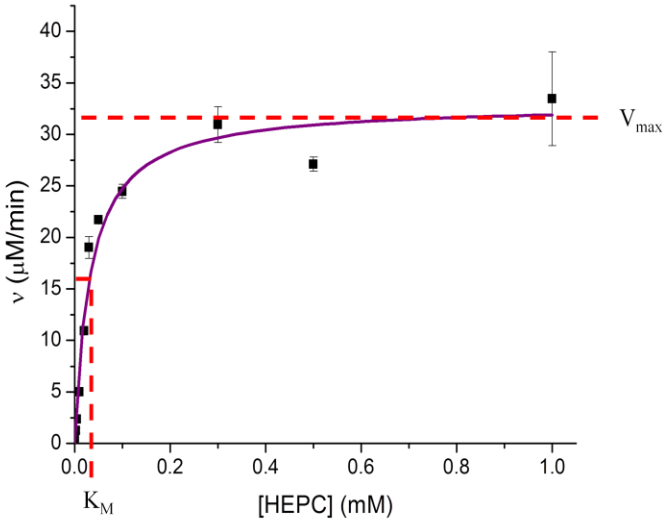

Figure 3.7. Example of Michaelis-Menten for OMPLA. OMPLA function was assayed in OG at different substrate concentrations. The initial reaction rates vs. substrate concentration were graphed and fit Michaelis-Menten kinetics curves. The maximum reaction rate (V_{max}) and substrate specificity (K_M) were determined from these plots; these values were used to determine the substrate turnover rate (k_{cat}) and enzyme efficiency (k_{cat}/K_M).

$[E]_0$ is the initial enzyme concentration. k_{cat} is the substrate turnover rate, the maximum number of substrate molecules converted to product per enzyme molecule per second. The catalytic efficiency, k_{cat}/K_M, is a measurement of enzyme efficiency and how well the enzyme converts substrate into a product.

There are a few assumptions made for Michaelis-Menten kinetics.[8] First, the enzyme-substrate (ES) complex is a steady state intermediate—that is, the concentration of ES remains relatively constant because the complex is being broken down and produced at the same rate.[8] Second, there is no product at the start of the reaction and the product cannot be converted to substrate.[8] Third, the [S] represents the free substrate concentration, but is assumed to be close to the total substrate concentration.[8] This is valid as long as [E] << [S]. Fourth, the binding and unbinding of substrate to enzyme is much faster than the release of product.[8] The Michaelis-Menten kinetic parameters, K_M, V_{max}, k_{cat}, and k_{cat}/K_M, were reported for OMPLA activity in different PDCs.

The substrate turnover rate, k_{cat}, is derived from the initial enzyme concentration and the maximum reaction rate (V_{max}). OMPLA k_{cat} values represent the speed in which OMPLA hydrolyzes HEPC when the system is saturated with enzyme. Trends identified for OMPLA substrate turnover rates reflect the protein's overall catalytic function. The Michaelis constant, K_M, is a measurement of the affinity of the substrate for the enzyme. OMPLA K_M values represent how well the substrate binds to the enzyme. Trends with OMPLA substrate affinity indicates how well the substrate interacts with the protein in certain detergent conditions and also highlights any possible competitive inhibition from detergents interacting with the OMPLA binding site. k_{cat} and K_M affect one another, and when used together, the k_{cat}/K_M reflects both the OMPLA binding and catalytic events;

however, when distinguishing trends with OMPLA activity in detergents, it is more practical to analyze the values separately.

3.4 Structural considerations for OMPLA activity

OMPLA activity in different PDCs will vary depending on how the detergent micelle impacts the structure of the protein and its active site. For a complete commentary on OMPLA function in varying environments, structural features important in protein function should be highlighted and monitored. Perturbations to these components can impact both substrate turnover rate and specificity. Examination of the OMPLA atomic resolution structure elucidates two important structural components for protein function.

First, OMPLA has an approximate 29 Å tall hydrophobic barrel with the active site residues located 4 Å from the top of the barrel (Figure 3.8). Typically buried within the hydrophobic domain of the lipid bilayer, maintaining this hydrophobic environment around the hydrophobic barrel may be essential to protein activity. Second, the OMPLA active site residues extend out 4.8 Å from the barrel, potentially interacting with lipid head groups at the bilayer interface (Figure 3.8). For optimum activity, the placement of the barrel and active site residues in these micelle mimics must be considered. OMPLA will likely have more activity in micelles with hydrophobic cores that can encompass the 29Å long barrel length. Increased protein activity may also be observed with OMPLA in PDCs with thicker head groups that can accommodate the 4.8 Å extension of the active site residues from the barrel.

3.5. OMPLA activity in varying detergents

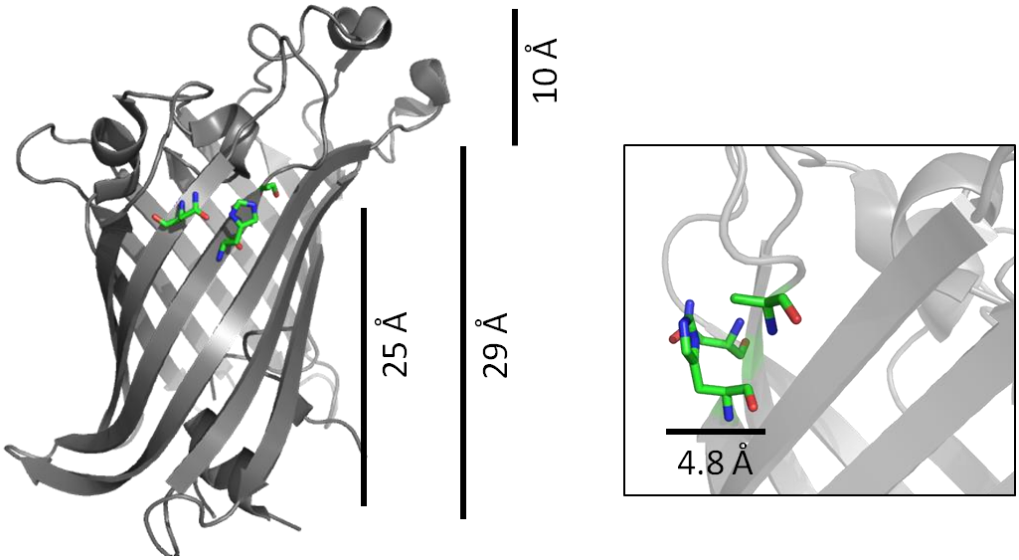

Figure 3.8. Structural considerations for OMPLA activity. The length of the OMPLA barrel is ~29 Å with the active site located 4 Å from the extracellular surface. The extracellular loops of OMPLA extend ~10 Å from the top of the β-barrel. The active site residues extend from the barrel as far as 4.8 Å. Micelles used for solubilization of OMPLA should accommodate this bicelle length and active site location and orientation.

OMPLA functional assays conducted in different PDCs confirm that OMPLA is active in 19 different detergent micelles. The detergents studied were the phosphocholine detergents (FC10, FC12, FC14, and FC16), the Anzergents (310, 312, and 314), the Cyclofos detergents (CF3, CF5, and CF7), glucosides (7G, OG, and NG), maltosides (NM, DM, and DDM), and the Cymal detergents (C5, C6, and C7). The numbered nomenclature is indicative of the carbon tail length – FC12 detergents have a phosphocholine head and 12-carbon tail, while decyl maltoside (DM) detergents have a maltoside head and 10-carbon tail. Figure 2.2 has structures for all of these detergents.

All of the OMPLA PDCs had similar activity (k_{cat}), substrate affinity (K_M), and enzymatic efficiency (k_{cat}/K_M) (Figures 3.9 and 3.10 and Table 3.2). This confirms that OMPLA is a highly stable, robust enzyme with the ability to dimerize, properly form the catalytic active site, bind substrate, and perform calcium-dependent hydrolysis of HEPC in varying detergent environments. A negative control containing Ellman's reagent, HEPC, and the appropriate detergent was subtracted from each triplicate reaction to remove any contributions from HEPC and detergent without OMPLA.

According to the SECMALS data, the FC14, FC16, and 314 OMPLA PDCs have some aggregated protein as well as the OMPLA dimer. This aggregation can potentially impact the measured k_{cat} and K_M values. The function of these three PDCs could be reduced due to this aggregated protein or overestimated. With a portion of the protein aggregated, the actual concentration of OMPLA dimer, the effective enzyme concentration, is lowered. This lower $[E]_0$ will reduce the actual k_{cat}. The protein aggregation complication can be resolved by collecting only the OMPLA dimer fraction during SECMALS and using that for protein activity assays. Due to this aggregation, the

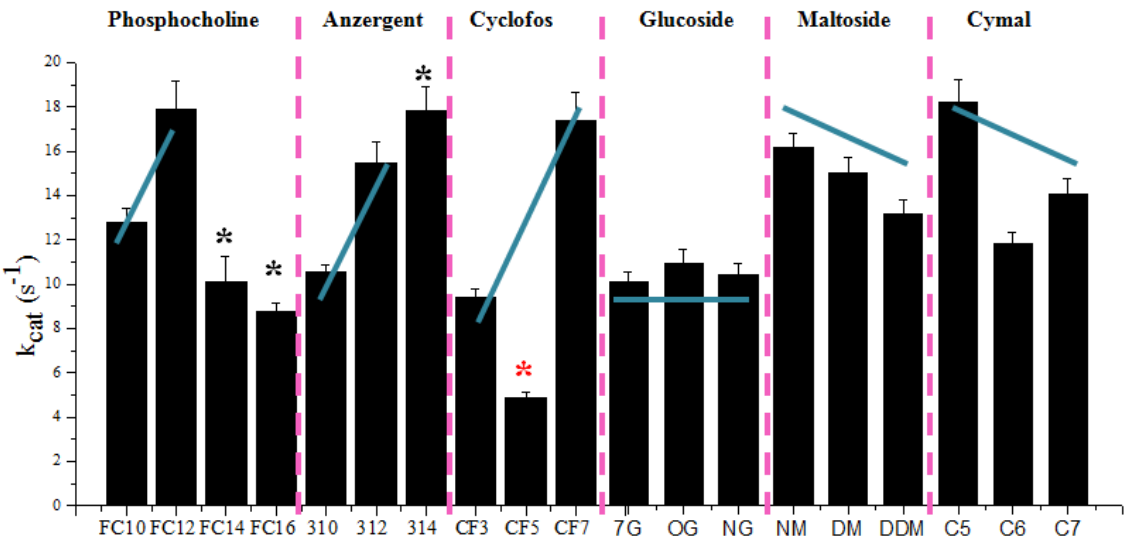

Figure 3.9. Substrate turnover rates (k_{cat}) of OMPLA PDCs. The determined k_{cat} values from the OMPLA kinetic assays are displayed graphically. All of these assays were performed in triplicate, and corrected with a negative control (reaction buffer + $CaCl_2$ + HEPC + detergent, without OMPLA). The results are separated by head group (top). PDCs with aggregation are denoted with black asterisks. Trends were made with the non-aggregated PDCs, and are highlighted with the teal lines. Cyclofos5 OMPLA activity (red asterisk) must be repeated for confirmation of kinetic parameters. Error bars represent standard deviation (n = 3).

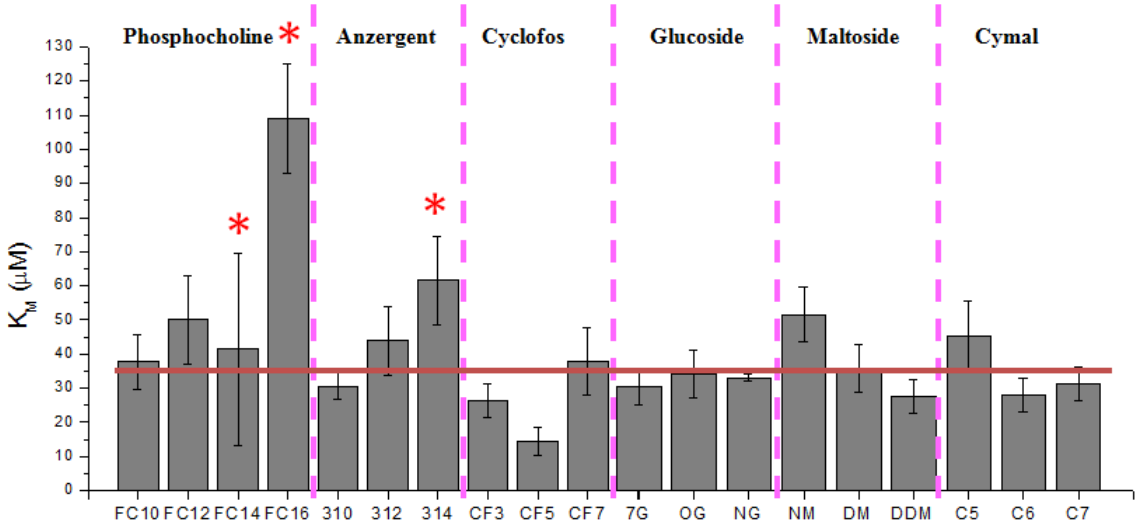

Figure 3.10. Substrate specificities (K_M) of OMPLA PDCs. The determined K_M values from the OMPLA kinetic assays are displayed graphically. All of these assays were performed in triplicate, and corrected with a negative control (reaction buffer + $CaCl_2$ + HEPC + detergent, without OMPLA). The results are separated by head group (top) and head group type (bottom). Trends are highlighted with the teal line. PDCs with aggregation are denoted with an asterisk. Error bars represent standard deviation (n = 3).

	FC10	FC12	FC14	FC16	310	312	314	CF3	CF5	CF7	7G	OG	NG	NM	DM	DDM	Cymal 5	Cymal 6	Cymal 7
[OMPLA] (μM)	21	22	6	8	15	15	19	10	5	16	11	13	22	23	15	7	18	9	8
[Det] (mM)	15	5	8	4	44	14	12	54	8	12	71	23	15	12	3	6	12	5	7
[Micelle] (μM)	127	44	64	25	109	154	117	---	---	---	21	71	154	242	17	50	179	46	48
micelle:OMPLA	6:1	2:1	1:1	3:1	7:1	10:1	6:1	---	---	---	2:01	5:01	7:01	10:1	1:1	7:1	10:1	5:1	6:1
K_M (μM)	38±8	50±13	41±28	109±16	31±4	44±10	62±13	26±5	14±4	38±10	30±5	34±7	33±1	52±8	36±7	28±5	45±10	28±5	31±5
V_{max} (μM/min)	38±2	54±4	30±3	26±1	32±1	46±3	54±3	28±1	15±1	52±4	32±1	34±2	33±1	51±2	47±2	41±2	57±3	37±1	44±2
k_{cat} (s^{-1})	13±1	18±1	10±1	9±0.4	11±0.3	15±1	18±1	9±0.4	5±0.3	17±1	11±1	11±1	11±1	17±1	16±1	14±1	19±1	12±1	15±1
k_{cat}/K_M ($M^{-1}s^{-1}$) * 10^5	3.4	3.6	2.4	0.80	3.4	3.5	2.9	3.6	3.4	4.6	3.5	3.4	3.3	3.3	4.4	5.0	4.2	4.5	4.7

Table 3.2. OMPLA PDC detergent, micelle, and protein concentrations as well as activity kinetic parameters in varying detergents. Aggregation numbers for the Cyclofos detergents have not been determined; therefore the micelle concentrations for these PDCs are unknown.

trends identified with OMPLA k_{cat} and K_M omit contributions from the FC14, FC16, and 314 PDCs.

3.5.1. Effects of detergent micelles on OMPLA substrate turnover rates (k_{cat})

Although OMPLA has similar activity in all of the detergents, modest trends can be identified with the detergent head groups. Removing the contributions from the aggregated samples, the average substrate turnover rate for OMPLA activity was approximately 13 s^{-1}. There are eight PDCs with activity above average: FC12, 312, Cyclofos7, NM, DDM, and Cymal 6. For better understanding of how OMPLA is more active in these PDCs, the micelle hydrophobic thicknesses and head group thicknesses are correlated with the dimensions of the OMPLA barrel and the orientation of the enzymatic active site (Figure 3.11).

The OMPLA PDCs with above average k_{cat} are composed of micelles with larger hydrophobic and shell thicknesses. The hydrophobic thicknesses of the PDCs with higher k_{cat} range from 26 to 34 Å with an average of 31 Å and the head group thicknesses average 4.75 Å. This is compared to the PDCs with lower k_{cat} values that have hydrophobic thicknesses that range from 21 to 30 Å with an average of 26 Å and head group thicknesses that average 3.6 Å. This larger micelle core and shell may better accommodate the 29 Å OMPLA barrel; proteins embedded in smaller micelles may undergo conformational dynamics that can perturb the enzymatic active site.

OMPLA substrate turnover changes with carbon tail length. For the Cymal and maltoside detergents, an increased tail length decreases k_{cat}. Cymal 5 and NM provide the optimum environment necessary for OMPLA function, with the catalytic residues near

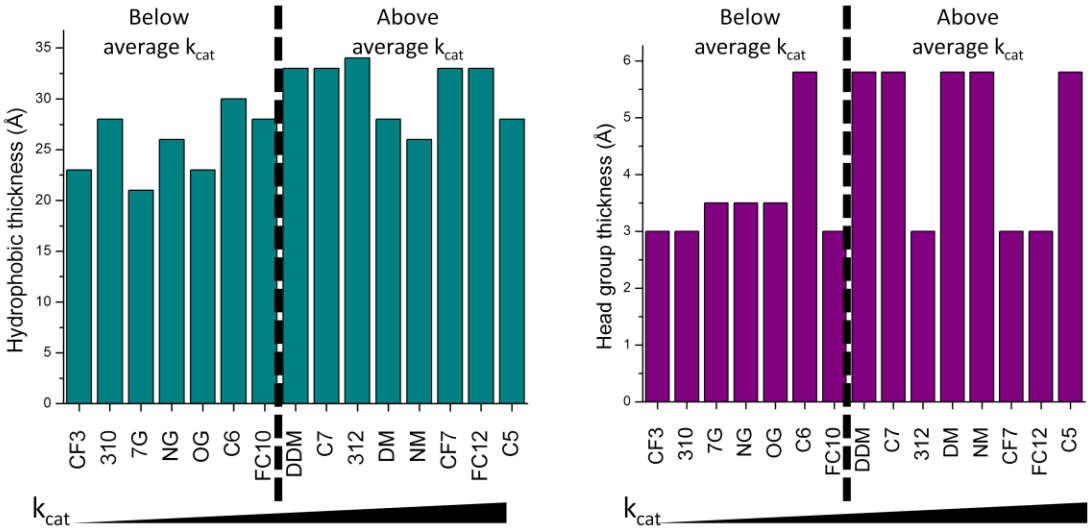

Figure 3.11. Hydrophobic and shell thicknesses of OMPLA PDCs. The hydrophobic thicknesses and shell thicknesses of OMPLA PDCs are organized by increasing substrate turnover rate (bottom). OMPLA with above average substrate turnover rate have thicker hydrophobic cores and head group shells.

the head group interface of the micelle. An increase in the carbon tails results in a burying of the active site residues, decreasing catalytic turnover (Figure 3.12A).

The opposite trend is observed with the phosphocholine, Anzergent, and Cyclofos detergents. Removing the contributions from the aggregated samples and the Cyclofos5 OMPLA outlier, an increase in substrate turnover is observed with detergent tail length. For these PDCs, the micelles have hydrophobic cores smaller than what may be required to accommodate the OMPLA barrel and active site, leading to exposed active site residues and attenuating substrate turnover. (Figure 3.12B).

The substrate turnover rate for the three glucoside detergents are within error of one another. This is attributed to the three micelles having similar structure. With the same glucose head group and a minor increase of 5 Å for 7G to NG micelles, the environment for OMPLA stability and activity remains very similar, resulting in comparable k_{cat} values for all three PDCs.

3.5.2. Effects of detergent micelles on OMPLA substrate affinity (K_M)

OMPLA has similar substrate affinity (K_M) in all of the detergent micelles. Analysis of OMPLA activity in respect to head group highlights modest trends between the detergent and substrate binding. Removing the contributions of the aggregated samples, the average K_M for the OMPLA PDCs is approximately 35 μM. Four of the seven OMPLA complexes with below average substrate affinity (FC10, FC12, 312, and Cyclofos7) are composed of zwitterionic detergents. These zwitterionic detergents have

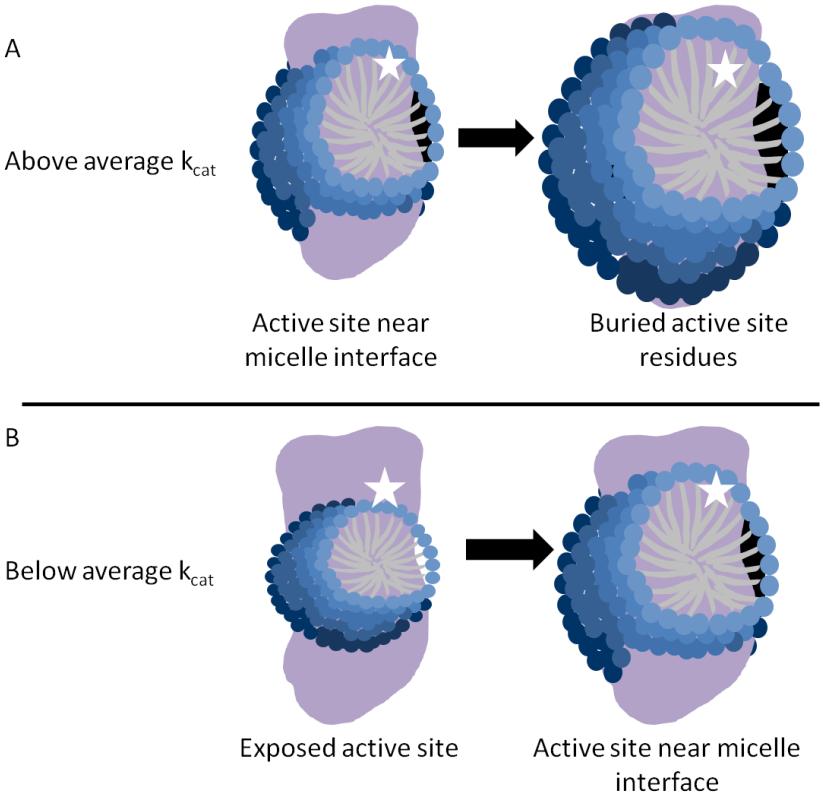

Figure 3.12. Effects of increased detergent carbon tail lengths on the OMPLA active site. Trends were identified with OMPLA substrate turnover and carbon tail length. (A) For the OMPLA with an above average k_{cat}, the Cymals and maltoside detergents, the enzymatic active site was located at the optimum location for Cymal5 and NM PDCs. An increase in carbon tail length results in a burial of the active site, attenuating the substrate turnover rate. (B) For OMPLA with below average k_{cat}, such as the phosphocholine, Anzergent, and Cyclofos detergents, these smaller micelles were enlarged with an increase in detergent carbon tail length, providing a better environment for the OMPLA active site and raising the k_{cat}.

the potential to interact with the OMPLA extracellular surface and catalytic residues. The active site residues, Ser144, His142, and Asn156, are positioned at the extracellular interface between the β-barrel and loops (Figure 1.5). This extracellular surface is highly charged with more negative surface potential than positive (Figure 3.13). It is likely that the zwitterionic head groups on the smaller detergents are associating with portions of the OMPLA extracellular surface and possibly the active site residues, attenuating substrate specificity.

3.5.3. Additional remarks on OMPLA activity

A carbon ring in the nonpolar tail of the detergents does not impact substrate binding and enzyme catalysis. Both Cymal and Cyclofos PDCs have k_{cat} and K_M similar to their corresponding maltosides and phosphocholine micelles. The concentration of free micelle was kept low with a maximum micelle to protein ratio of 10:1, maintaining activity in all detergents, including 7G (CMC = 70 mM) and FC16 (CMC = 0.013 mM). The PDCs with 10:1 micelle to protein ratios (312, NM, and Cymal 5) had reasonable K_M and k_{cat} values in relation to the other PDCs. High micelle concentrations can reduce enzyme activity, as seen with 12-SB detergents; however, this was not a problem for these assays.[2]

The most efficient PDC is DDM OMPLA, while the least efficient detergent is FC16. DDM OMPLA has a low K_M, enabling it to bind substrates, but the μM affinity prevents an interaction that is too tight that it would hinder turnover. FC16 OMPLA has less substrate affinity, resulting in less activity. The aggregation in FC16 OMPLA is likely responsible for the decreased enzymatic efficiency.

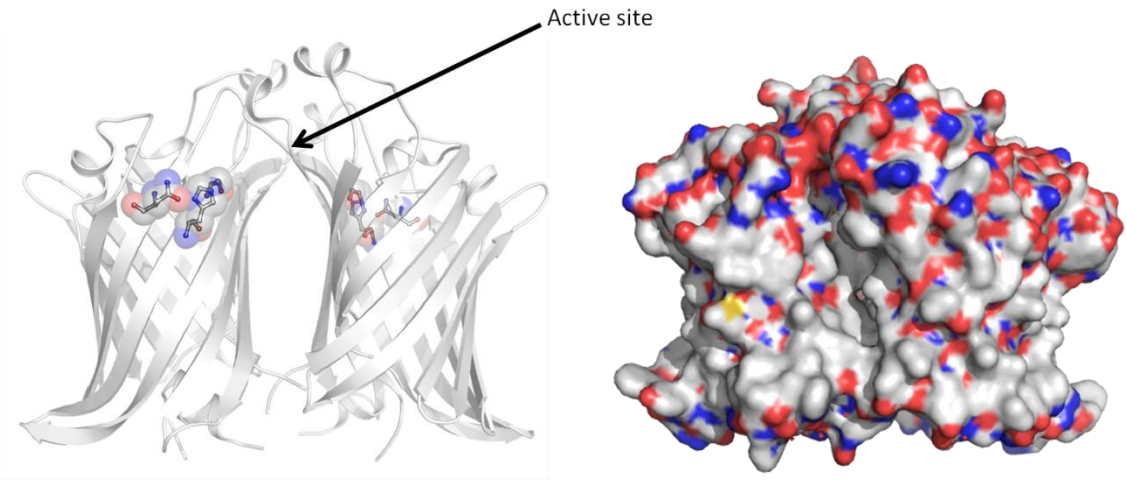

Figure 3.13. Surface representation of the OMPLA dimer and active site. The OMPLA catalytic residues as well as the extracellular surface have positive (blue) and negative (red) potentials that can interact with charged detergent head groups, impacting substrate specificity.

3.6. Future directions

To further explore and test the hypotheses on OMPLA activity, mixed micelles can be utilized. Mixed micelles enable a measurement of OMPLA activity in micelles with intermediate properties of both detergents. With mixed micelles, specific contributions to protein activity can be elucidated, including distinguishing head group or hydrophobic thickness effects on function. Mixing NM and DDM detergent will tune the hydrophobic thickness of the micelles, and the protein's activity as a function of increased size will provide conclusions on how the core thickness modifies protein activity. Similar studies can be pursued with head group thickness and surface charge.

SECMALS of OMPLA in mixed micelles can be conducted to not only confirm that mixed micelles are being formed, but to also monitor trends with protein aggregation in the larger micelles. 314/310 or FC16/FC12 PDCs can be used to identify the dependence of OMPLA aggregation on micelle size. Also, SECMALS dimer fractions without aggregation can be assayed to confirm the determined k_{cat} and K_M values.

All of these experiments with mixed micelles will help identify which physical properties of detergent micelles impact OMPLA activity. In addition to exploring the influence of detergents on OMPLA function, similar pursuits are currently being conducted with other membrane proteins. Results from these multiple studies can be compiled to give a complete picture on how well detergents mimic the bilayer.

3.6.1. PagP purification and activity in detergent micelles

The activity of the PhoPQ-activated gene protein (PagP) 8-stranded β-barrel membrane enzyme is also being characterized in varying detergent micelles. PagP expression, refolding, and purification procedures are similar to OMPLA protocols. PagP

inclusion bodies were resuspended similarly to OMPLA, but rapid dilution and refolding occurs in FC12 micelles instead of DM. Refolded PagP is added to a DEAE column for detergent exchange. PagP has been successfully purified in 15 detergents (Figure 3.14).

PagP functions in the transfer of a palmitate group from a phospholipid to the hydroxyl group of the N-linked *R*-3-hydroxymyristate chain on the proximal glucosamine unit of lipid A (Ref. Chapter 1). The PagP activity assay is designed to mimic the first step in PagP activity, the cleavage of the palmitate group from the phospholipid. Instead of a phospholipid, the chromophore *p*-nitrophenyl phosphate (pNPP) is used as the substrate (Figure 3.15). Addition of PagP to pNPP in buffer results in the hydrolysis of the substrate, yielding yellow *p*-nitrophenol. The absorbance of *p*-nitrophenol at 405 nm is measured over time to obtain initial rates of reaction. Preliminary PagP activity assays indicate that PagP is active in Cyclofos7 PDCs (Figure 3.16). Cyclofos7 detergent was initially used for PagP assays because the cyclic ring in the tail prevents the detergent from fitting into and interacting with the PagP binding cavity like other detergents.[10] PagP function will continue to be assayed, identifying trends between PagP activity and micelle properties.

3.6.2. OmpT purification and activity assay design

The β-barrel membrane enzyme OmpT will also be assayed in different detergent micelles. Functional information on all three β-barrel enzymes will be used to correlate physical properties of detergents with active membrane proteins. OmpT is expressed and purified with similar methods as OMPLA and PagP. OmpT is refolded overnight in FC12, and also applied to a DEAE column for detergent exchange. OmpT has been

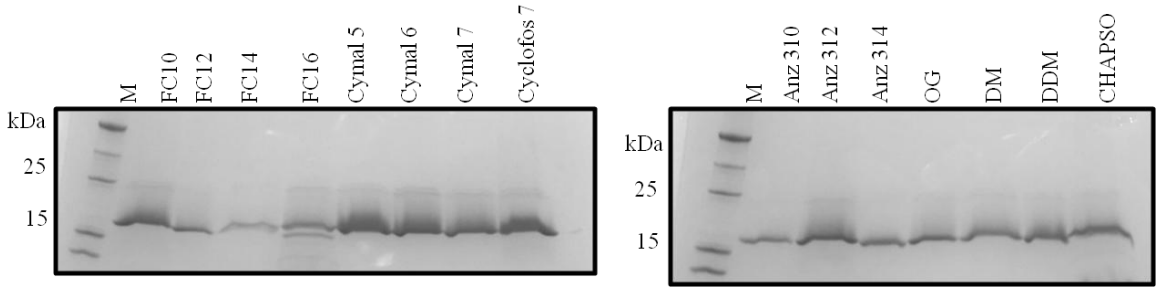

Figure 3.14. PagP purified in several detergents. SDS-PAGE was used to confirm the successful purification of PagP in 15 detergents. Folded PagP runs at a molecular weight of 19 kDa.

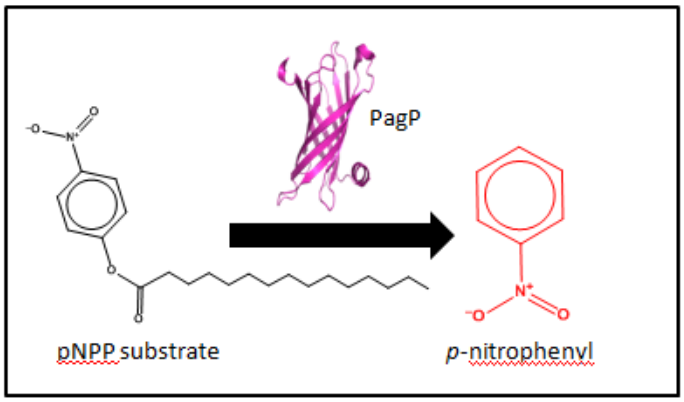

Figure 3.15. PagP activity assay. PagP function is assayed by measuring the change in absorbance obtained upon cleaving the p-nitrophenyl phosphate substrate with PagP.

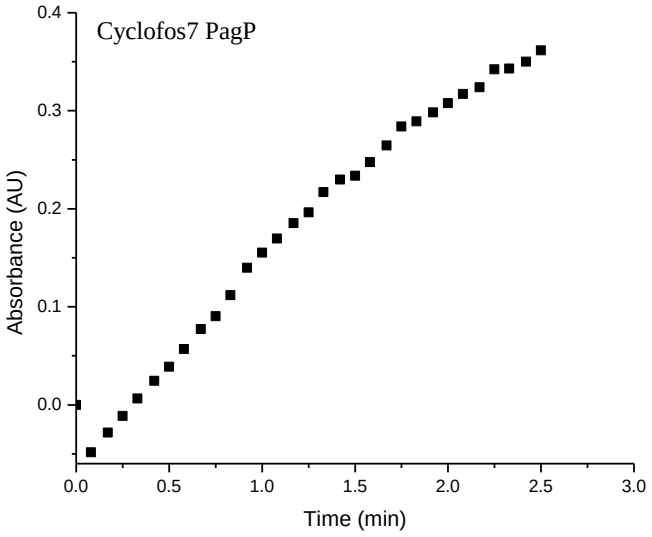

Figure 3.16. Activity of Cyclofos7 PagP. Triplicate PagP assays were conducted in Cyclofos7 detergent. The increase in color over time is indicative of PagP cleaving the pNPP substrate. A negative control containing pNPP in detergent without enzyme was subtracted from the data.

successfully purified into 16 detergents, but purification optimization is ongoing (Figure 3.17).

The OmpT activity assay is designed to monitor the cleavage of a custom peptide (Figure 3.18). OmpT cleaves antimicrobial peptides preferentially between two basic residues. The substrate for OmpT cleavage contains the basic amino acid sequence required for OmpT hydrolysis (Arg-Arg-Glu) along with an indole-3-acetic acid (IAA) cap at the N-terminus and the chromophore *p*-nitroaniline (pNA) at the C-terminus. The assay is coupled with a second enzyme, aminopeptidase M, an exopeptidase. Upon cleavage of the custom peptide with OmpT, the free amine group is exposed and subsequently cleaved by aminopeptidase M. This second hydrolysis releases the pNA chromophore, yielding a yellow color change that is monitored spectrophotometrically.

3.7. Conclusions

The OMPLA functional studies in varying detergent micelles are a first step toward elucidating the relationship between detergent characteristics and protein activity. OMPLA remained active in all 19 detergent micelles, with modest trends in substrate turnover rate and specificity. The enzyme is more active in detergents with larger, nonionic head groups such as the glucosides, maltosides, and Cymal detergents. These nonionic polar heads are less repulsive and form less perturbing interactions with the charged extracellular surface of OMPLA. An increase in the carbon tail length of the phosphocholine, maltoside, and glucoside PDCs attenuates substrate turnover, potentially due to hydrophobic mismatch destabilizing the OMPLA catalytic residues near the micelle head group – tail interface. Smaller micelles such as 7G, OG, and NG provide active site accessibility and less electrostatic repulsions at the interface, resulting in PDCs

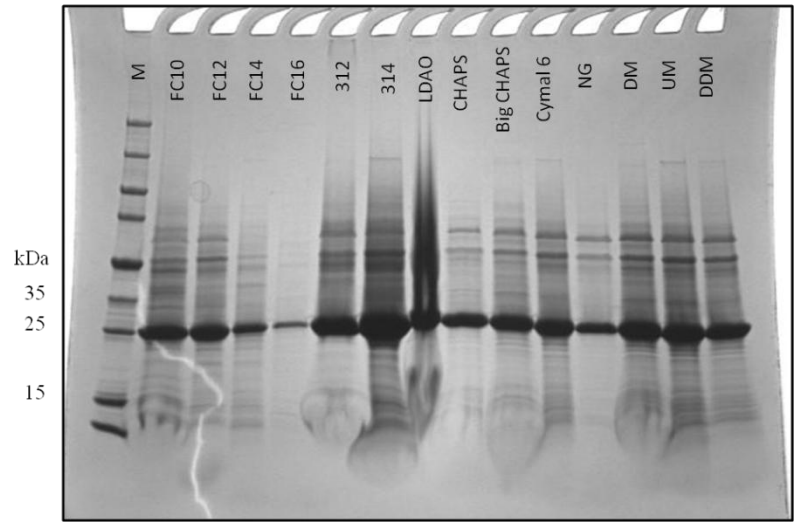

Figure 3.17. OmpT purified in several detergents. SDS-PAGE was used to confirm the successful purification of OmpT in 14 detergents. Folded OmpT runs at a molecular weight of 25 kDa. Purification optimization is required to obtain clean, pure OmpT PDCs.

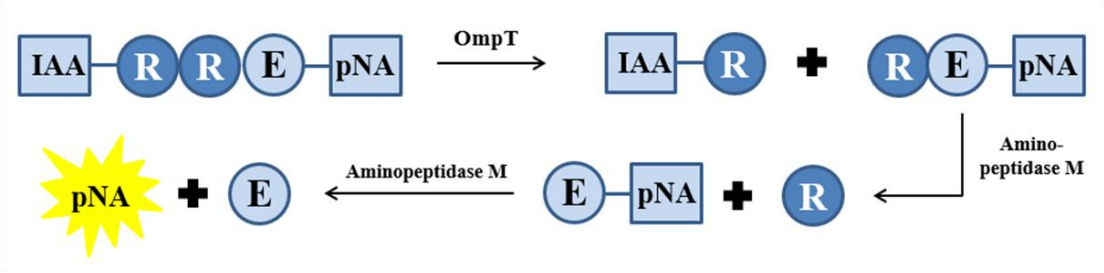

Figure 3.18. OmpT activity assay. The custom substrate for the OmpT assay will be hydrolyzed by OmpT between the two basic arginine residues. Aminopeptidase M targets the resulting free amine, cleaving the remaining arginine from the *p*-nitroaniline chromophore. The released *p*-nitroaniline is the colored species that occurs as a result of OmpT cleavage. Spectrophotometric measurements of the assay will yield OmpT reaction rates.

with almost identical k_{cat} and K_M. The OMPLA PDCs all bind HEPC at μM affinity, but protein aggregation may attenuate substrate specificity for the enzyme, as seen with FC14, FC16, and 314 K_M values.

This systematic characterization of activity in respect to detergent micelle properties is ongoing. PagP and OmpT function in bilayer mimics will be compiled with OMPLA activity, forming a complete commentary on optimal β-barrel membrane protein-detergent complexes.

3.7. Materials and Methods

3.7.1. Expression and purification of β-barrel enzymes

OMPLA, PagP, and OmpT genes in pET11a vectors were generously provided by the Karen Fleming laboratory (Johns Hopkins University, Baltimore, MD). All three proteins have similar expression and purification procedures. For expression, the plasmids were transformed into a BL21(DE3) *Escherichia coli* strain. Cell cultures were grown to an OD_{600} ~ 0.7 at 37°C in Luria-Bertani media supplemented with ampicillin (100 μg/mL). Protein expression to inclusion bodies was induced for 4 hours at the same temperature with 1 mM isopropyl-β-thio-D-galactoside (IPTG). Cells from 1-L culture were harvested by centrifugation (6000g, 15 min, 10°C), resuspended with 30 mL lysis buffer (50 mM tris, pH 8, 40 mM EDTA, 2.5 g lysozyme), and lysed using a microfluidizer (Microfluidics model 110L, Newton, MA).

The insoluble fraction was pelleted (6000 rpm, 30 min, 4°C), washed with wash buffer (10 mM tris, pH 8, 2 mM EDTA), and then pelleted again. The proteins were solubilized from inclusion bodies in 5 mL resuspension buffer (10 mM borate, pH 10, 2 mM EDTA, 8 M urea, 2 mg/mL final protein concentration). 500 μL of the resuspended

protein was rapidly diluted into 12.5 mL refolding buffer (10 mM borate, pH 10, 2 mM EDTA, 1 M urea) with detergent (4.5 mM FC12 for OmpT and PagP, 5.4 mM DM for OMPLA) and refolded overnight at 50°C with shaking.

The refolded protein was applied to a DEAE resin (Sigma, St. Louis, MO.) equilibrated with Buffer A (20 mM tris, pH 8.3, 2 mM EDTA) for OMPLA and OmpT purifications and Buffer B (10 mM Tris, pH 8) for PagP. Detergent exchange was conducted by washing the column with 50 mL of Buffer A or B with the appropriate detergent above CMC. The protein was eluted with 15 mL of elution buffer (Buffer A with 1 M KCl or Buffer B with 1 M NaCl) in the new detergent above CMC. The eluate was concentrated (MWCO = 10 kDa) to 2 mL volume. Concentration was determined by measuring the absorbance at 280 nm. The predicted molar extinction coefficients for OMPLA, PagP, and OmpT are 82280, 82390, and 78270 $M^{-1}cm^{-1}$, respectively. Proteins were stored at room temperature. Detergent concentrations were measured by 1-D ^{1}H NMR spectroscopy by comparison of the integrated methyl peak with samples of known detergent concentrations. To adjust the micelle concentration, the protein was dialyzed in 4 L equilibration buffer for an appropriate time to remove excess detergent.

3.7.2. SECMALS

A Waters 1525 binary pump HPLC and 2489 UV/visible detector was coupled to a Wyatt technology miniDAWN TREOS light scattering detector and Optilab T-rEX refractometer for SECMALS. Size exclusion chromatography was performed on a Superdex 200 Increase 10/300 GL column (GE Healthcare, Uppsala, Sweden) equilibrated with SECMALS buffer (20 mM tris, pH 8.3, 2 mM EDTA, 150 mM NaCl). To normalize the Astra V SECMALS software, 1 mg BSA (Sigma, St. Louis, MO.) was

separated with SECMALS. Following normalization, 12 to 73 mg OMPLA was separated for 1 hour in SECMALS buffer (0.45 mL/min flow rate). The light scattering and refractometer collected data over time to use for molecular weight determination.

3.7.3. OMPLA activity assay

The OMPLA activity assay mixture was a 100 μL volume of 50 mM tris, pH 8.3, 20 mM $CaCl_2$, 0.8 mM DTNB, and 0.05 μM OMPLA. For Michaelis-Menten kinetics, triplicate assays were conducted with 1, 0.5, 0.3, 0.1, 0.05, 0.03, 0.02, 0.01, 0.005, 0.003, 0.001, 0.0005, 0.0003 mM HEPC substrate concentrations. The absorbance at 412 nm was measured for 2.5 minutes in 10 second intervals. A negative control containing the reaction buffer components with the appropriate detergent sans OMPLA was subtracted from each reaction. Absorbance vs. time was plotted for each assay. The slope of this data over the first 1.5 minutes was translated into initial reaction rates (ν) using the extinction coefficient of the TNB^{2-} product, 13600 $M^{-1}cm^{-1}$. Initial reaction rate vs. [S] were plotted to determine Michaelis-Menten kinetic parameters.

3.7.4. PagP activity assay

The PagP functional assay was conducted with 45 μM Cyclofos7 PagP in 100 μL water. A final concentration of 225 μM pNPP substrate was added to the reaction, and the absorbance over 2.5 minutes was measured spectrophotometrically at 405 nm. The negative control containing the appropriate concentration of Cyclofos7 detergent in water with substrate was subtracted from the triplicate PagP assays.

3.8. References

1. Burgess, N., T. Dao, A. Stanley, and K. Fleming. 2008. β-barrel proteins that reside in the Escherichia coli outer membrane in vivo demonstrate varied folding behavior in vitro. J Biol Chem 283: 26748-26758.

2. Slotboom, D., R. Duurkens, K. Olieman, and G. Erkens. 2008. Static light scattering to characterize membrane proteins in detergent solution. Methods 46: 73-82.

3. Zhao, H., P. Brown, and P. Schuck. 2011. On the distribution of protein refractive index increments. Biophys J 100: 2309-2317.

4. Stanley, A., P. Chuawong, T. Hendrickson, and K. Fleming. 2006. Energetics of outer membrane phospholipase A (OMPLA) dimerization. J Mol Biol 358: 120 – 131.

5. Dekker, N., J. Tommassen, A. Lustig, J. Rosenbusch, and H. Verheij. 1997. Dimerization regulates the enzymatic activity of *Escherichia coli* outer membrane phospholipase A. J Biol Chem 272: 3179 – 3184.

6. Kingma, R., H. Snijder, B. Dijkstra, N. Dekker, and M. Egmond. 2002. Functional importance of calcium binding sites in outer membrane phospholipase A. Biochim Biophys Acta 1561: 230 – 237.

7. Stanley, A. and K. Fleming. 2007. The role of a hydrogen bonding network in the transmembrane β-barrel OMPLA. J Mol Biol 370: 912-924.

8. Luckey, M. 2008. Membrane Structural Biology with Biochemical and Biophysical Foundations. Cambridge University Press, New York, NY.

9. Oliver, R., J. Lipfert, D. Fox, R. Lo, S. Doniach, and L. Columbus. 2013. Dependence of micelle size and shape on detergent alkyl chain length and head group. PLoS ONE 8: e62488.

10. Ahn, V., E. Lo, C. Engel, L. Chen, P. Hwang, and L. Kay. 2004. A hydrocarbon rule measures palmitate in the enzymatic acylation of endotoxin. EMBO J 23: 2931-2941.

Chapter 4: The Influence of Detergents on LspA function

Bilayer mimics have different effects on every membrane protein. Monitoring the influence of detergent micelles on β-barrel membrane enzymes provides an opportunity to find trends with physical detergent properties and β-barrel enzyme function. This research targets not only β-barrel membrane enzymes, but aims to correlate function with all types of proteins, including α-helical bundles. The stability and function of the α-helical membrane enzyme, lipoprotein signal peptidase A (LspA), in varying detergent environments is the focus of this chapter.

While α-helical bundles have structural differences from β-barrels, they are significantly less stable. Entire β-sheets of barrels are stabilized via an internalized hydrogen bonding network among the backbone carbonyls and amides.[1] These β-sheet interactions are stronger than the local hydrogen bonds formed between individual residues along the α-helix (Figure 4.1).[1,2] The ΔG_{unf} of β-barrels can be as high as 32 kcal/mol compared to ~4 kcal/mol for α-helical bundles.[3,4] α-helical proteins differ in structure, stability, and even native membrane. Therefore, investigations on the stability and activity of LspA is another interesting strategy to explore protein-mimic complexes.

4.1. Protein-detergent complex formation with LspA

Recombinant LspA from *Chlamydia trachomatis* was expressed in *E.coli* cells. Unlike with the three β-barrel enzymes, LspA did not express into inclusion body pellets. To isolate the membrane-bound LspA protein, the E. coli cells were lysed with a high pressure homogenizer and the cell debris was removed via centrifugation. The supernatant containing the membrane-bound LspA was pelleted using high speed ultra-

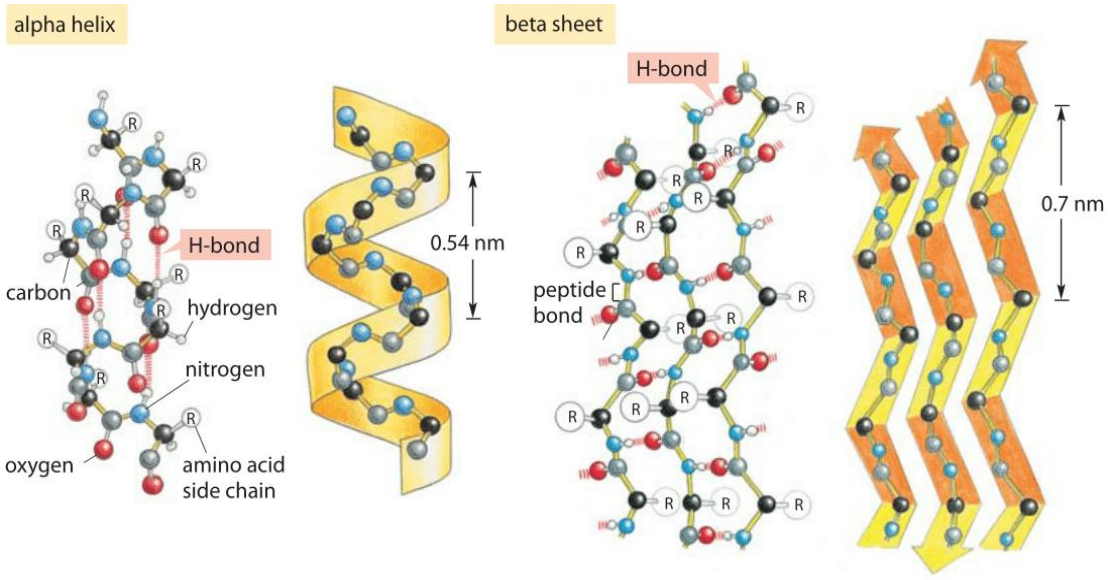

Figure 4.1. Hydrogen bonding and protein secondary structure.[2] α-helix and β-sheet structures both depend on upon hydrogen bonding for stabilization. β-sheets more stable than α-helices.

centrifugation (35,000g). To solubilize the protein from the membrane, the pellet was resuspended in FC12 detergent for 3 hours.

To study LspA in varying detergents, the FC12 was exchanged for several different detergents via immobilized metal ion affinity chromatography (IMAC). Recombinant LspA was expressed with a polyhistidine tag for affinity chromatography purposes. These 6 histidine residues on the N-terminus of the protein interacted with the Co^{2+} applied to the IMAC column, immobilizing the protein on the resin. Once immobilized on the column, the FC12 detergent was exchanged for other detergents, similar to the OMPLA detergent exchange in Section 3.1 (Figure 4.2). Protein solubility was monitored 3 days after detergent exchange via centrifugation of the purified protein. The supernatant and pellet were separated with SDS-PAGE; LspA in the supernatant indicated stable, solubilized protein, while protein in the pellet suggested that LspA was unstable and precipitated.

4.1.1. Results: LspA PDC stability in detergent enzymes

LspA detergent exchange was conducted in 27 detergents including phosphocholines, glucosides, maltosides, Cymals, bile salt derivatives, thiomaltosides, an Anzergent, and dimethylglycine (Figure 4.3 and Table 4.1). A first difference from the β-barrel enzymes, LspA was not soluble and stable in many detergents. There were 3 outcomes from detergent exchange depending on the micelle: 1) purification of a stable PDC, 2) purification of an instable PDC, and 3) protein precipitation during detergent exchange.

LspA exchanged into the phosphocholine and Anzergent detergents produced soluble, stable PDCs (Figure 4.4). The maltosides as well as Cymal 3, 4, and 5,

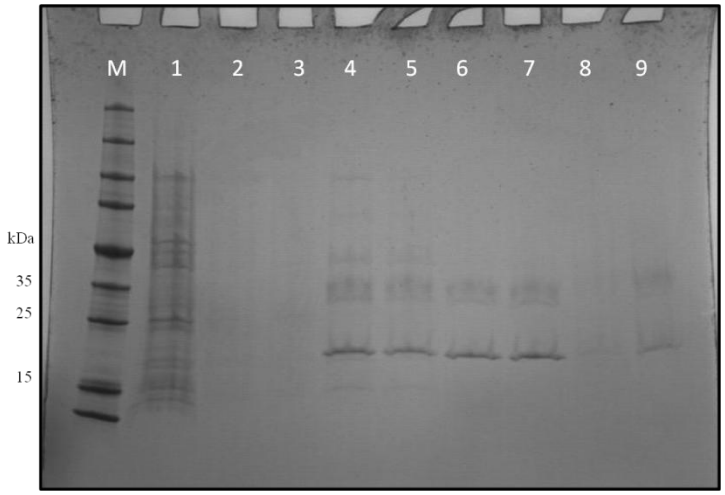

Figure 4.2. LspA purification in FC12 detergent micelles. LspA purification and was immobilized with IMAC for detergent exchange into FC12 micelles. Fractions from the detergent exchange were analyzed with SDS-PAGE. The gel depicts the column flowthrough (lane 1), wash 1 (2 & 3), wash 2 (4 & 5), elution (6 & 7), and resin (8 & 9). The molecular weight of LspA is 21 kDa.

Dodecylthiomaltoside (DDTM)

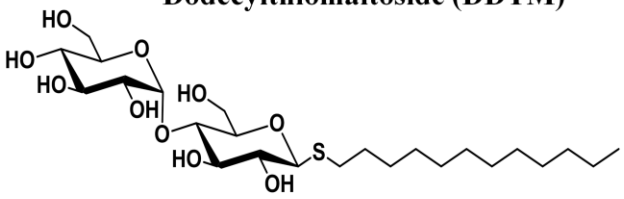

Dodecyldimethylglycine (DDMG)

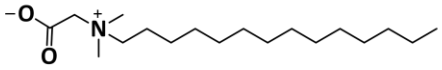

Figure 4.3. Structures of dodecylthiomaltoside and dodecyldimethylglycine detergents. Other detergent structures were depicted in Chapter 1.

Phosphocholines					Anzergents
FC-10	FC-12	FC-14	FC16	DHPC	Anz 3-12
+	+	+	+	-	+
Glucosides					
6G	7G	OG	NG	DG	DDG
-	-	-	-	-	-
Maltosides				**Thiomaltosides**	
NM	DM	UM	DDM	DTM	DDTM
-	-	+	-	-	-
Cymals					
Cymal 1	Cymal 2	Cymal 3	Cymal 5	Cymal 6	
-	-	-	-	-	
Dimethylglycines			**Bile Salts**		
DDMG			CHAPS	BigCHAPS	CHAPSO
-			-	-	-

Table 4.1. LspA purification in varying detergents. Of the 25 detergents screened for solubility, 5 detergents formed stable LspA PDCs.

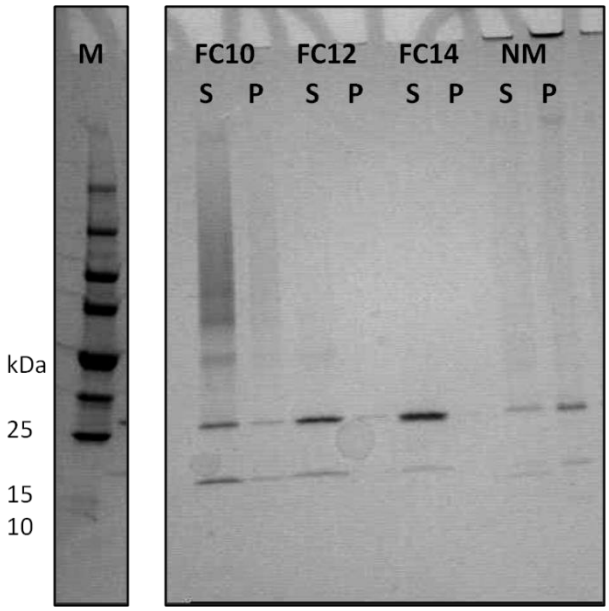

Figure 4.4. LspA PDC solubility in phosphocholine and maltoside detergents. LspA PDCs (21 kDa) were centrifuged and supernatant (S) and pellet (P) were separated on a protein gel three days after purification to analyze solubility and stability. FC10, FC12, and FC14 LspA samples were in the supernatant, indicating stable, soluble proteins. NM was less stable, and precipitated after a few days.

solubilized an unstable PDC, as the protein precipitated from the micellar solution just hours later (Figure 4.4). The protein immediately precipitated on the IMAC column when exposed to the glucoside, thiomaltoside, bile salt, and dimethylglycine detergents.

This detergent screen suggests that independent of tail length, LspA is more stable in detergents with the smaller, zwitterionic head groups. This trend can be due to several reasons. First, the phosphocholine and Anzergent detergents share greater similarities with the native lipids within the inner membrane (Figure 4.5).[5] The phosphocholine and Anzergent detergents may be close enough mimics to the bilayer to provide the protein with enough stability and the electrostatic contacts necessary to fold and remain soluble in these detergents. Second, Asp-14 within the conserved region A of LspA is essential for protein folding and stability.[6] This aspartate residue, potentially near the micelle head group shell, may be impacted by a bulkier, nonionic head group, causing instability and protein precipitation on the column or after purification.

Circular dichroism was completed on the successfully exchanged LspA PDCs to further confirm the protein's fold. Circular dichroism (CD) is a qualitative spectroscopic technique that uses the differential absorbance of right and left circular polarized light when applied to chiral molecules to analyze the secondary structure of proteins.[7] Although the change in absorbance is usually measured, CD measurements are often reported in degrees of ellipticity, which are absorbances corrected for protein concentration.[7] With Beer's law, the differences in absorbance (ΔA) is converted to $\Delta\varepsilon$, and the mean residue ellipticity $[\theta]$ is determined with the following equation:

$$[\theta] = 3298.2\Delta\varepsilon \quad [1]$$

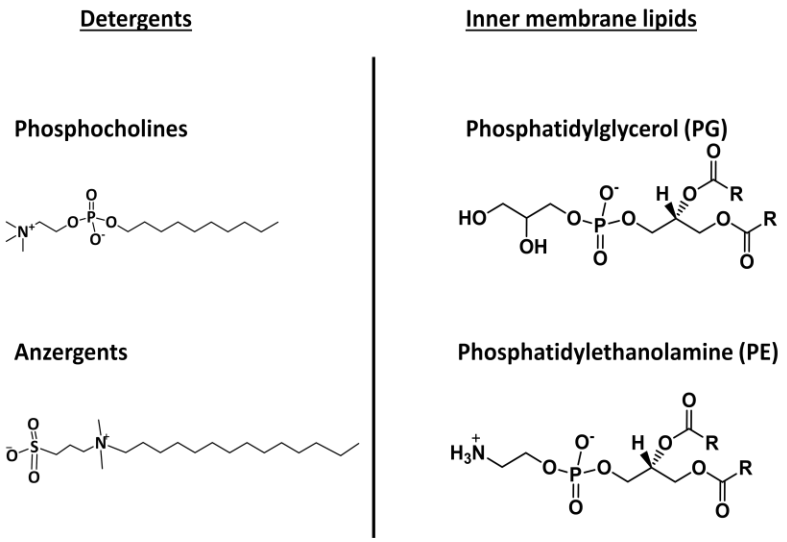

Figure 4.5. Structures of similar detergents and lipids. A few of the inner membrane lipids, PG and PE, have similar head group size and charges as the phosphocholine and Anzergent detergents.

where [θ] are in units of degrees•cm^2•$dmol^{-1}$.[7] CD spectra are depicted in molar ellipticity vs. wavelength, and have characteristic trends depending on the protein's secondary structure (Figure 4.6).[7,8] α-helical proteins have CD spectra with two minima, one at 208 nm and the other at 222 nm wavelength.[9]

CD was performed on the purified LspA, and the spectra have minima at 209 and 222 nm wavelengths, confirming that the protein is forming a α-helical protein fold (Figure 4.7). LspA stability is not dependent on tail length (FC10 and FC16 produce stable, folded PDCs); this exemplifies the flexibility within the detergent micelles, as the carbon tails must shift to accommodate the protein.

4.2. LspA function in detergent micelles

4.2.1. Development of a custom signal peptide substrate for LspA cleavage

LspA activity assays involved monitoring the cleavage of a signal peptide with two methods: HPLC and fluorescence.[10] Designing an optimal custom signal peptide substrate for LspA cleavage was vital in obtaining reliable, consistent activity results. To engineer the substrate peptide, sequences for other signal peptide were used as a template. The sequences included three signal peptides from *Chlamydia trachomatis* and three from *Bacillus subtilis* (Table 4.2).[11-13] Analysis of the signal peptides from other bacteria highlighted several characteristics that the LspA peptide should contain: 1) a lipobox cleavage sequence of L-X-X-C in the C-terminus, 2) 1 to 3 polar residues at the N-terminus, and 3) 1 to 3 hydrophobic residues at the N-terminus. Common lipobox sequences varied from LSSC, LAGC, LAAC, and IAAAC.[11-13]

With this information, three signal peptide substrates were designed containing the following sequences: GSALSLSSCDNG (named UVAB2), YSGALAACGN

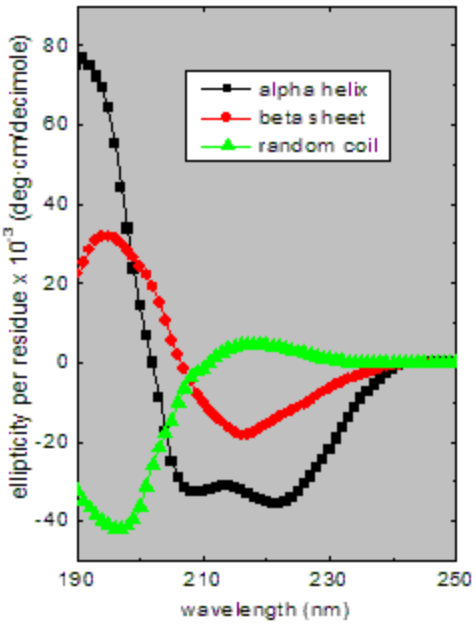

Figure 4.6. Typical circular dichroism spectra.[8] Far-UV CD spectra of α-helices, β-sheets, and random coil structures have characteristic trends. Typical CD spectra for α-helices contain two minima at 209 and 222 nm wavelength.

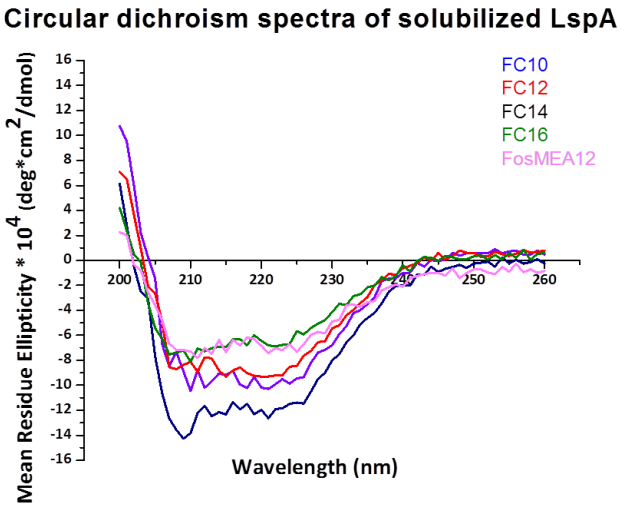

Figure 4.7. CD spectra of LspA in varying detergents. LspA maintains α-helical fold in zwitterionic detergents as indicated with the minima of the CD spectra at 209 and 222 nm wavelength.

Protein	N-region	H-region	Lipobox (C-region)
C. tch MipL2	MKK	TALLAALCSVVS	LSSCC
C. tch YtgA	MSFFHTRKYKLILR	GLLC	LAGCF
C. tch PAL	MRKTIFK	AFNLLFSLLF	LSSCY
B. sub PrsA	MKK	TGVYIGA	LAACG
B. sub OpuAC SBP	MLKK	IAIAAITATSIL	LAACG
B. sub PstS	MKKNK	LVLMLLMAAFMM	IAAACG
Signal peptide sequences			
UVAB2		GSALSLSSCDNG	
UVAB3		YSGALAACGN	
UVAB4		GSALSLSSCSRI	

Table 4.2. Signal peptides and the custom substrate sequences. The LspA substrate was designed using known signal peptide sequences in *Chlamydia trachomatis* and *Bacillus subtilis*. The custom substrate has similar H-region and lipobox sequences to signal peptides from the literature.

(UVAB3), and GSALSLSSCSRI (UVAB4). The C-terminal domains were derived from signal peptides from CccA, MipL, and CRPL2, from *C. tch* and *B. sub* (Table 4.2). Each peptide was tested to confirm cleavage via LspA with HPLC, and the best peptide was tagged for fluorescence activity assays.

4.2.2. LspA HPLC assay optimization and results

Positive and negative controls for the HPLC and fluorescence activity assays were required for accurate interpretation of purified LspA function. Cell extract from *E. coli* cells transformed with and without *lspA* in the pET28 vector were used as controls. pET28b + LspA cell extract was the positive control, and contained LspA in the bacterial membrane. The negative control was pET28b – LspA, an empty pET28b vector expressed in *E. coli* cells. The cell extracts are useful controls; however, the extracts contain other cell contents and contaminants. Accurate LspA concentrations cannot be determined with cell extract.

Prior to conducting the LspA activity assays, several controls were completed. pET28b – LspA and pET28b + LspA cell extracts were monitored with HPLC. The two chromatograms contained early eluting peaks with retention times between 2 and 4 minutes (Figure 4.8). HPLC runs with peptide only were also completed. The UVAB2, 3, and 4 all eluted with a single peak at a later retention time (Figure 4.8). Knowing what retention time to expect the peptide and the cell extract is important when interpreting the LspA assay results.

The activity assay was designed as follows: prepare a reaction buffer containing the positive or negative control cell extract, tris buffer at pH 8, EDTA, and DMF. The substrate is added to the reaction buffer and the mixture is incubated for up to an hour at

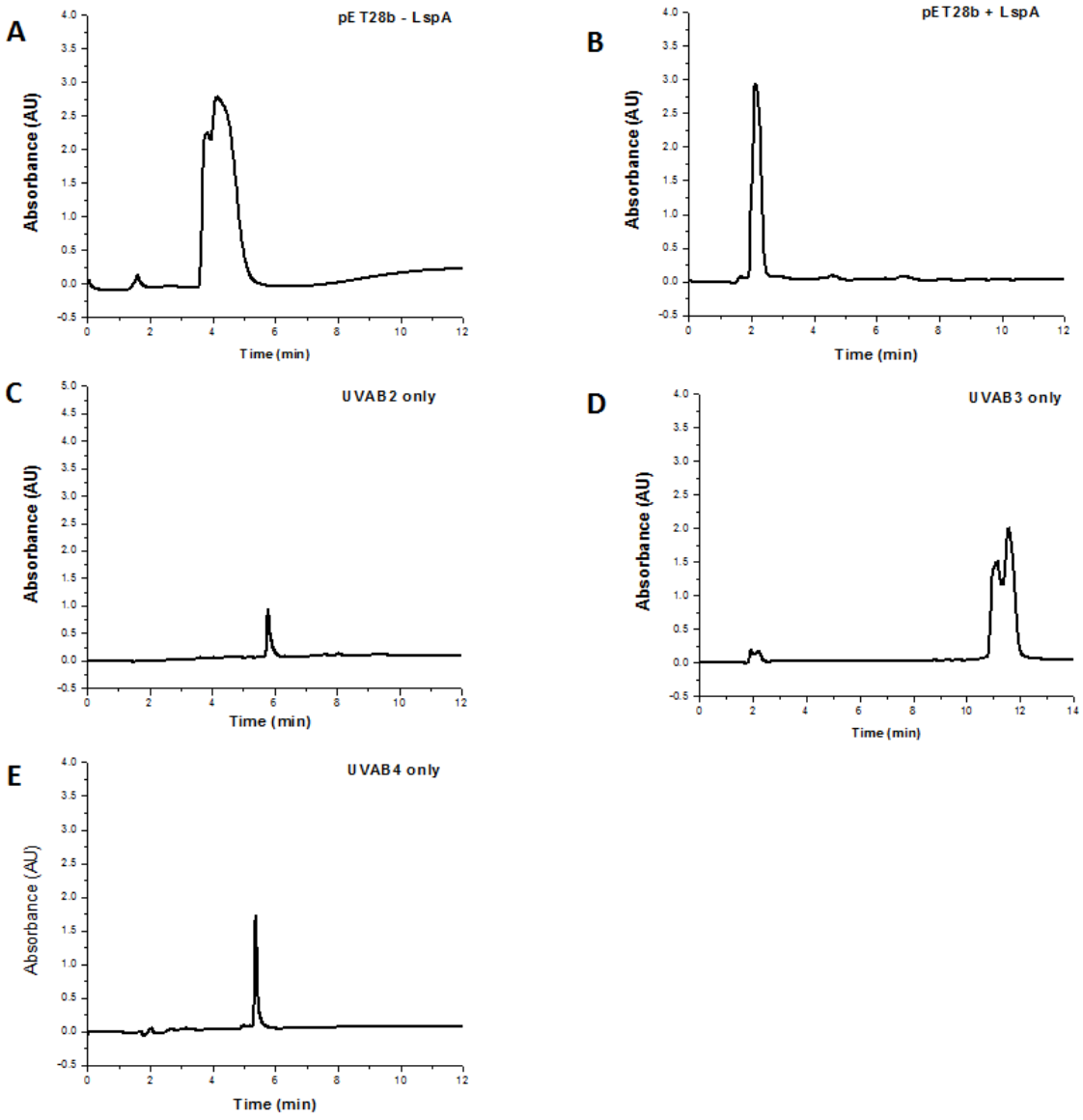

Figure 4.8. HPLC activity assay controls. The negative and positive controls were analyzed with HPLC (A & B) along with substrate only samples (C – E). Early eluting peaks are indicative of the cell extract, this is useful when comparing with other chromatograms.

37°C. This was completed with UVAB2, 3, and 4 to determine which substrates show the potential to be a viable substrate for these assays. All three peptides showed signs of cleavage in both the positive and negative controls (Figure 4.9), with smaller fractions eluting between 3 and 5 minutes. Although these initial controls were inconclusive, the peptides with more cleavage products, UVAB3 and UVAB4, were generated with fluorescent tags for use in all of the following HPLC and fluorescent assays.

UVAB3 and UVAB4 signal peptide substrates were tagged with a fluorescent donor/quencher pair. With the 3-nitrotyrosine donor and aminobenzamide on opposite ends of the peptide, LspA activity can be quantitated (Figure 4.10). Upon addition of LspA, the peptide will be cleaved, the donor/quencher pair will be separated, and the fluorescence will increase. Initial reaction rates can be determined from the change in fluorescence. The fluorescence and HPLC activity assays allow for a qualitative and quantitative measurement of LspA function.

4.2.2.1. Results: LspA activity assayed with HPLC

As before, HPLC was completed on the fluorescently tagged UVAB3 and UVAB4 peptide only samples (Figure 4.11). Upon addition of the positive and negative controls, the results were significantly different. UVAB3 with pET28b – LspA did not show any signs of peptide cleavage while UVAB3 with pET28b + LspA showed distinct cleavage peaks at retention times between 4 and 5 minutes (Figure 4.12). These results established a viable positive and negative control and substrate (UVAB3) for the purified LspA samples. Because the UVAB4 substrate chromatograms did not depict any peptide cleavage fragments in the positive control (Figure 4.12), the remaining LspA activity assays focused on the cleavage of UVAB3.

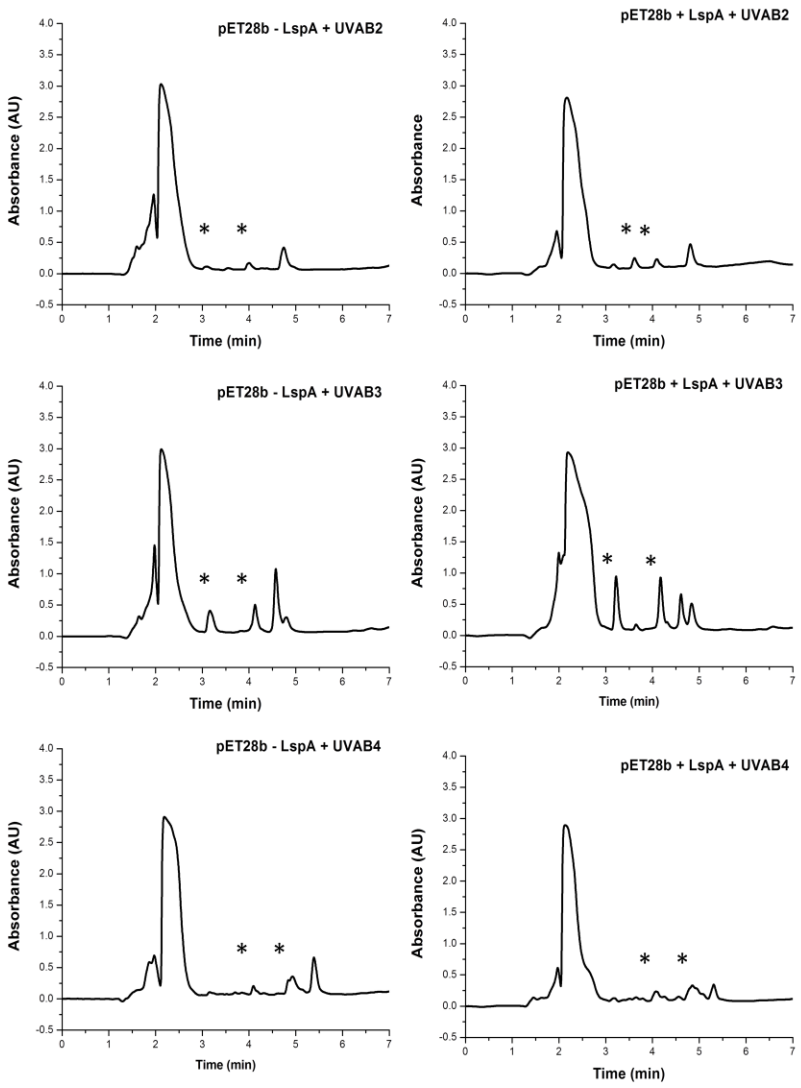

Figure 4.9. LspA activity with each substrate. Negative (pET28b – LspA) and positive (pET28b + LspA) cell extracts were incubated with the 3 different signal peptide substrates (UVAB2, 3, and 4) for 30 minutes prior to HPLC. Cleavage of the signal peptides is observed for both positive and negative controls. Cleavage peaks are designated with asterisks, the full substrate peak elutes at approximately 5 minutes, and the cell extract elutes early, at approximately 2 minutes.

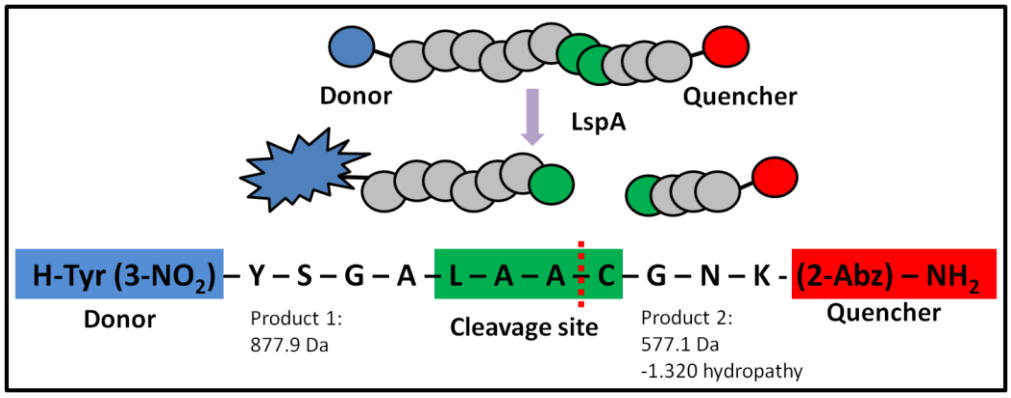

Figure 4.10. UVAB3 engineered with the donor/quencher pair. A 3-nitrotyrosine donor and aminobenzamide quencher was added to the opposite ends of the UVAB3 peptide. Upon LspA cleavage, the donor and quencher are separated, resulting in an increase in fluorescence.

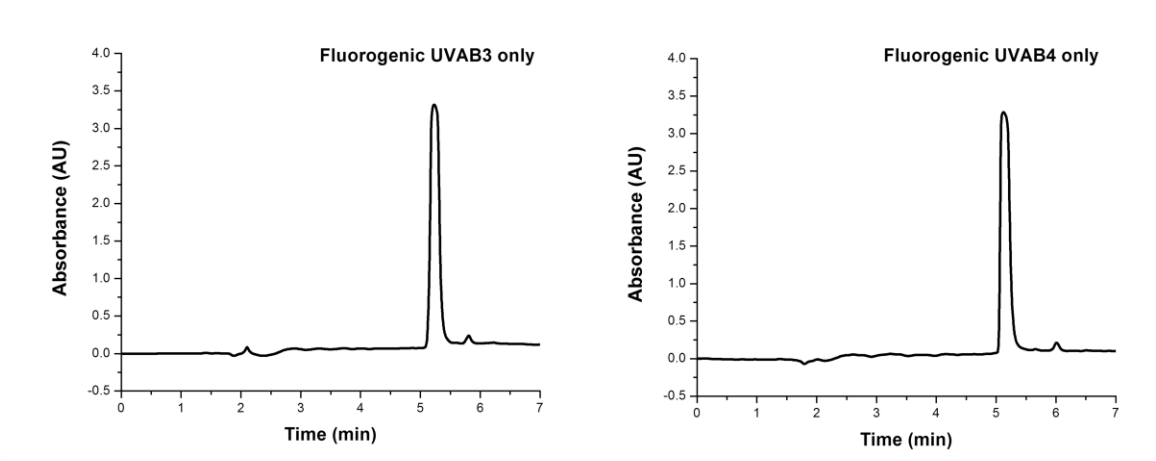

Figure 4.11. Fluorogenic signal peptide only chromatograms. UVAB3 and UVAB4 were analyzed on HPLC as peptide only samples prior to conducting the positive and negative controls. The peptides eluted as a single peak.

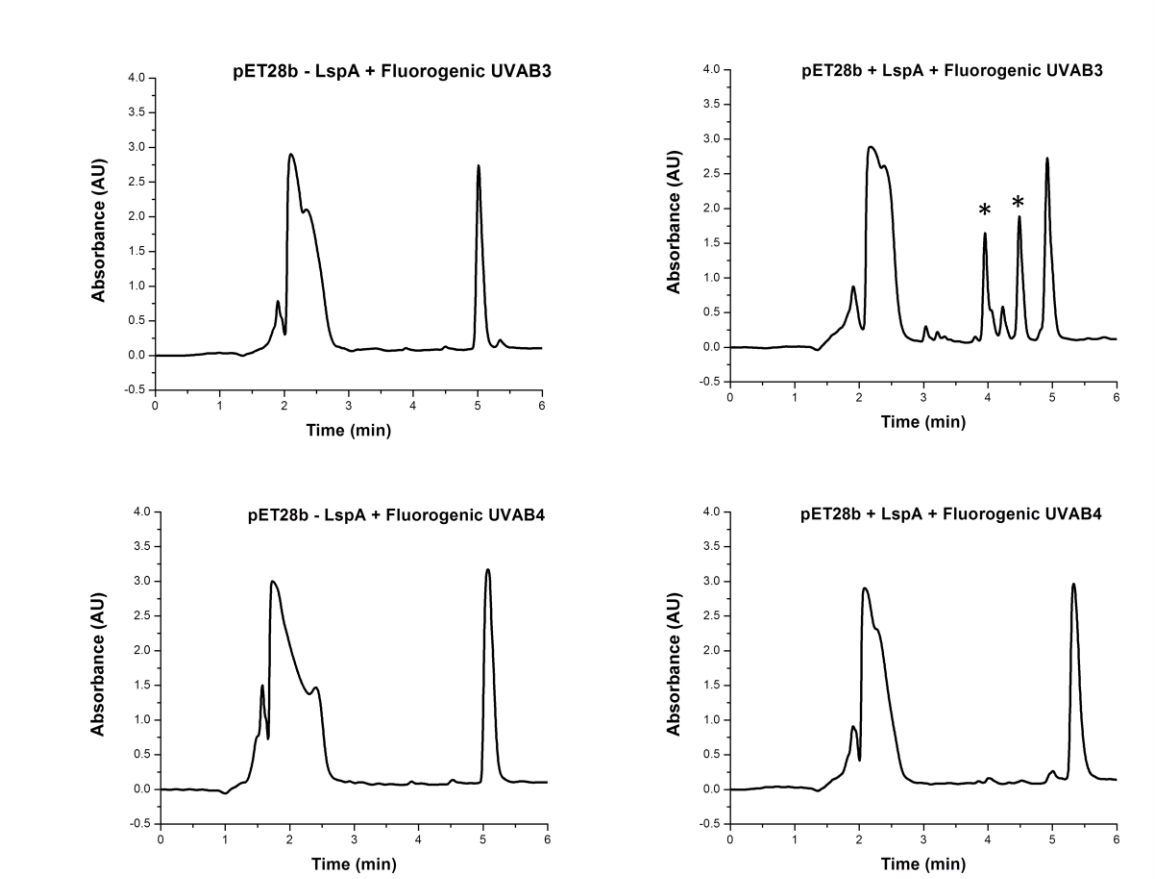

Figure 4.12. Fluorogenic UVAB3 and UVAB4 positive and negative controls. The positive and negative control cell extracts were incubated with UVAB3 (top) and UVAB4 (bottom) for 60 mins. Peptide cleavage occurred for UVAB3 with the positive control (asterisk).

Purified LspA activity was monitored with HPLC in FC10, FC12, and FC14 PDCs. While HPLC chromatograms contained peaks for both peptide and LspA at ~ 2 and 5 minutes, respectively, there were no cleavage fragments detected, suggesting that the detergent-solubilized LspA is inactive (Figure 4.13). For confirmation, these reaction mixtures were incubated for up to 60 minutes prior to applying to the HPLC column.

These results indicate that even as stable PDCs, LspA solubilized in detergent is inactive. The active site residues that are located within TMDs 3 and 4 are likely significantly affected by the membrane mimic. With every purified LspA sample inactive, it is more challenging to determine which specific detergents affect the LspA functional fold and what key physical micelle properties are disrupting LspA activity. Before concluding that LspA is inactive in all detergent mimics, fluorescent assays on the UVAB3 with purified LspA was completed. The results of these assay show promising, yet contradictory results.

4.2.3. LspA fluorescence assay optimization and results

The LspA fluorescence assay involved exciting the reaction mixture at 340 nm and measuring the fluorescent emission at 411 nm every 5 minutes for 30 minutes. The positive and negative cell extract controls were initially assayed with UVAB3. Upon addition of UVAB3 to both positive and negative controls, there was an increase in fluorescence. This is expected, as the cell extract contains not only the target protein, but other proteins and debris that could cleave the signal peptide. With the change in fluorescence calculated for enzyme specific activity, the pET28b + LspA positive control has twice the activity of the negative control (Figure 4.14).

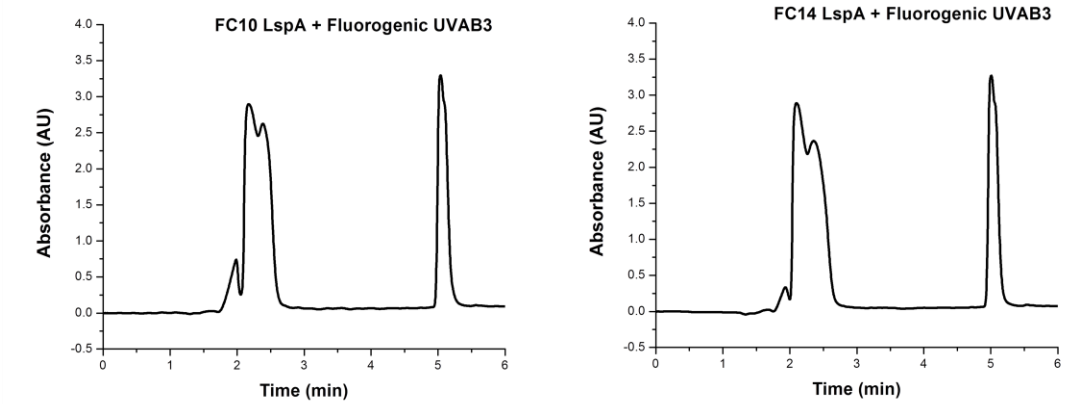

Figure 4.13. Purified LspA HPLC activity chromatograms. FC10 and FC14 LspA PDCs were incubated with UVAB3 signal peptide substrate for 60 min. No peptide cleavage peaks were observed.

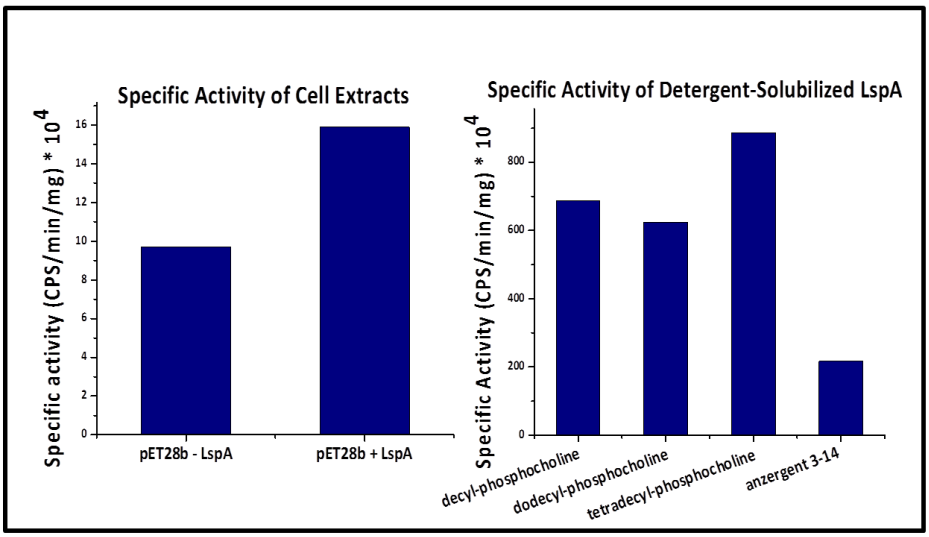

Figure 4.14. LspA fluorescence assay results. LspA specific activity in counts per second (CPS) per minute per mg is reported by measuring the change in fluorescence upon the addition of enzyme. The positive control, pET28b + LspA, has almost twice the activity of the negative control. The activity of the LspA PDCs is significantly greater than the controls, with FC14 LspA having the highest specific activity.

4.2.3.1. Results: Purified LspA function assayed with fluorescence

With established controls, fluorescent activity was assayed with the controls, FC10, FC12, FC14, and Anzergent 314 LspA PDCs. All of the purified LspA PDCs were active, with specific activities an order of magnitude higher than the positive control (Figure 4.14 and Table 4.3). Fluorescence methods are 1000x more sensitive than UV measurements. With increased sensitivity, the fluorescence assay was able to measure signal peptide cleavage, unlike the HPLC assay. FC14 LspA has the highest activity while Anzergent 314 has significantly lower activity than the other PDCs.

As with the LspA detergent exchange results, enzyme activity is independent of carbon tail length. The FC14 and 314 detergents have the same nonpolar carbon tails yet differ four-fold in specific activity. The phosphocholine and Anzergent head groups have similar size and charge; however, the charge distribution across the head group shell is opposite. The positive charge on FC detergents is on the outside of the shell while the negative charged is closer to the micelle core; Anzergents have an opposite distribution. The LspA catalytic aspartate residues are located at the micelle interface. There is a possibility that these residues are interacting with the positive choline on the Anzergent head group rather than the negative charged phosphate on the phosphocholine detergents. The electrostatic interactions formed between the LspA catalytic aspartates and the Anzergent head group could potentially attenuate protein function. Association between protein and micelle head group not uncommon. NMR experiments suggests hydrogen bond formation between FC head groups and the arginine side chains of FXYD2, a Na/K-ATPase as well as association between the protein hormone epidermal growth factor (EGF) with SDS and FC12 micelles at the surface.[14,15]

	Specific activity (CPS/min/mg * 10^4)
pET28b – LspA	10
pET28b + LspA	16
FC10 LspA	624
FC12 LspA	687
FC14 LspA	886
314 LspA	217

Table 4.3. LspA fluorescence assay results. Specific activity values for positive and negative controls as well as purified LspA.

To further explore LspA activity, globomycin, a known LspA inhibitor, was added to the reaction mixture. The addition of globomycin to FC12 and FC14 LspA significantly attenuated protein function (Figure 4.15). Globomycin reduced FC12 LspA activity by approximately 50% and decreased FC14 LspA activity by 70%.

Preliminary LspA fluorescence activities demonstrate reliable negative and positive controls, active LspA PDCs, and attenuated function with a known inhibitor. This assay shows great potential for monitoring LspA in varying detergents and identifying correlations between detergents and protein properties. Typically, fluorescence sensitivity can be three times higher than that of a UV detector.[16] It is possible that the both HPLC and fluorescence activities were successful, but the fragments were not resolved with UV.

4.3. Future directions and conclusions

With these promising results, efforts to monitor LspA activity in varying detergent micelles are ongoing. The preliminary work on this α-helical protein optimized LspA solubilization, purification, and activity assays. Initial data suggests that LspA is not stable in all detergents, and its activity is significantly affected by the membrane mimics. This work exemplifies the arduous trial-and-error detergent screening that is required for studying a membrane protein and emphasizes the difference between outwardly similar detergent micelles.

A major drawback to this research is obtaining a reliable signal peptide substrate. Although the sequences remained as designed, signal peptides synthesized from the same

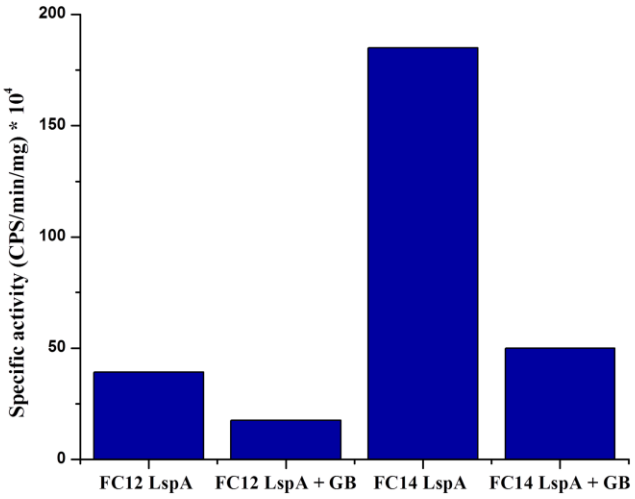

Figure 4.15. LspA PDC activity in the presence of globomycin. Globomycin (GB) attenuates the specific activity of LspA PDCs. The inhibition is more significant for FC14-solubilized LspA.

and different companies produced very different results in respect to both the HPLC and fluorescence assay. With the replicability issues, this project will benefit greatly with in-house peptide synthesis to ensure similar results with every experiment. Peptide synthesis and substrate production will be a beneficial component added to this research.

In addition to obtaining a more replicable substrate peptide, LspA detergent exchange and purification will continue; it is likely that there will be more success when purifying in Anzergent 310, 312, and potentially Cyclofos micelles. Stable PDCs will be confirmed with circular dichroism and assayed with fluorescence. There is potential for HPLC to be used to qualitatively confirm LspA cleavage; however, other methods may be more successful. With a combination of biophysical techniques, the activity of LspA PDCs will be elucidated.

4.4. Methods

4.4.1. LspA expression and purification

The pET28b plasmids containing the *lspA* gene was transformed into BL21(DE3) *E. coli* cells for protein expression. Cell cultures were grown to an OD_{600} ~ 0.8 at 37°C in terrific broth media supplemented with kanamycin (50 μg/mL). Protein expression was induced for 4 hours at the same temperature with 1 mM IPTG. Cells from 6-L culture were harvested by centrifugation (6000g, 15 min, 10°C), resuspended with 300 mL lysis buffer (50 mM tris, pH 8, 150 mM NaCl, 1 μL DNAse, ½ EDTA-free protease inhibitor pellet (Roche)), and lysed using a microfluidizer (Microfluidics model 110L, Newton, MA). The cell debris was pelleted with low speed centrifugation (10,000g, 30 min, 4°C) and discarded. The supernatant containing the membrane bound fraction was pelleted with high speed centrifugation (35,000g, 90 min, 4°C). The pellet was resuspended in 160

mL extraction buffer (20 mM phosphate, pH 7.8, 150 mM NaCl, 4.5 mM FC12, 1 EDTA-free protease inhibitor pellet) for 3 hours at room temperature.

The resuspended protein was applied to cobalt chelating sepharose fast flow resin (GE Healthcare, Uppsala, Sweden) for detergent exchange. The column was washed with 10 mL wash buffer 1 (20 mM phosphate, pH 7.8, 500 mM NaCl, and the appropriate detergent), followed by 5 mL wash buffer 2 (20 mM phosphate, pH 7.8. 500 mM NaCl, 45 mM imidazole, and the appropriate detergent). LspA was eluted with 10 mL elution buffer (20 mM phosphate, pH 7.8, 150 mM NaCl, 600 mM imidazole, and the appropriate detergent). The eluate was concentrated (MWCO = 10 kDa) to 2 mL volume. Concentration was determined by measuring the absorbance at 280 nm. The predicted molar extinction coefficient for LspA is 29973 $M^{-1}cm^{-1}$. To remove imidazole, the protein was dialyzed in 4 L equilibration buffer for 1 hour, 3 times. Detergent concentrations were measured by 1-D ^{1}H NMR spectroscopy by comparison of integrated methyl peak with samples of known detergent concentrations. After a few days, protein solubility was verified by centrifuging the protein (18,000g, 30 min, 10°C) and analyzing the pellet and supernatant with SDS-PAGE. For CD, 1 mL of 0.05 mg of dialyzed LspA in varying detergents was added to a quartz cuvette and the differential absorbance of the sample was measured at 180 to 260 nm. The CD spectra were background subtracted with measurements of buffer and detergent.

4.4.2. LspA activity assays

The pET28 – LspA and pET28b + LspA cell extract controls were produced by transforming the plasmids into BL21(DE3) *E. coli* cells, expressing bacterial cells in

terrific broth media supplemented with kanamycin (50 μg/mL) to an OD_{600} ~ 0.8, and inducing the cultures with IPTG for 4 hours. The bacterial cells were harvested and pelleted via centrifugation (6000g, 15 min, 4°C) and resuspended in 10 mL lysis buffer. The cells were lysed with pulse sonication for 30 mins with 30 second pulses. After sonication, the cell debris was pelleted with centrifugation (10,000g, 30 min, 4°C) and the supernatant cell extract was used for the LspA activity assays.

The LspA signal peptide substrate (sequenced YSGALAACGN) was produced by multiple companies (Anaspec, Fremont, CA and Genscript, Piscataway, NJ) with and without the 3-nitrotyrosine/aminobenzamide donor/quencher pair. The signal peptide without the donor and quencher was used for the HPLC assays and the tagged substrate was used for the fluorescence experiments.

The hydrolysis of the peptide substrate was performed in assay buffer (50 mM tris, pH 8, 1 mM EDTA, 1% DMF, and the appropriate detergent). Varying amounts (μL) of cell extract were incubated at 37°C for up to an hour in assay buffer with 10 to 200 μM substrate. After preincubation, the mixture was quenched with 0.2% TFA, centrifuged at 14,000 rpm for 5 min, and the supernatant was applied to a reversed-phase XBridge BEH 130 C18, 5μm, 4.6 x 100 mm HPLC column (Waters, Milford, MA). The mobile phase separation procedure is a 1 mL/min linear gradient of 10 to 70% solvent B (0.1% TFA in acetonitrile) in 8 min (solvent A is 0.1% TFA in water), followed by 95% solvent A for 7 min. The substrate and products were detected with the UV detector at 255 nm.

The fluorogenic LspA assay was completed using varying amounts of cell extract for the controls and 1 μM LspA PDCs in assay buffer. Upon addition of 100 to 500 μM

tagged substrate, the mixture was excited every 5 minutes at 340 nm and the fluorescent emission at 411 nm was collected over 30 minutes with a Fluoromax-3 fluorometer (Horiba, Kyoto, Japan). Reaction rates were reported in counts per second (CPS) per minute. For the LspA PDC inhibition assays, a final concentration of 0.1 μM globomycin was added to the reaction buffer with enzyme and substrate.

4.5. References

1. Buehler, L. 2015. Cell membranes. Garland Science, New York, New York.

2. Milo, R. 2015. Cell Biology by the Numbers. Garland Science, New York, New York.

3. Moon, C. N. Zaaccai, P. Fleming, D. Gessmann, and K. Fleming. 2013. Membrane protein thermostability may serve as the energy sink for sorting in the periplasm. Proc Natl Acad Sci USA 110: 4285-4290.

4. Mayor, U., N. Guydosh, C. Johnson, G. Grossmann, S. Sato, G. Jas, S. Freund, D. Alonso, V. Daggett, and A. Fersht. 2003. The complete folding pathway of a protein from nanoseconds to microseconds. Nat 421: 863-867.

5. Silhavy, T., D. Kahne, and S. Walker. 2010. The bacterial cell envelope. Cold Spring Harb Perspect Biol: 1-17.

6. Tjalsma, H., G. Zanen, G. Venema, S. Bron, and J. van Dijl. 1999. The potential active site of the lipoprotein-specific (type II) signal peptidase of *Bacillus subtilis*. J Biol Chem 274: 28191-28197.

7. Greenfield, N. 2006. Using circular dichorism spectra to estimate protein secondary structure. Nat Protoc 1: 2876-2890.

8. “Circular dichroism.” *Alliance Protein Laboratories*. 2016. Web. 30. Mar. 2016. < http://www.ap-lab.com/circular_dichroism.htm>

9. Kelly, S. and N. Price. 2000. The use of circular dichroism in the investigation of protein structure and function. Curr Prot Pept Sci 1: 349-384.

10. Zhong, W. and S. Benkovic. 1998. Development of an internally quenched fluorescent substrate for *Escherichia coli* leader peptidase. Anal Biochem 225: 66 – 73.

11. Sutcliffe, I. and D. Harrington. 2002. Pattern searches for the identification of putative lipoprotein genes in Gram-positive bacterial genomes. Microbiol 148: 2065-2077.

12. Lundemose, A., D. Rouch, C. Penn, J. Pearce. 1993. The Chlamydia trachomatis Mip-like protein is a lipoprotein. J Bacteriol 175: 3669-3671.

13. Heinz, E., P. Tischler, T. Rattei, G. Myers, M. Wagner, and M. Horn. 2009. Comprehensive *in silico* prediction and analysis of *Chlamydiae*. BMC Genomics 10: 1-18.

14. Gong, X., Y. Ding, J. Yu, Y. Yao, and F. Marassi. 2015. Structure of the Na/K-ATPase regulatory protein FXYD2b in micelles: implication for membrane-water interfacial arginines. Biochim Biophys Acta 1848: 299-306.

15. Mayo, K., A. De marco, E. Menegatti, and R. Kaptein. 1987. Interaction of epidermal growth factor with micelles monitored by photochemically induced dynamic nuclear polarization-1H NMR spectroscopy. J Biol Chem 262: 4899-4904.

16. Aulisa, E. and D. Gilliam. 2015. A practical guide to geometric regulation for distributed parameter systems. CRC Press, Boca Raton, FL.

Chapter 5: Small angle scattering of detergent-rich bicelles

Scattering techniques have been employed for the studies of biological systems over the last thirty years with the introduction of many powerful X-ray and neutron facilities around the world.[1] Small angle scattering (SAS) can be used to study the structure, kinetics, and interactions of macromolecules, nanocomposites, alloys, and synthetic polymers in the 10 to 1000 Å range.[2] Common biological structures studied with these methods are complex macromolecular aggregates, protein assemblies, organic polymers, and protein-surfactant complexes.

Small angle scattering was introduced in 1930s with the thesis work of Andre Guinier on metallic alloys.[3] Guinier's early observations in 1938 on the Al-Cu alloy led to the discovery that the scattering of X-rays at small angles can provide not only information on the sizes and shapes of particles but also the internal structure of disordered and partially ordered systems.[4] The method gained popularity in the study of biological systems in solution in the 1960s when low-resolution structural information, shape, and internal composition of the system could be determined without crystallography.[2] Since the 1970s the construction of large scale facilities, such as high flux reactors and spallation sources for neutrons and synchrotron radiation X-ray sources, has been a major advancement for SAS.[2]

Although there was a decline of interest in SAS with progress in other structural methods in the 1980s, the 1990s brought another breakthrough in the technique.[2] SAS data analysis methods were greatly improved, allowing *ab initio* shape and domain structure determination and detailed modeling of macromolecular complexes.[2] The instrumentation also advanced, with sub-millisecond time resolution achieved on the

third generation synchrotron radiation sources.[2] Bertram Brockhouse and Clifford Schull brought SAS to the forefront most recently with their work in the development of neutron scattering techniques and neutron spectroscopy, winning a Nobel Prize in Physics in 1994.

In this chapter, these advanced SAS methods, specifically, small angle neutron scattering (SANS), are being utilized for the structural characterization of detergent-rich bicelles.

5.1. Small angle scattering principles and methodology

5.1.1. Small angle scattering theory

Scattering measurements can be done with X-rays or neutrons. Upon interaction of the beam with the sample (called the incident) X-rays or neutrons scatter from the sample. The scattering results from differences in the sample's electron density in the case of X-rays, and differences in nuclear density in respect to neutron scattering. While the fundamental principles of small angle scattering remain the same, there are differences, benefits, and disadvantages of small angle X-ray scattering (SAXS) vs. SANS methods that will be discussed in the next section.

X-rays and neutrons have wavelike properties, including amplitude and phase. In a typical SAS experiment, the X-rays or neutrons are directed toward a dilute, homogeneous sample in physiological buffer. The sample is then exposed to the collimated X-ray or neutron beam. Upon interaction, the X-rays or neutrons are scattered from their original straight trajectory at a small angle, 2θ, of 0.1 to 10° (Figure 5.1) with a scattering vector of Q (The scattering vector Q is typically lowercased; however, to

prevent confusion with the bicelle lipid-to-detergent ratio, q, uppercase Q for the scattering vector is used in this thesis).[2] The light can scatter elastically or inelastically. In elastic scattering, the kinetic energy of the incoming X-ray or neutron does not change after being scattered from the sample, resulting in no loss in the magnitude of the wave vector. With inelastic scattering the kinetic energy of the scattered X-rays or neutrons is altered from those coming from the beam source. Inelastic scattering changes both the direction and magnitude of the wave vector. The scattering can also be described with respect to coherence. Coherent scattering is dependent on the scattering vector, Q, and can provide structural, spatial correlation, and collective motion information. Incoherent scattering is Q-independent and contributes to the background scattering noise. It is the elastic, coherent scattering that provides the useful structural information from small angle scattering.

The scattering vector, Q, specifically refers to the difference between the incident wave vector k_i and the final wave vector, k_f, after sample interaction. Q typically has units in reciprocal space, nm^{-1} or $Å^{-1}$, and is defined as:

$$Q = \left|k_i - k_f\right| = \frac{4sin\theta}{\lambda} \quad [1]$$

This equation can be substituted into Bragg's Law of Diffraction

$$\lambda = 2dsin(\frac{\theta}{2}) \quad [2]$$

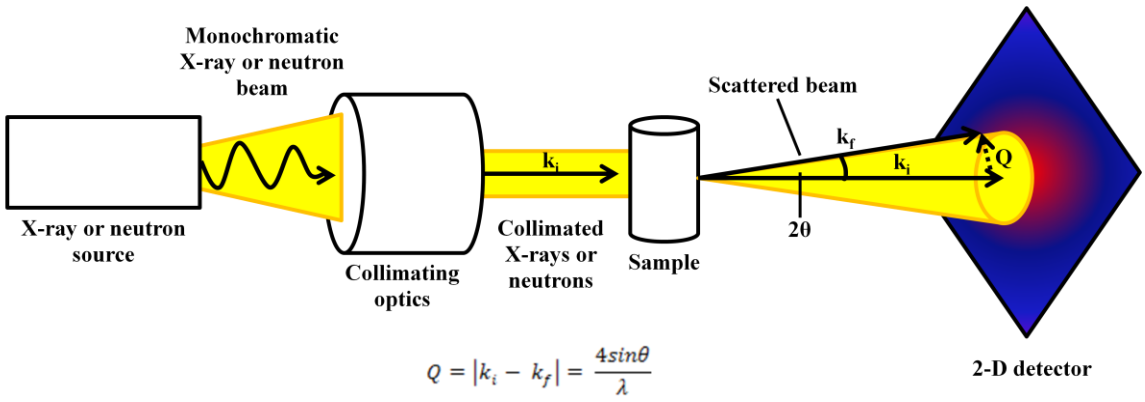

Figure 5.1. SAS experiment design. Collimated X-rays and neutrons contact the sample via an incident wave vector, k_i. The light scatters at a small angle, 2θ, along a final wave vector, k_f. The scattering vector, Q, is the difference between the incident and final wave vectors, and also relates to the wavelength of the light source, λ.

to yield a useful expression that relates Q with d, distance.

$$Q = \frac{2\pi}{d} \text{ [3]}$$

Low-Q (0.01 $Å^{-1}$) scattering data is indicative of larger interactions (500 Å) and high-Q (0.3 $Å^{-1}$) scattering gives more information about smaller distances (10 Å).[1]

The most fundamental difference between X-ray and neutron scattering is the mechanism by which the incident radiation interacts with matter. This interaction can be described in terms of the scattering length, b, and scattering cross-section, σ. X-rays are scattered by the electrons surrounding atomic nuclei, and its scattering length is defined as

$$b = Zr_0 \text{ [4]}$$

where Z is the number of electrons and r_0 = 2.82 x 10^{-13} cm is the Thomson electron radius. Scattering length is typically in units of cm. The X-ray scattering cross-section is

$$\sigma = 4\pi(Zr_0)^2 \text{ [5]}$$

where the units for σ is cm^2. The scattering length and cross-section for SAXS vary in direct proportion to the number of electrons present, increasing with atomic number.

Contrary to X-ray scattering, the scattering length and cross-section of neutrons depends on the interaction between the neutron and a given nucleus and varies irregularly with each element; even isotopes of the same element have different b and σ (Table 5.1). Herein lies an advantage of SANS over SAXS: hydrogen and deuterium have different b and σ, and unlike X-rays, neutrons can "see" deuterium and differentiate it from

Element	b_N (10^{-12} cm)	σ (10^{-24} cm^2)
H	-0.374	1.76
D	0.667	5.59
C	0.665	5.56
N	0.940	11.1
O	0.580	4.23
P	0.517	3.31
S	0.284	2.16

Table 5.1. Neutron scattering lengths and cross-sections. The neutron scattering lengths (b_N) and scattering cross-sections (σ) of different elements, including the isotope deuterium, is tabled. An advantage of SANS is the differences between the scattering of hydrogen and deuterium, which can be exploited with contrast variation experiments.

hydrogen. This is essential to the benefits of SANS experiments, and will be described in further detail in the Section 5.1.3.

Regardless of the differences in scattering lengths and cross-sections, both SAXS and SANS scattering are dependent on the scattering length density (SLD), ρ. SLD is defined as the scattering length of N atoms divided by the volume of the atoms:

$$\rho = \frac{\Sigma^N b}{V_m} \text{ [6]}$$

Σ^N is the sum of the scattering length contributions from N atoms and V_m is the molecular volume. The molecular volume can be computed using the bulk density of the material (ρ_m), molecular weight (M), and Avogadro's constant (N_A)

$$V_m = \frac{M}{\rho_m N_A} \text{ [7]}$$

to yield this solvable equation for SLD with units of $Å^{-1}$.

$$\rho = \frac{\rho_m N_A \Sigma^N b}{\Sigma M} \text{ [8]}$$

The SLD difference between the particle and solvent, also known as the net particle scattering or contrast (Δρ), is essential to SAS experiments. Without this contrast, there is no scattering.

The basic Rayleigh-Gans-Debye scattering equation defining the scattering intensity, I(Q), for an ensemble of a randomly oriented macromolecule is:

$$I(Q) = \Delta\rho^2 \varphi_P V_P P(Q) S(Q) \text{ [9]}$$

This equation takes into account the SLD difference in scattering, or contrast ($\Delta\rho$), the volume fraction of particles (φ_P), volume of each particle (V_P), form factor (P(Q)), and structure factor (S(Q)). The form factor accounts for the particle size and shape, while the structure factor represents particle interactions, interference, or matrix effects. Most scattering data is plotted in terms of I (Q) vs. Q, or is Fourier transformed into a P(r) distance distribution function, and these scattering profiles provide structural information about the sample.

5.1.2. SAXS vs. SANS

SAXS and SANS are advantageous for several reasons. These techniques can probe structures of 1 nm to 1 μm lengths, providing information on the overall size, shape, and spatial relationship of the sample. This information can be learned in real time, allowing for the analysis of the system under a variety of environmental conditions.

As mentioned earlier, SAXS and SANS experiments are distinguished by their beam source and the process in which the incident radiation interacts with the sample. X-rays interact with electrons surrounding the atomic nuclei, while neutrons interact with the nuclei, resulting in more uniform scattering lengths and cross-sections for X-ray scattering that increases with atomic number in comparison to the random values for neutron scattering. This irregular scattering pattern for SANS experiments has three advantages: 1) Identifying light atoms, such as hydrogen, in the presence of heavier ones, is easier 2) neighboring elements in the periodic table have significantly different scattering and can be identified, and 3) isotopes of the same element can be distinguished.[2] This difference in hydrogen vs. deuterium scattering is a major advantage

for SANS methods. SANS contrast variation experiments use this advantage to distinguish different components of a sample, i.e. a hydrogenated micelle vs. deuterated protein. Contrast variation experiments can be completed only with SANS, and will be described in depth in Section 5.1.3.

Due to its relatively weak interaction with the nucleus, the neutron is a highly penetrating probe. Therefore, SANS experiments can characterize the interior of a sample, rather than only the surface layer probed by SAXS. The neutron is also nondestructive, unlike X-rays, and is suitable for high temperatures. Neutron experiments are completed over a few hours, while SAXS measurements can be completed in minutes. SAXS has the superior time resolution as well, with millisecond time-resolved structural and conformational analysis compared to the second time regime of SANS experiments.

The major disadvantage of SAXS and SANS is that both methods provide only low resolution structural information (> 10 Å).[1] This low resolution regime gives an idea of aggregation, conformation, stoichiometry, and particle size and shape. Also, there are no small laboratory sources available to conduct SANS, and less than 50 SANS instruments exist worldwide. While SAXS instruments are more common, the higher resolution data can only be obtained at the few facilities with a high flux synchrotron.

5.1.3. SANS contrast variation and multi-component systems

As stated previously, small angle scattering can only occur when there is contrast, $\Delta\rho$, between the scattering length densities of the particle and the solvent. Hydrogen and

deuterium have significantly different scattering lengths in SANS; similarly, the SLDs of H_2O and D_2O vary considerably (Table 5.2). Contrast variation, or contrast matching, experiments can be completed that exploit this contrast requirement, using the differences in hydrogen and deuterium scattering to identify structural features of a system.

Biological SAS methods are typically completed by obtaining the scattering of the overall system, which is usually a sample (e.g. a protein in a bicelle) in water. These experiments would not be able to distinguish between the two components, and the scattering profile would be representative of the entire system. Contrast variation is completed by deuterating one component of the system (i.e. a perdeuterated protein) and leaving the other component (i.e. a bicelle) fully hydrogenated (Figure 5.2).

This example of the perdeuterated protein in a hydrogenated bicelle can be used to describe a typical contrast variation experiment. SANS of the protein-bicelle complex in water will result in a loss of contrast between the H_2O and the hydrogenated bicelle, and all scattering of this system will only result from the deuterated protein. Inversely, the scattering of the perdeuterated protein in the bicelle in D_2O solvent will only represent the hydrogenated bicelle. With these contrast variation experiments, each component of the system can be distinguished depending on the D_2O concentration in the solvent. In addition to the scattering of each system, experiments can be completed to determine the overall percentage of D_2O in the solvent required to eliminate the scattering for the entire system. This percentage of D_2O is called the contrast match point, or CMP.

Material	**ρ (10^{-6} Å^{-2})**
0% D_2O (100% H_2O)	-0.56
10% D_2O	0.14
20% D_2O	0.83
30% D_2O	1.52
40% D_2O	2.20
50% D_2O	2.91
60% D_2O	3.59
70% D_2O	4.28
80% D_2O	4.96
90% D_2O	5.65
100% D_2O	6.33

Table 5.2. Scattering length densities (SLD) of water with increasing D_2O concentrations. Water has a different SLD (ρ) than D_2O, which is utilized for SANS contrast variation experiments.

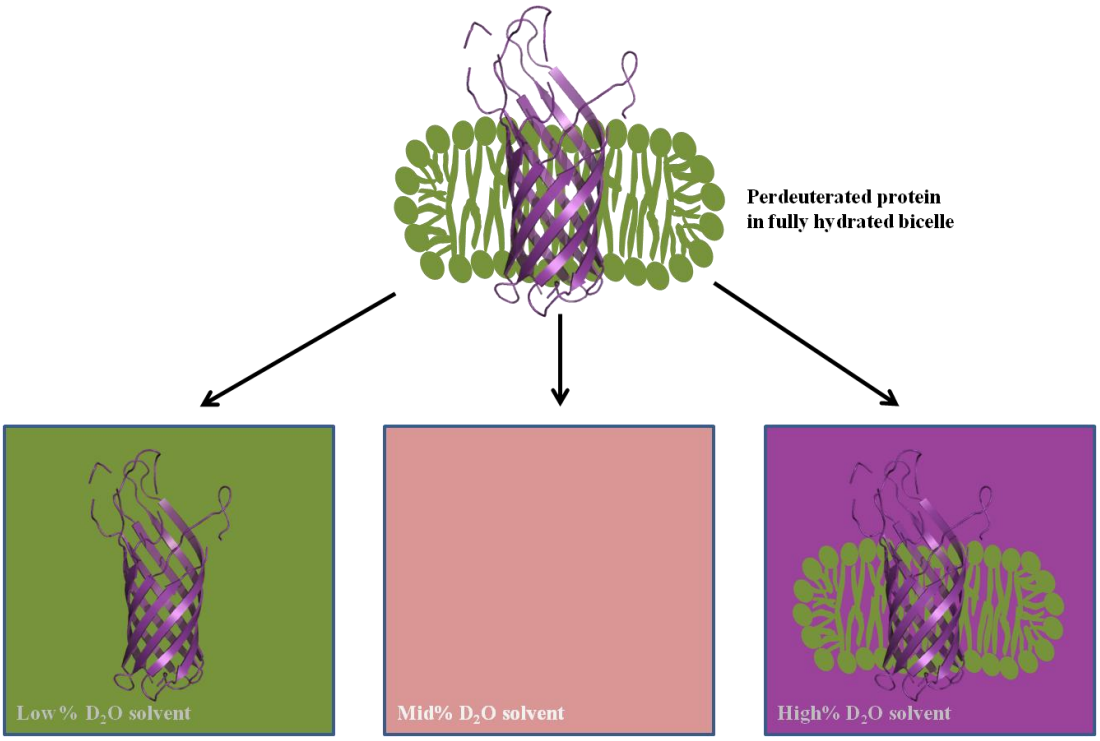

Figure 5.2. Example of SANS contrast variation. The perdeuterated protein (purple) embedded in the fully hydrated bicelle (green) can be dialyzed into buffers with varying D_2O concentrations. When exposed to 0% D_2O solvent, contrast is lost between the hydrated bicelle and the solvent, and resulting scattering is only from the protein. By dialyzing the complex in 100% D_2O buffer, contrast between the protein and solvent is abolished, and scattering is representative of only the bicelle. There is a CMP between 0 and 100% D_2O that matches out the entire complex, and there is no scattering.

Typical contrast variation experiments are completed on the same partially deuterated system at multiple concentrations of D_2O in the buffer, called contrast points. This enables the researcher to obtain systematic snapshot views of the complex. The scattering observed from this system at each contrast point is described as:

$$I(Q) = \Delta\rho_1{}^2 I_{11}(Q) + \Delta\rho_2{}^2 I_{22}(Q) + \Delta\rho_1\Delta\rho_2 I_{12}(Q) \quad [10]$$

where $I_{11}(q)$ and $I_{22}(q)$ describe the basic scattering functions originating from each component, and $I_{12}(q)$ represents the cross-term scattering.

Contrast variation experiments described in this thesis were completed with d54-DMPC lipids that contained deuterated alkyl tails and hydrogenated phosphocholine head groups, and fully hydrogenated DHPC detergent. These bicelles represent a three component system containing: 1) the identical d54-DMPC and DHPC hydrogenated phosphocholine head groups, 2) the deuterated d54-DMPC carbon tails, and 3) the hydrogenated DHPC alkyl tails (Figure 5.3).

5.2. Previous work and project motivation

The ideal bicelle is often discussed by researchers as the hybrid between detergent micelles and liposomes, consisting of distinctly separated lipid bilayer and detergent rim domains. This notion of complete separation between the bicelle components is often debated, and yields interesting questions about bicelle formation and composition.

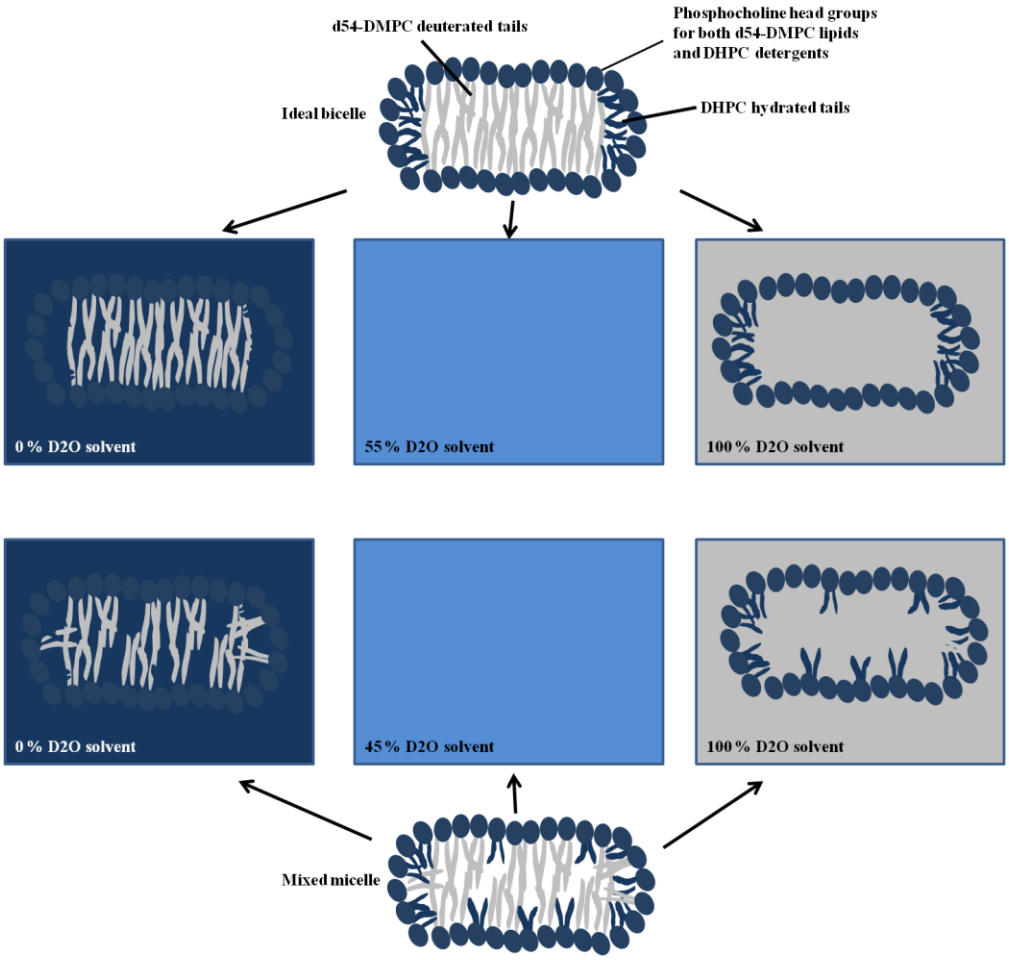

Figure 5.3. d54-DMPC/DHPC bicelle SANS contrast variation experimental design. The three component bicelle composed of deuterated DMPC lipid tails and fully hydrated DHPC tails surrounded by a hydrated phosphocholine head group shell. Contrast variation highlights the differences between the ideal bicelle and a "mixed micelle" bicelle. In 0% D_2O solvent, scattering is observed for the lipid core and depicts an ellipsoidal shape. In 100% D_2O, scattering is seen for the hydrated head groups and rim, forming a shell-like structure. Between 40 and 65% D_2O, depending on q-ratio, the CMP is reached, abolishing scattering from the entire system. With more hydration within the bicelle core, the CMP for "mixed micelle" bicelles will be slightly lower than the CMP for ideal bicelles.

While biophysical investigations of lipid-rich bicelles confirm ideal bicelle-like structures, it is less likely that detergent-rich bicelles follow the same trend.[5] Detergents have the propensity to form micelles in aqueous environments; therefore, detergent-rich bicelles are likely to have some degree of mixing between its amphiphile components, forming mixed micelles instead of ideal bicelles. To test the validity of the ideal model, the size and shape of detergent-rich bicelles are being investigated.

SAS techniques are useful tools to probe bicelle structure. Initial bicelle SAXS experiments by Ryan Oliver were conducted with DMPC and DHPC mixtures of lipid-to-detergent ratios (q-ratios) from 0.1 to 1.0 in 0.1 increments. These low q-ratios represented the detergent-rich bicelle regime. Several total amphiphile concentrations, C_L, were studied, including 1.5 and 6% (w/v) at 6, 25, and 40°C. A major observation of the SAXS data was that an increase in lipid concentration results in the aggregate transitioning from smaller structures to a larger system. As q was increased from 0.1 to 0.5, each SAXS profile was different, indicating that the DMPC and DHPC are well mixed and form a different structure with each systematic addition of the lipid component (Figure 5.4). Scattering profiles from q = 0.5 to 1.0 depict only minor differences, indicating that the overall size and shape formed by the aggregates are similar.

Radii of gyration (R_g) were measured with Guinier analysis of the data, and L, the dominant head group to head group distance, was determined by using the position of the second maximum ($L = 2\pi/Q_{max}$) (Table 5.3). L is measured from the center of one head group to the center of the opposing head group on the opposite side of the bicelle.

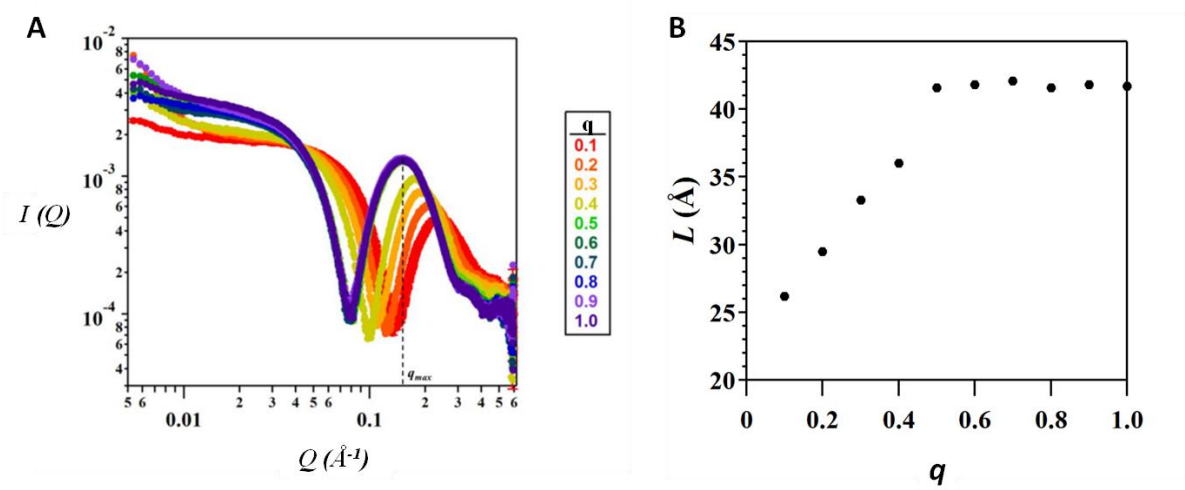

Figure 5.4. Experimental SAXS profiles of DMPC/DHPC bicelles. (A) SAXS data collected for bicelles at incremental q-ratios (0.1 to 1.0) at C_L = 6% (w/v) and 25°C. Dominant head group to head group distance, L, is determined from the position of the 2nd maximum, Q_{max}. The Q_{max} of q = 1.0 bicelles is designated with a dotted line. (B) Dominant head group to head group distances (L) measured in respect to q-ratio. SAXS profiles reflect a linear transition from q = 0.1 to 0.5, followed by a plateau from 0.5 to 1.0.

q	R_g (Å)	L (Å)
0.1	18.0	26.2
0.2	19.7	29.5
0.3	22.8	33.3
0.4	27.1	36.0
0.5	33.5	41.6
0.6	33.2	41.8
0.7	33.9	42.1
0.8	32.5	41.6
0.9	34.5	41.8
1.0	34.3	41.7

Table 5.3. Measured radii of gyration and dominant head group to head group distances of DMPC/DHPC bicelles. SAXS profiles of DMPC/DHPC bicelles at C_L = 6% at 25°C were analyzed with a Gunier fit to determine R_g. Dominant head group to head group distance, L, is determined from the position of the 2nd maximum.

Therefore, using carbon bond lengths and the phosphocholine head group size, the expected L for a pure DMPC bilayer is approximately 44.4 Å and 24.2 Å for a pure DHPC micelle. The L for the q = 0.1 bicelles is 26.2 Å, and increases until q = 0.5, where the average L remains approximately 41.8 Å. These values indicate that detergent-rich bicelles (q = 0.1) form DHPC-like micelles and transition to a DMPC bilayer morphology with increased lipid concentration. The R_g of the data provided by Guinier analysis corresponds well to the trends in L. These promising initial results led to the interest in gaining more structural information about these detergent-rich bicelles.

To capture this transition from micelle-sized aggregates to bicelle-like structures, SANS was utilized to probe more dimensions of the lipid-detergent mixtures. SANS contrast variation experiments were completed with q = 0.3 and 0.7 d54-DMPC/DHPC bicelles at C_L = 1.5 and 6% (w/v) and T = 25 and 40°C in solvents with varying D_2O concentrations (Figure 5.5). q = 0.3 and 0.7 were chosen to analyze with SANS because these structures represent both the mixed micelle and bicelle regimes. Contrast match points were determined using the x-intercept of a 2^{nd} order polynomial fit to I(0)/c vs. fraction of D_2O in the solvent. The match point for q = 0.3, C_L = 6% bicelles was 34.1% D_2O, slightly less than the 43.6% CMP for q = 0.7 bicelles. Because the deuterated lipid tails are matched with higher D_2O concentration in the solvent, this increase in CMP with higher Q values was expected. These CMP values did not differ substantially with the C_L = 1.5% bicelles.

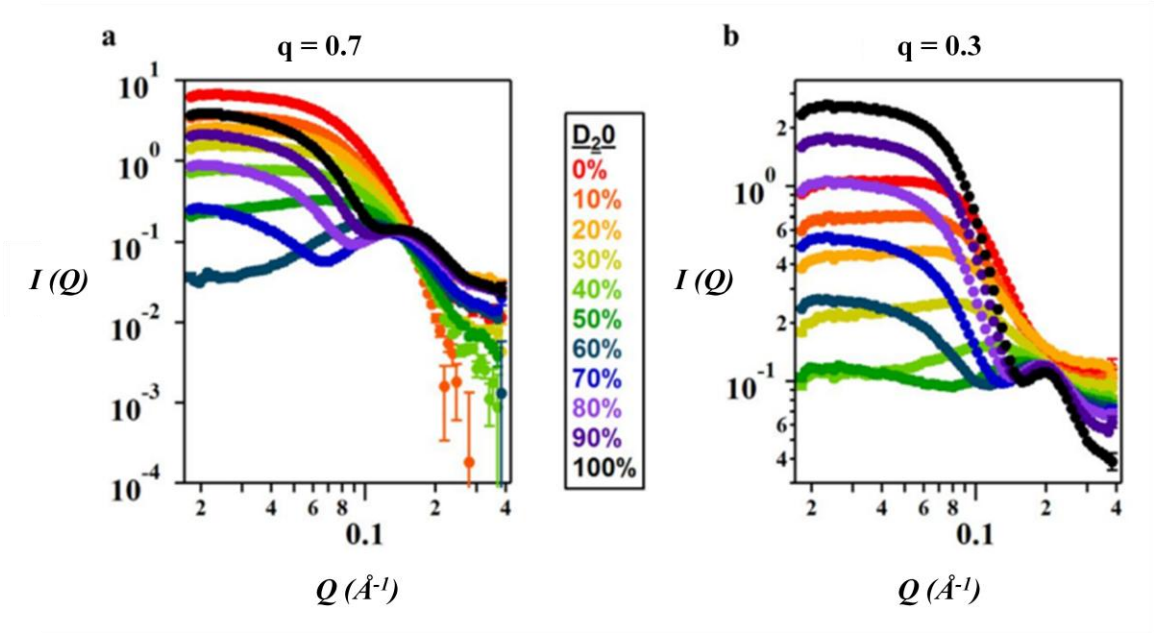

Figure 5.5. SANS contrast variation series of DMPC/DHPC bicelles. Scattering was collected at C_L = 6% (w/v) and 1.5% (not pictured) and 25°C of a) q = 0.7 and b) q = 0.3 bicelles. D_2O concentration in solvent is designated by color.

Although preliminary analysis of the scattering data resulted in determining the Rg, L, and CMP of these low-Q bicelles, the head group shell thickness, overall length, and radius can be determined by fitting the SANS data with a core-shell bicelle model. The dimensions obtained from properly fitting the SANS data can confirm a change in aggregate size with q-ratio and monitor the transition from micelle to bicelle, challenging the ideal bicelle model for detergent-rich bicelles.

5.3. Structure and composition of d54-DMPC/DHPC bicelles

5.3.1. Core-shell bicelle model

SANS data is analyzed using multiple software packages. SASView facilitates the fitting of the data to shape-dependent, shape-independent, and custom models. Choosing the correct model is essential to obtaining accurate dimensions of the bicelles. Because the d54-DMPC/DHPC aggregates consist of a hydrocarbon core surrounded by an outer shell of phosphocholine head groups, the model used for the analysis is the core-shell bicelle model (Figure 5.6). Core-shell models allow for variations in the SLDs for the shell vs. core. The core-shell bicelle model is a derivative of the cylinder and core-shell cylinder models. The cylinder model represents a circular cylinder, while the core-shell cylinder model is almost identical but accounts for an outer shell layer. The difference between the core-shell cylinder and core-shell bicelle model is that the bicelle shell parameters are separated into a face-shell and rim-shell, and these values can be varied for different shell thicknesses and SLDs around the aggregate.

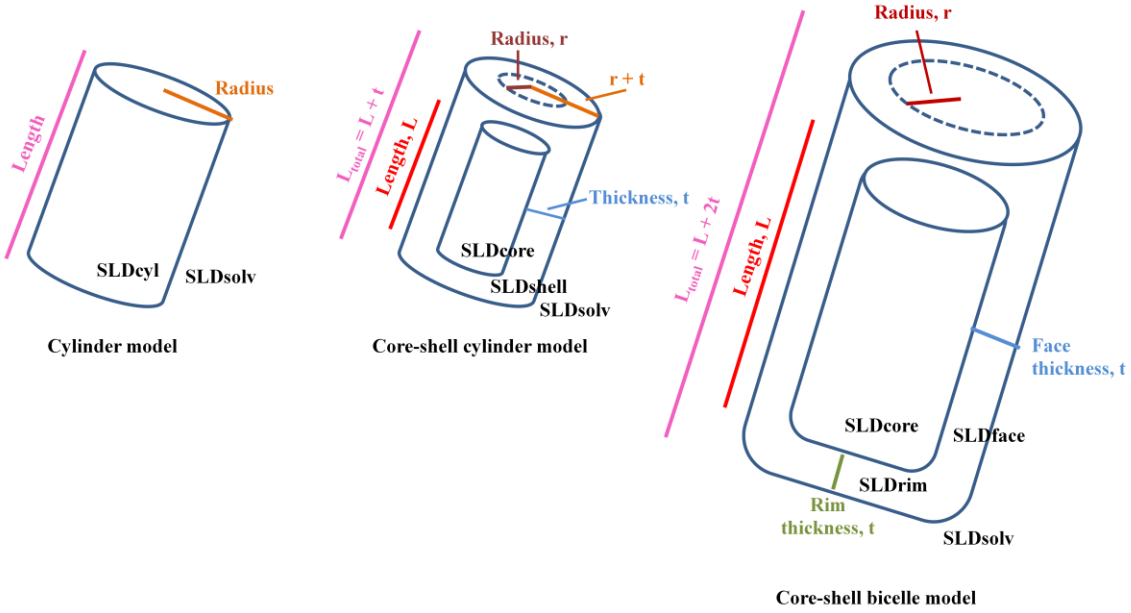

Figure 5.6. Core-shell models for SANS fitting. The core-shell bicelle model used to fit the SANS contrast variation data is derived from the cylinder and core-shell cylinder models. The addition of the different face and rim shell thicknesses and SLDs distinguish the core-shell bicelle fit from the other models.

The cylinder model provides the form factor for a monodisperse circular cylinder and is normalized by the particle volume. As mentioned above, the form factor represents the particle size and shape, and for the cylinder model is calculated as:[4]

$$P(Q) = \frac{scale}{V_{cyl}} f^2(Q) + bkg \quad [11]$$

where

$$f(Q) = 2\left(\rho_{cyl} - \rho_{solv}\right)V_{cyl} \frac{\sin\left(QLcos\frac{\alpha}{2}\right)}{QLcos\frac{\alpha}{2}} \frac{J_1(Qrsin\alpha)}{(Qrsin\alpha)} \quad [12]$$

and

$$V_{cyl} = \pi r^2 L \quad [13]$$

V_{cyl} is the volume of the cylinder. α is defined as the angle between the cylinder axis and the scattering vector, Q. The function *f(Q)* averages the form factor over all possible orientations of the cylinder with respect to Q. L is the length of the cylinder and r is the radius. j_1 is a first order Bessel function representing cylindrical symmetry and coordinates. The returned value is in units of cm^{-1} on an absolute scale.

The core-shell cylinder form factor is derived from the cylinder model but includes the contrast between the core and shell and the shell and solvent such that:[6]

$$f(Q,\alpha) = 2(\rho_{core} - \rho_{shell})V_{core} \frac{\sin\left(QLcos\frac{\alpha}{2}\right)}{QLcos\frac{\alpha}{2}} \frac{J_1(Qrsin\alpha)}{(Qrsin\alpha)} + 2(\rho_{shell} -$$

$$\rho_{solv})V_{shell} \frac{\sin\left(Q(L+2t)cos\frac{\alpha}{2}\right)}{Q(L+2t)cos\frac{\alpha}{2}} \frac{J_1(Q(r+t)sin\alpha)}{(Q(r+t)sin\alpha)} \quad [14]$$

where t is the shell thickness, r is the radius of the core, the outer radius of the shell is given by r + t, and the total length is given by L + 2t. V_{shell} is the volume of the outer shell (i.e. the total volume, including the shell):

$$V_{shell} = \pi(r+t)^2(L+2t)[15]$$

The core-shell bicelle model is a more general case of this core-shell cylinder model form factor, enabling differences in the face and rim shells.

The core-shell bicelle model allows for the tuning and determination of several parameters including scale (unit-less), background (cm^{-1}), radius, length, rim thickness, and face thickness in Angstroms. SLDs (in units of $Å^{-2}$) of the core, rim, face, and solvent can be altered as well to get a fit to the scattering data (Table 5.4).

5.3.2. Determination of scattering length densities for core-shell bicelle fits

The experimental SANS data for the 0.3 and 0.7 bicelles were fit using the core-shell bicelle model described above. Although there are 10 parameters that can be adjusted to obtain the best fit, there are several parameters such as the scattering length densities (SLDs) that are held constant based on several assumptions placed on the system. By keeping the SLDs constant, the fitting process is more systematic and allows for trends in bicelle size and shape to be identified.

SANS contrast variation experiments were utilized by measuring the contrast of bicelles in solvents with different concentrations of D_2O. The solvent SLD was set at different values depending on this D_2O percentage in solution. As demonstrated with Equation 8, each solution has a different SLD depending on the scattering length of the

Parameter	Units	Default value
Background	cm-1	0
Scale	none	1
SLDcore	$Å^{-2}$	1×10^{-6}
SLDrim	$Å^{-2}$	4×10^{-6}
SLDface	$Å^{-2}$	4×10^{-6}
SLDsolvent	$Å^{-2}$	1×10^{-6}
Face thickness	Å	10
Rim thickness	Å	10
Radius	Å	20
Length	Å	400

Table 5.4. SASView core-shell bicelle parameters. The several parameters for fitting the bicelles are tabled. The SLD values of the core, face, rim, and solvent can be assigned to the core-shell bicelle fit as well as the face and rim thickness, radius, and length. Background and scale are useful when overlaying the fit with the experimental data.

molecule and the molecular volume. Therefore, H_2O has a smaller SLD (-5.61 x 10^{-7} $Å^{-2}$) than D_2O (6.33 x 10^{-6} $Å^{-2}$). Table 5.2 is a table representing all of the SLD values given to the different experimental solvents.

The face and rim SLDs of the d54-DMPC/DHPC bicelles were determined by assuming a uniform phosphocholine head group shell around the entire bicelle. To determine the SLD of the face and rim shells with Eqn. 8, the chemical composition of the head group ($C_8H_{14}NOP$) was used to estimate the sum of the scattering lengths. The

density of the phosphocholine head group was determined at 1.69 g/cm^3 by estimating the molecular weight and head group volume; this density was used to determine the molecular volume. The SLD of the phosphocholine head group was estimated with these values at 2.21 x 10^{-6} $Å^{-2}$. Preliminary fits of the scattering data constrained the face SLD and rim SLD to ± 1.0 x 10^{-6} $Å^{-2}$ to get an initial size and shape of the bicelles. As the fits were refined, this wide range of SLDs was narrowed significantly.

The core SLD was determined using the d54-DMPC and DHPC tail SLDs. Both tail SLDs were estimated similarly to the SLD of the phosphocholine head groups, using the molecular volume and the chemical composition. The SLD of d54-DMPC tails is 6.91 x 10^{-6} $Å^{-2}$ and the SLD of the DHPC tails is -4.65 x 10^{-7} $Å^{-2}$. Because of the unknown degree of mixing between the d54-DMPC and DHPC molecules, preliminary bicelle fits were completed allowing this wide range of core SLD values. As the fits improved, the core SLDs of the bicelles were refined.

5.3.3. Systematic generation of bicelle fits

5.3.3.1. Preliminary q = 0.3 bicelle fits

Preliminary q = 0.3 bicelle fits contained the fit parameters outlined in Table 5.5. The initial fits allowed for a wide range of core SLDs, compensating for possible mixing between the deuterated and hydrated tails. The fits also had a wide range of face and rim SLDs ($2.21 \pm 1 \times 10^{-6}$ Å^{-2}) and bicelle size dimensions. The face and rim thickness was allowed to vary between 5 and 10 Å, the length from 40 to 100 Å, and the radius ranged from 20 to 35 Å. These preliminary fits were generated for two purposes: 1) gain familiarity with the software, and 2) to get an idea of the size and shape of the bicelle without over-constraining the fits.

With widely ranged parameters, trends were identified with initial q = 0.3 bicelle fits in 0, 20, 60, 80, and 100% D_2O solvent (Figure 5.7 and Table 5.6). The fits suggested a face and rim thickness of 6.5 to 8 Å, a radius between 20 and 30 Å, and a length that varied from 30 to 60 Å. These values were reasonable, given the dimensions of a phosphocholine head group size and the lengths of the DMPC tails; however, the wide values for the core SLD required more constraining to confirm the fit and size dimensions.

Scattering experiments explore systems in reciprocal space, and the scattering vector, Q, can act as an inverse yard stick. Thus, low-Q scattering data relates to large structures and aggregates while high-Q data represents shorter distances. To monitor this inverse relationship, plots of the face/rim thickness vs. radius, face/rim vs. length, and radius vs. length were generated using the preliminary q = 0.3 bicelle fits (Figure 5.8). As expected, alterations in larger bicelle dimensions, such as length and radius, resulted in vast changes in the low-Q domain of the fits. Differences in the radius also affected the fits in the mid-Q range, specifically the slope in that region. Changes in the shorter

Parameter	1st gen.	2nd gen.	3rd gen.	4th gen.
SLDcore (* 10^{-6} Å^{-2})	3.22 ± 3.7	3.22 ± 3.7	3.22 ± 3.7	q = 0.3, 1.75 q = 0.7, 4.74
SLDrim (* 10^{-6} Å^{-2})	2.21 ± 1.0	2.50 ± 0.5	2.50 ± 0.3	2.1
SLDface (* 10^{-6} Å^{-2})	2.21 ± 1.0	2.00 ± 0.5	2.10 ± 0.3	2.1
Face thickness (Å)	7.5 ± 2.5	5.5 ± 4.5	5.5 ± 4.5	5 ± 3
Rim thickness (Å)	7.5 ± 2.5	5.5 ± 4.5	5.5 ± 4.5	5 ± 3
Radius (Å)	27.5 ± 7.5	20 ± 15	20 ± 15	20 ± 5
Length (Å)	70 ± 30	55 ± 45	55 ± 45	q = 0.3, 24 ± 4 q = 0.7, 70 ± 4

Table 5.5. Four generations of core-shell bicelle fit constrained parameters. Initial bicelle fits were generated with q = 0.3 bicelles and wide ranges for the SLDs and size dimensions. As the fits improved, narrowed restraints were placed on the bicelle parameters to obtain uniform SLDs and constrained dimensions to compare with other q-ratios.

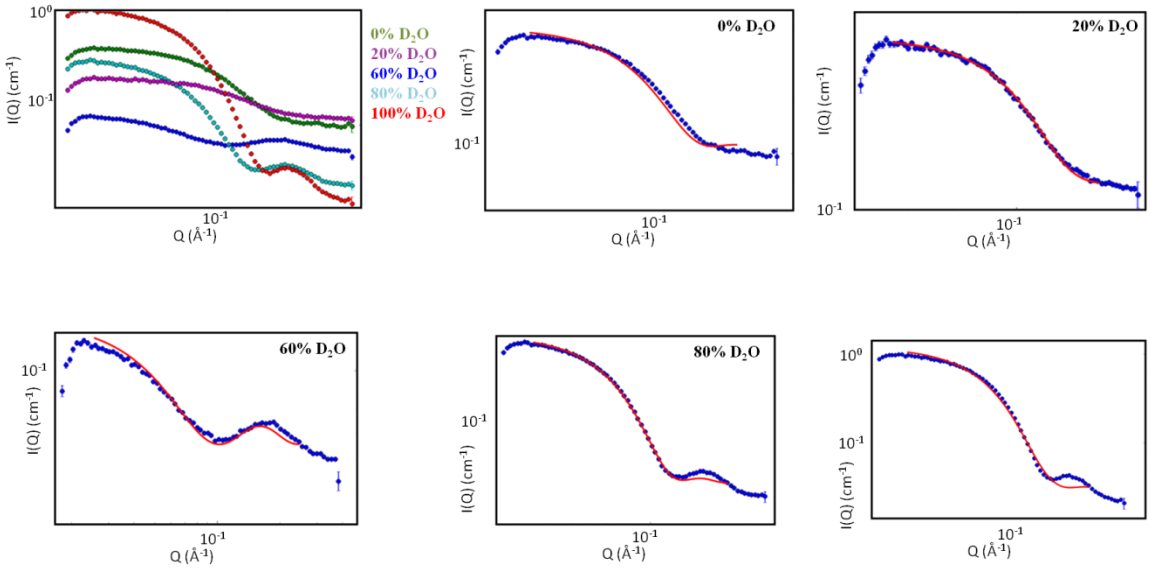

Figure 5.7. First generation q = 0.3 bicelle fits. The q = 0.3 contrast series was measured at C_L = 1.5% in 0, 20, 40, 60, 80, and 100% D_2O at 25°C. The 40% D_2O scattering profile was near the CMP, resulting in little contrast and scattering, and omitted for fitting. Fit shown in red. The bicelles in solvent with D_2O concentrations before CMP had less intensity, and flatter scattering profiles. For a better view of the fits, these profiles were zoomed in.

	0% D_2O	20% D_2O	60% D_2O	80% D_2O	100% D_2O
SLDcore (* 10^{-6} Å^{-2})	6.33	-0.93	4.63	2.50	-0.47
SLDrim (* 10^{-6} Å^{-2})	1.21	1.48	1.21	1.21	2.04
SLDface (* 10^{-6} Å^{-2})	2.99	1.86	2.99	3.00	2.99
Face thickness (Å)	7	7	7.5	7.5	7.5
Rim thickness (Å)	7	7	7.5	7.5	7.5
Radius (Å)	20	20	20	20	20
Length (Å)	40	30	40	30	60

Table 5.6. First generation q = 0.3 bicelle fits. The q = 0.3 bicelles in varying D_2O concentrations were analyzed with the core-shell bicelle fit (Figure 5.8). Because of the wide range of SLDs allowed for the SLD core, the SLDcore differs greatly between the q = 0.3 samples. The 1st generation fits identified starting values for the face and rim thickness, radius, and length.

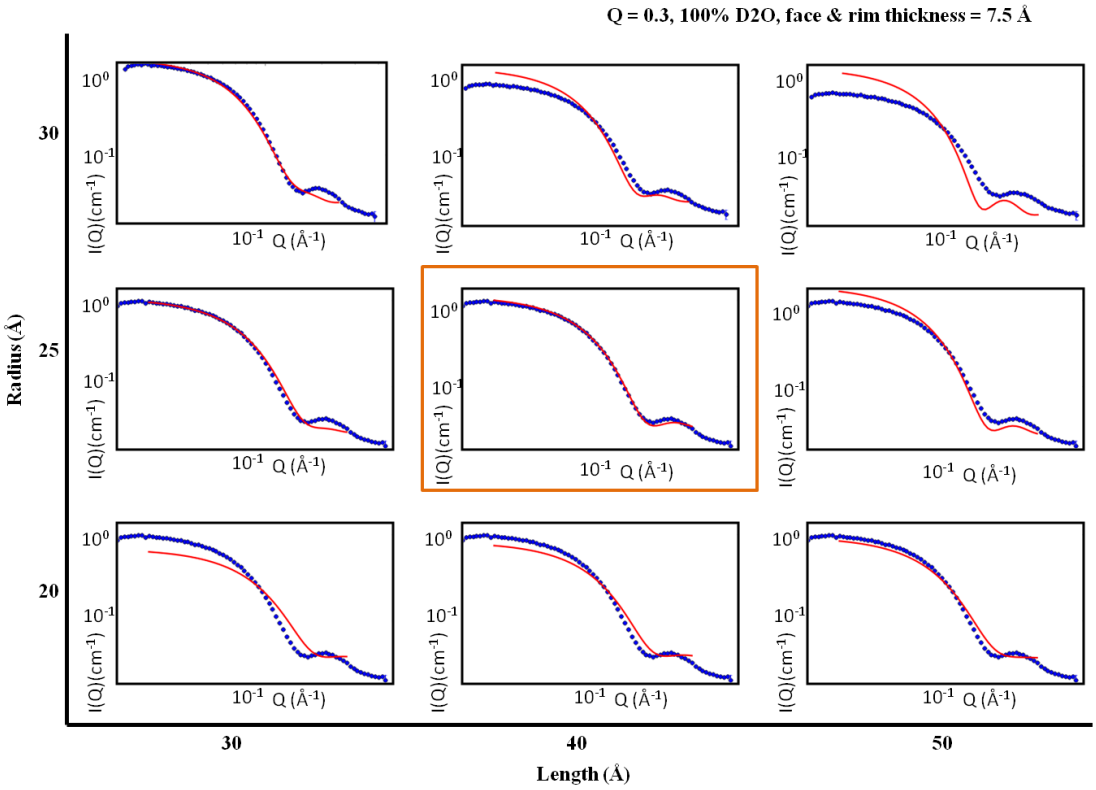

Figure 5.8. Preliminary bicelle fits plotted in respect to radius vs. length. Bicelle scattering data was collected with q = 0.3 bicelles in 100% D_2O at C_L = 1.5% (w/v) at 25° C. With the face and rim thickness at 7.5 Å, the radius and length were varied to monitor how each parameter contributes to the fit to the data. Face and rim thickness contribute to changes in the high-Q, while radius and length differences greatly impact the mid to low-Q range. The best fit to the data is boxed.

distances of the face and rim did not have a significant effect on the fits generated as expected, only producing minor high-Q alterations. Understanding how each dimension contributes to the bicelle model fits is important when refining and constraining this data.

5.3.3.2. Second and third generation fits of q = 0.3 bicelles

Because the preliminary fit bicelle parameters contained wide ranges and allowed for a wealth of bicelle sizes, further constraints were put on the parameters to enable a more accurate depiction of the d54-DMPC/DHPC bicelles (Table 5.5). These constraints were modified a total of 4 times before achieving reliable fits. Therefore, there are 4 generations of bicelle fits that can be followed to understand the methodological process in SANS data fitting. The final parameter values are shown in Table 5.5 in comparison with the initial constraints.

The second and third fit generations resulted in a narrowing of the face and rim SLDs from the original $2.21 \pm 1 \times 10^{-6}$ Å^{-2} to 2.5 and $2.1 \pm 0.3 \times 10^{-6}$ Å^{-2}, respectively. The core SLD kept its wide range, representing the unknown amount of mixing between the fully hydrogenated detergents and fully deuterated lipid tails. The face and rim thickness range was widened from 7.5 ± 2.5 Å to 5.5 ± 4.5 Å, to accommodate a thinner head group shell indicated by the experimental data fits. The radius values were lowered and the range extended; preliminary fits restricted the radius to 27.5 ± 7.5 Å and 3rd generation fits allowed radii to extend to 20 ± 15 Å. Bicelle length range also widened significantly, extending from 70 ± 30 Å to 55 ± 45 Å. Changes in the bicelle parameters represent the exploration of a possibly smaller structure than what was originally observed with preliminary fits.

5.3.3.3. Final generation bicelle fits

To significantly narrow the range used for the core SLD, the value was calculated using the mole fraction of the deuterated and hydrated tail SLDs with the following formula:

$$SLD_{\chi} = (\chi(SLD_{deut.tails})) + ((1-\chi)(SLD_{hyd.tails}))$$

The core SLDs of the q = 0.3 bicelles was calculated at 1.75 x 10^{-6} $Å^{-2}$ and the q = 0.7 bicelles were estimated similarly, equaling 4.74 x 10^{-6} $Å^{-2}$. These values were set as invariable parameters (Table 5.5).

The face and rim SLDs were set to an unchanging 2.1 x 10^{-6} $Å^{-2}$. This value was correlates with the expected SLD of a phosphocholine head group. The face and rim thickness was ultimately restrained to 4.80 ± 0.75 Å, almost the size of a phosphocholine head group shell thickness (~ 3 Å). The radius was restricted to 20 ± 5 Å, and the length increased with q-ratio from 24 to 70 ± 4 Å for q = 0.3 and 0.7, respectively. This trend in increased bicelle length with q-ratio will be further explored in Section 5.2.4. All of these values were converged upon during previous fits and emphasizes the importance of conducting systematic SAS data fitting for accurate size and shape values.

5.3.4. Results: SANS-determined bicelle dimensions

SANS scattering profiles for the C_L = 1.5%, q = 0.3 and q = 0.7 bicelles fit relatively well using the core-shell bicelle fit (Figure 5.9 and 10). Bicelle samples in solvents with 40 to 70% D_2O were omitted for a few bicelles systems. Depending on q-ratio, these D_2O concentrations in solvent are near the entire bicelle CMP, and there is

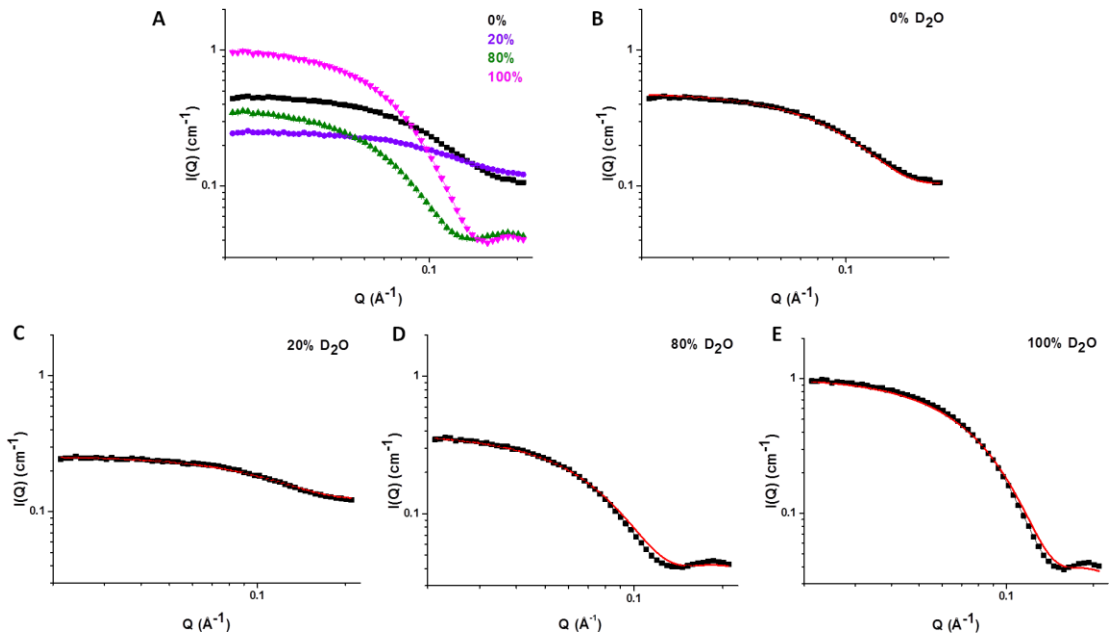

Figure 5.9. Small angle neutron scattering profiles of q = 0.3 DMPC/DHPC bicelles. Contrast variation experiments were conducted on d54-DMPC/DHPC bicelles at q = 0.3, C_L = 1.5% (w/v), 25°C at varying solvent D_2O percentages. 40% and 60% D_2O scattering profiles were omitted due to lack of scattering near the contrast match point (40.4% D_2O). (A) SANS contrast variation of d54-DMPC/DHPC bicelles in solvents with 0%, 20%, 80%, and 100% D_2O. (B-E) Experimental profiles at varying solvent D_2O concentrations (black) were analyzed with the core-shell bicelle fit (red) at $0.021 < Q < 0.21$ for determination of the sizes and dimensions of the detergent-rich complexes.

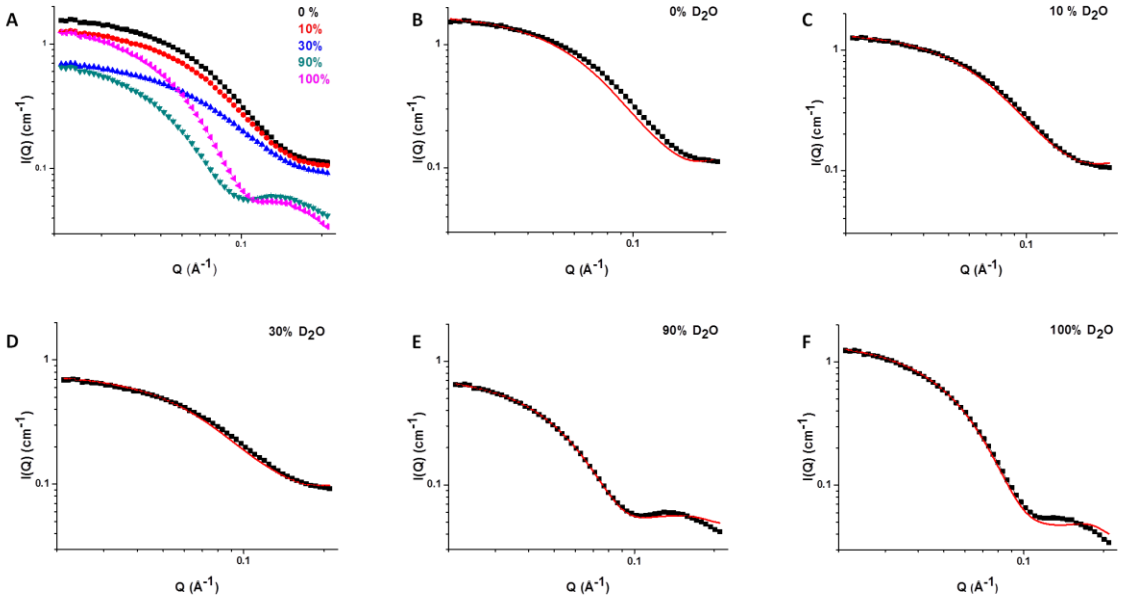

Figure 5.10. Small angle neutron scattering profiles of q = 0.7 DMPC/DHPC bicelles. Contrast variation experiments were conducted on d54-DMPC/DHPC bicelles at q = 0.7, C_L = 1.5% (w/v), 25°C at varying solvent D_2O percentages. 50% and 70% D_2O scattering profiles were omitted due to lack of scattering near the contrast match point (56.0% D_2O). (A) SANS contrast variation of d54-DMPC/DHPC bicelles in solvents with 0%, 10%, 30%, 90%, and 100% D_2O. (B-F) Experimental profiles at varying solvent D_2O concentrations (black) were analyzed with the core-shell bicelle fit (red) at $0.021 < Q < 0.21$ for determination of the sizes and dimensions of the lipid-rich complexes.

minimal scattering to fit. All of the bicelles were analyzed at a low-Q of 0.021 $Å^{-1}$ to a high-Q of 0.21 $Å^{-1}$.

Bicelle data before the CMP (40.4% and 56.0% D_2O for q = 0.3 and 0.7) are characterized by a smooth curve with a negative slope that flattens out at high Q. This curve is indicative of a spherical or elliptical globular structure. Data after the CMP is characterized by a sharp negative slope at low to mid-Q and second maxima in the high-Q. This difference in lineshape is indicative of a shell structure. The changes in scattering profiles with D_2O concentration are expected. With low D_2O concentration in the solvent, the DHPC tails and all of the PC head groups are matched out, and the only contrast observed derives from the deuterated lipid core. This core would adopt a more spherical or ellipsoidal geometry. At higher solvent D_2O concentrations, the deuterated lipid core would be matched out; scattering would only represent the PC head group shell and the DHPC detergent rim, and this will result in a shell-like pattern in the scattering profile (Figure 5.4).

The core-shell bicelle model fits the experimental data relatively well. The model fits the low-Q data better than the high-Q data. The high-Q region depicts more features indicative of the curvature and shell structure and shorter distances. The core-shell bicelle model is a derivative of the cylinder model while the complex studied likely has more curvature. Therefore, these differences in high-Q fit between the data and model are reasonable.

Error for these fits are determined by identifying the best fit to the scattering profiles, followed by changing the parameters slightly to identify how far the fit can be

varied before significantly impacting the data (Table 5.7). There are less variations allowed for face thickness, rim thickness, and radius before modifying the fit while length can be varied by approximately ±5 Å for q = 0.7 bicelles. Generally, the structural parameters for the face and rim thickness and radius have approximately ± 1 Å error. Length is an overall larger dimension; the larger error determined for this structural parameter is reasonable.

The outer shell of the d54-DMPC/DHPC bicelles are composed of a layer of phosphocholine head groups in the face and rim. The phosphocholine head group has an estimated size of 3 Å.[7] The q = 0.3 bicelle fits suggested both an average face thickness and rim thickness of 4.9 Å while the q = 0.7 aggregates contained an average face thickness of 4.5 and rim thickness of 4.6 Å (Table 5.7).

The bicelle radius corresponds to half of the diameter of the bicelle core. Unlike L, which represents the head group to head group distance, the radius represents half of the thickness of the hydrocarbon core. The SAXS-determined L for the q = 0.3 and 0.7 bicelles were 33.3 and 42.1 Å. Removing the 1.5 Å contribution from the head groups and halving this value gives an estimate of the radii at 15.9 and 20.3 Å. The q = 0.3 bicelles had an average radius of 21 Å while q = 0.7 bicelles was 22 Å (Table 5.7).

Unlike with shell thickness and radius, the increase in lipid concentration significantly impacts the length of the bicelle. q = 0.3 bicelles have an average length of 22 Å, while the q = 0.7 bicelles have a length of 71 Å (Table 5.7). With these different lengths, the q = 0.3 and 0.7 aggregates form completely different shaped structures. Correlations between q-ratio and these bicelle dimensions will be explored in the

	0.3				0.7				
% D_2O	0%	20%	80%	100%	0%	10%	30%	90%	100%
Face thickness (Å)	4.5 ± 0.5	5.3 ± 0.8	5.8 ± 0.8	6.3 ± 1.3	3.7 ± 2.7	3.0 ± 2.0	3.5 ± 1.5	4.3 ± 1.3	5.0 ± 1.0
Rim thickness (Å)	4.5 ± 0.5	4.9 ± 0.4	5.0 ± 1.0	4.8 ± 0.8	3.5 ± 1.5	3.3 ± 1.8	4.5 ± 0.5	5.3 ± 0.4	4.5 ± 0.5
Radius (Å)	17 ± 0.8	12 ± 0.5	25 ± 1.0	24 ± 0.8	19 ± 0.5	19 ± 0.6	19 ± 0.5	25 ± 0.5	25 ± 0.5
Length (Å)	18 ± 1.8	22 ± 2.0	31 ± 2.5	27 ± 2.5	68 ± 5.0	68 ± 5.0	71 ± 4.5	73 ± 8.5	70 ± 3.0

Table 5.7. Final d54-DMPC/DHPC bicelle dimensions. Q = 0.3 and 0.7 bicelle sizes determined with the core-shell bicelle fitting using constrained core, face, and rim SLD values in varying solvent D_2O concentrations.

following discussion section along with implications for the ideal bicelle model.

5.4. Discussion

5.4.1. Dimensions of detergent-rich bicelles

The q = 0.3 and 0.7 bicelles have similar head group shell thicknesses and radii. The face and rim thicknesses of these two aggregates are approximately 4.7 Å. This value corresponds well with the 3 Å thickness of a phosphocholine head group. The radii of both bicelles are 21 to 22 Å, relating with what is expected for half of the thickness of a DMPC bilayer (~ 21 Å). An increase in q-ratio does not impact the radii and shell thickness, according to the equivalent values for these dimensions. However, the addition of lipids to these detergent-rich systems significantly impacts the length of the bicelles, affecting the overall bicelle shape of the bicelles.

With a length of approximately 22 Å and a radius of 18 Å, the q = 0.3 bicelles form a shape far different than what is expected of an ideal bicelle. The q = 0.3 bicelle structure has an ellipsoidal shape, with dimensions similar to a DHPC micelle (Rg = 25 Å). In contrast, the q = 0.7 aggregate adopts a more bicellar shape, with its 22 Å radius and 71 Å length. This q = 0.3 and 0.7 data suggests remarkable implications for bicelle formation: 1) the transition from mixed micelle to bicelle with increasing q-ratio occurs with an increase in the structure length, and 2) the ideal model does not adequately represent these low-q bicelles.

The transition to bicellar structures occurring predominantly with the bicelle length suggests that the lipids added to the system partition into the DMPC bilayer, expanding the aggregate size from the core while retaining the shell thickness and radii

sizes (Figure 5.11). This is expected; the change in the length of bicelles as lipid concentration is altered has been mentioned in the literature. Vold and Prosser reported the increase in bicelle size with q-ratio in 1996, and this observation was later confirmed with dynamic light scattering by other researchers.[8,9] However, the experimental data suggests that the q = 0.3 and 0.7 aggregates are not expanding from smaller to larger bicelles, but are transitioning from mixed micelle to bicelle. This implication contradicts the ideal bicelle model.

The ideal model implies that lipid and detergent mixtures at any q-ratio forms bicelles with completed separated bilayer and rim domains. The data presented in this thesis suggests otherwise for several reasons. First, SANS profiles of the q = 0.3 bicelles demonstrate that low-q bicelles have an ellipsoidal micelle structure and as q-ratio is increased, the aggregates adopt a bicelle structure. These micelle-like aggregates do not contain the bilayer domain that is predicted by the ideal bicelle model. Second, the SAXS profiles of the q = 0.1 to 0.5 bicelles are very different with each incremental addition of lipid, suggesting that there is some degree of mixing between the DMPC and DHPC. Even at low q-ratios, the SAXS profiles of ideal bicelles would have the same L, and subsequently Q_{max}, indicative of the 42 Å DMPC bilayer thickness, but the experimentally determined Q_{max} and L are different for each q-ratio. Third, the SANS data was fitted using a core SLD of a mixed complex. The goodness of the fits with this mixed SLD further suggests that there is mixing of the lipid and detergent components in solution. To monitor the structure and arrangement of the detergent-rich bicelles, molecular dynamic simulations in conjunction with experimental studies have been pursued.

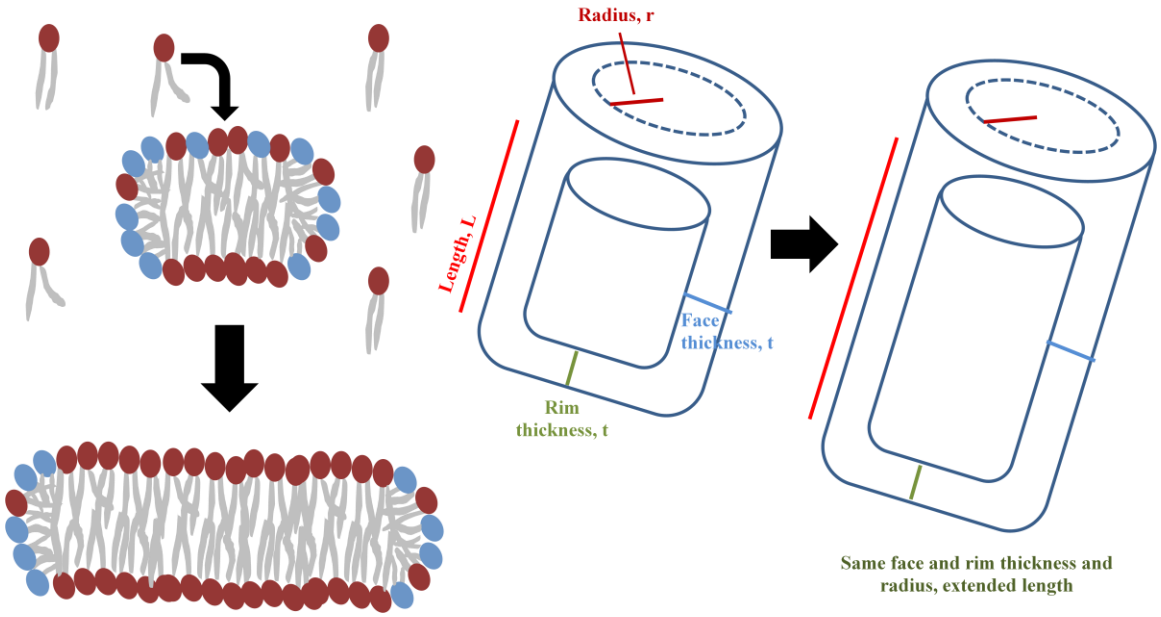

Figure 5.11. Suggested route for lipid partitioning with increased q-ratio. With an increased q-ratio, the length of the bicelles expands, not impacting the face and rim thickness or the radius. This suggests that the increased amount of lipids partition into the lipid core interior of the bicelle, only changing one dimension.

5.4.2. Utilizing molecular dynamics simulations to observe low-q bicelles

To get a better understanding of the size and shape of these detergent-rich bicelles, collaborators Svetlana Baoukina and Peter Tieleman at the University of Calgary generated molecular dynamic (MD) simulations of the DMPC/DHPC bicelles at q = 0.3 and 0.7 (Figure 5.12). The bicelles were simulated over 1 μs with Gromacs v.4.6.5., in a hydration level of 400 water molecules per amphiphile, and a C_L of 100 mM, or 9% (w/v). The simulations added the bulk q-ratio of lipids and detergents in a box to generate the aggregates. These simulations were confirmed to have similar sizes to the experimental bicelles, and therefore, provide an accurate image of actual detergent-rich bicelles.

5.4.3. Bulk q-ratio vs. actual bicelle q-ratio

An interesting finding from the MD-simulated bicelles focuses on the actual q-ratios in the bicelle vs. the bulk q-ratio in solution. The generated q = 0.3 and 0.7 bicelles had different lipid-to-detergent concentrations than the bulk q-ratio in solution (Table 5.8). Although the appropriate ratio of lipids and detergents were added to the MD simulations, 100% of the bicelle components did not interact to form q = 0.3 and 0.7 bicelles. The complexes formed had different q-ratios, designated q*. The q = 0.3 bicelles had q*-ratios of 0.30 and 0.32 while the q = 0.7 simulated bicelles had a q* = 0.76 and 0.92. Atomic structures of the q* = 0.30 and 0.32 suggested a mixed micelle shape unlike the q* = 0.76 and 0.92 bicelle-like complexes. This correlates well with the structures observed with the SAXS and SANS data. This discovery implies

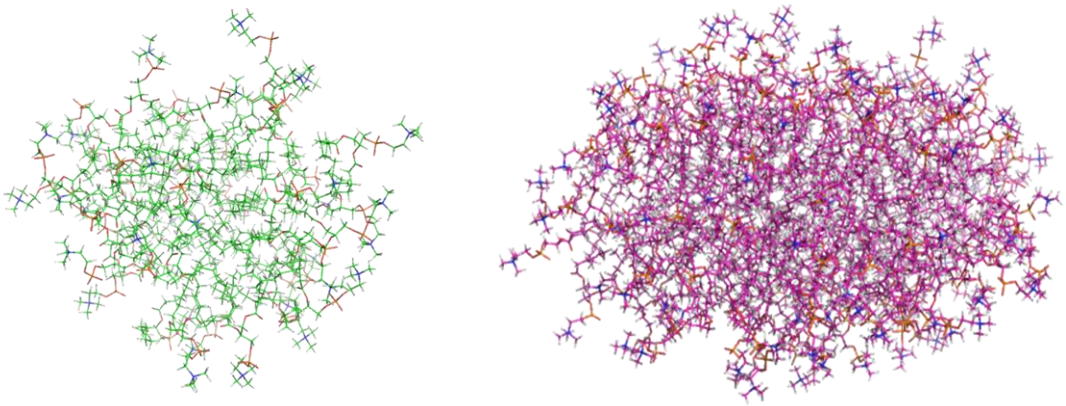

q = 0.30 (0.30*)) **q = 0.70 (0.92*)**

Figure 5.12. Simulated DMPC/DHPC bicelles at q-ratios of 0.3 and 0.7. Gromacs v. 4.6.5. was utilized to generate q = 0.3 and 0.7 bicelles at C_L = 9% (w/v)Although the appropriate q-ratio of lipids and detergents were added to the simulation box, these bicelles formed with slightly different q-ratios, designated q*.

q	q*	R_g (Å)	Shell thickness (Å)	Radius (Å)	Length (Å)
0.3	0.3	16	4.7	15	44
	0.32	17	4.8	16	42
0.7	0.76	26	4.8	20	75
	0.92	24	4.8	20	64

Table 5.8. Bicelle dimensions determined from the atomic MD-simulated bicelles. The simulated complexes at q = 0.3 and 0.7 formed structures with slightly different q-ratios than the bulk q-ratio introduced to the system. The q-ratios of these generated bicelles are denoted with q*. An ellipsoid fit of the complexes to the atomic data was used to calculate the R_g, shell thicknesses, radii, and lengths from averages over 10 time frames.

that the mimics designed by researchers may actually be structurally different than expected.

5.4.4. Dimensions of the simulated bicelles correlate well with experimental data

Before confirming that the MD-simulated bicelles were an accurate depiction of the low-q bicelles, several steps were taken to ensure that these generated bicelles represent similar sizes and shapes of the experimental aggregates. The sizes of the bicelles were determined using calculations from the atomic structures (Table 5.8) as well as CRYSOL and CRYSON programs in the ATSAS software package.

CRYSOL and CRYSON generate SAXS and SANS profiles from the atomic PDB files of the simulated bicelles (Figure 5.13 and 5.14). These profiles were analyzed similarly to the SAXS and SANS data. Guinier analysis and q_{max} determination of the generated SAXS profiles measured the R_g and L of the aggregates while core-shell bicelle model fitting of the generated SANS profiles identified the face and rim thickness, radius, and length. The R_g and L of the aggregates have similar trends as the SAXS data (Table 5.9). Considering the error in the experimental data, preliminary CRYSON-generated SANS profiles of the q = 0.7 bicelles also correlate with the SANS results, with a shell thickness of approximately 5 Å, radius of 17 Å, and length of 73 Å (Table 5.9).

Although the bicelle sizes are not identical with the experimental results, the differences in the computational and experimental methods must be considered. The bicelles used for the computational studies had a total amphiphile concentration of 9%

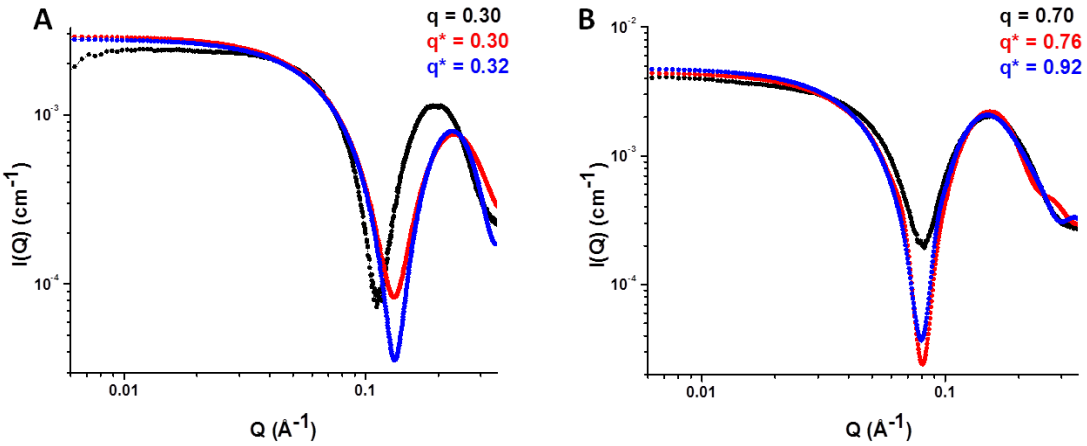

Figure 5.13 SAXS profiles generated from simulated DMPC/DHPC bicelles. Experimental SAXS data for the DMPC/DHPC bicelles were compared to CRYSOL-generated SAXS profiles from the simulated bicelles. (A) q = 0.3, C_L = 9% (w/v) experimental SAXS data (black) is depicted with the simulated profiles of q* = 0.30, C_L = 9% (w/v) (red) and q* = 0.32, C_L = 9% (w/v) (blue) bicelles. (B) q = 0.7, C_L = 9% (w/v) experimental SAXS data (black) is shown with q* = 0.76, C_L = 9% (w/v) (red) and q* = 0.92, C_L = 9% (w/v) (blue) simulated bicelles. SAXS profiles were analyzed with a Guinier fit and Q_{max} determination for identification of radii of gyration and dominant head group to head group distances.

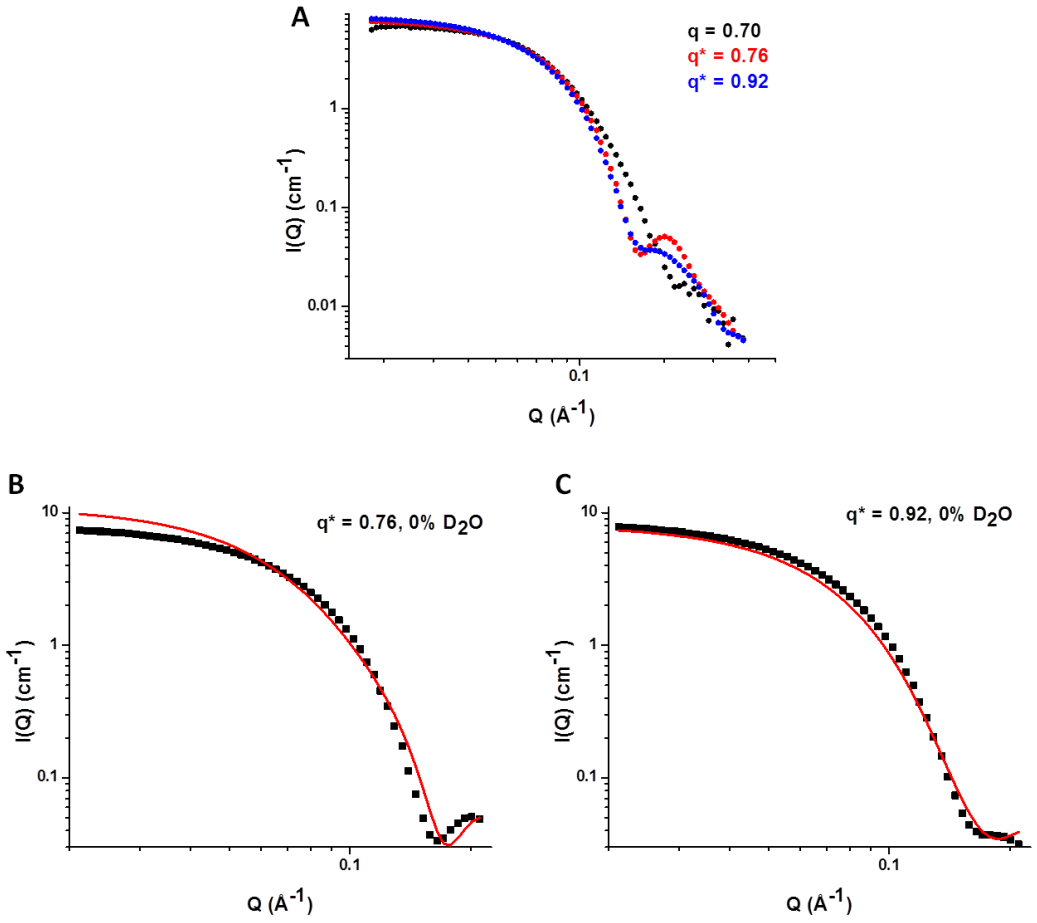

Figure 3.14. SANS profiles generated from simulated DMPC/DHPC bicelles. (A) Experimental SANS data for DMPC/DHPC bicelles at q = 0.7, C_L = 9% (w/v) (black) are depicted with CRYSON-generated SANS profiles from the simulated bicelles at q* = 0.76, C_L = 9% (w/v) (red) and q* = 0.92, C_L = 9% (w/v) (blue). (B and C) SANS profiles of the q* = 0.76 and q* = 0.92 bicelles (black) were fit with the core-shell bicelle model (red) to determine structural parameters of the simulated bicelles

q	q*	Crysol		Cryson			
		R_g (Å)	L (Å)	Face thickness (Å)	Rim thickness (Å)	Radius (Å)	Length (Å)
0.3	0.30	16	27	--	--	--	--
	0.32	17	28	--	--	--	--
0.7	0.76	26	41	3.5 ± 2.5	5.5 ± 1.0	20 ± 0.8	78 ± 4.5
	0.92	24	42	3.0 ± 1.0	3.3 ± 1.3	22 ± 0.8	62 ± 2.5

Table 5.9. Bicelles dimensions determined from SAXS and SANS profiles of simulated complexes. SAXS and SANS profiles of the simulated bicelles, with q-ratios denoted q*, were generated with CRYSOL and CRYSON, respectively. R_g and L of the SAXS profiles were determined with Guinier analysis and using the position of the 2nd maximum, Q_{max}. Core-shell bicelle model fits of the generated q* = 0.76 and 0.92 SANS data were used to determine structural parameters of the q = 0.7 DMPC/DHPC complexes.

(w/v) while the experimental bicelles had a concentration of 1.5% (w/v). This 10-fold difference in amphiphile concentrations can impact the comparison between the two methods. Therefore, comparing the sizes directly is useful, but monitoring the trends with the two bicelle complexes may also provide helpful information. However, with the disadvantages, the MD-simulated bicelles provide a reliable depiction of the low-q bicelles. The trends provided from these simulations can be trusted to reflect the actual systems.

5.4.5. Detergent-rich bicelles are mixed systems that contradict the ideal bicelle model

The MD-generated bicelles reflect the experimental data well. With that, the simulated bicelles also give a second confirmation that the ideal bicelle model does not represent detergent-rich bicelles. The simulated bicelles contain well-mixed DMPC and DHPC components. Because this well-mixed simulated complex correlates well with the experimental data, this suggests that the experimental bicelles formed by these mixtures are also mixed systems. Also, the SANS contrast variation experiments were well fit with the core-shell bicelle model using a core SLD of a mixed system. The goodness of the fits with this mixed core SLD also suggests that there is a more mixed arrangement of the bicelle components.

In addition to the mixed composition, SAXS, SANS, and MD data suggest that the q = 0.3 bicelles have an ellipsoid micelle-like structure that transitions into a more bicelle arrangement with an increase in lipid concentration. This contradicts the bicelle model that insists that the complex has bicellar features throughout the low and high q-

ratios. By using a combination of experimental and theoretical methods, the structure and composition of low-q bicelles has been well-investigated.

5.5. Closing remarks and future directions

This analysis of the SAXS and SANS scattering data in conjunction with MD simulations demonstrate that the size and shape of bicelles are largely dependent on the q-ratio, and unlike the ideal bicelle model, detergent-rich bicelles form mixed micelle structures. Preliminary SAXS data showed a transition from mixed micelle to bicelle with a q = 0.1 to 0.5 which was supported with neutron scattering data. By increasing the q-ratio of these systems, more lipids partition into the DMPC bicelle core, extending the overall length of the structure while retaining the same shell thickness and radius. These results correlate well to literature reported on these detergent-rich aggregates. MD and core-shell bicelle model fitting suggest that lipid and detergent domains of the bicelle have a higher degree of mixing than predicted with the ideal bicelle model, especially in highly detergent-rich bicelles. Because bicelles are increasingly popular in membrane protein research, confirming of the size and shape of these detergent-rich structures will enable researchers to make better choices when selecting an appropriate membrane mimic for their membrane protein.

To further monitor the transition from mixed micelles to bicelles, experimental and theoretical pursuits to elucidate the q = 0.5 bicelle structure is in progress. q = 0.5 is the q-ratio in which the bicelles first adopt the bicelle structure. Therefore, elucidating the structure of q = 0.5 is challenged with SANS profiles that may represent a hybrid of micelle and bicelle structure. Preliminary fits of the q = 0.5 bicelles suggests similar shell

thicknesses and radii to the other bicelle mixtures, and a length of approximately 77 Å (Figure 5.15 and Table 5.10). These fits are being improved systematically to give an accurate determination of the size of q = 0.5 bicelles. MD simulations of the q = 0.5 bicelles depict bicelles with both a mixed micelle shape (q* = 0.51) and bicelle shape (q* = 0.72) (Figure 5.16 and Table 5.11). Deciding which model accurately reflects the system will depend on the final size dimensions for the experimental bicelles and how they correlate with the CRYSON-generated q = 0.5 models.

In addition to determining bicelle size and shape, the structures of proteins embedded in bicelles, proteobicelles, are also being explored. Preliminary proteobicelle SANS experiments were completed using fully hydrated Opa β-barrel membrane proteins embedded in d54-DMPC/DHPC bicelles. The q = 0.3 proteobicelles were made using two methods: 1) adding DHPC to Opa-DMPC proteoliposomes, and 2) adding DMPC lipids to Opa-DHPC protein-detergent complexes (PDC). Initial data suggests that the proteobicelles produced by adding DHPC to the Opa proteoliposomes formed large, globular structures, not bicelles. The Opa proteobicelles prepared from Opa-DHPC PDCs produced better scattering profiles (Figure 5.17). Although scattering was obtained for these Opa proteobicelles, these experiments must be repeated along with a full contrast variation series to obtain information on the structure of Opa in this mimic. These preliminary experiments provided useful insight on the optimal formation of Opa proteobicelles.

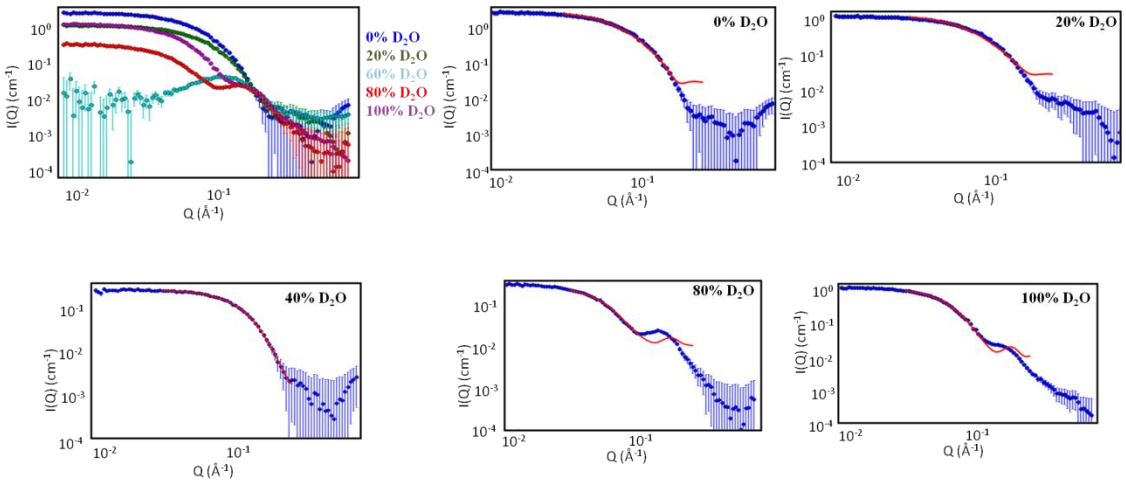

Figure 5.15. Core-shell bicelle fits to the q = 0.5 bicelles. Scattering collected of the d54-DMPC/DHPC bicelles at q = 0.7 and CL = 1.5% (w/v) at 25°C. The data in varying solvent D_2O concentrations was fit with the core-shell bicelle model. The 60% D_2O fit were omitted due to lack of scattering near the CMP. Optimization of these fits continues, and will provide key information on the transition from mixed micelle to bicelle. Fits shown in red.

	0.5				
	0%	**20%**	**60%**	**80%**	**100%**
Face thickness (Å)	4.30	4.79	4.30	5.21	5.30
Rim thickness (Å)	4.41	4.97	4.68	4.85	4.85
Radius (Å)	19.7	18.9	20.8	21.1	22.2
Length (Å)	78.4	75.0	76.1	81.0	75.3

Table 5.10. d54-DMPC/DHPC dimensions for q = 0.5 bicelles. Sizes determined with the core-shell bicelle fitting. The SLD for the core was 3.29 x 10^{-6} $Å^{-2}$. The solvent, face, and rim SLDs are the same values for the q = 0.3 and 0.7 fits. These values were converged upon via several generations of q = 0.5 fitting.

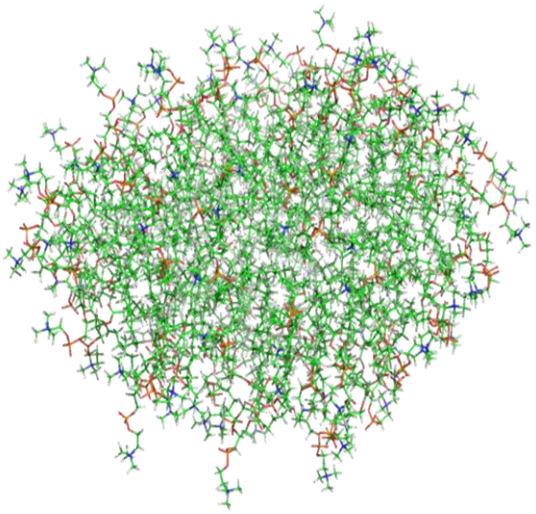

q = 0.50 (0.72*)

Figure 5.16. Simulated DMPC/DHPC bicelle at q = 0.5. Although the appropriate bulk q-ratio of lipids and detergents were added to the simulation, these bicelles formed with different structures with varying q-ratios, designated q*.

q	q*	Rg (Å)	L (Å)	structure
0.5	0.51	21	35	mixed micelle
0.5	0.72	25	42	bicelle

Table 5.11. Size and shape of MD-simulated q = 0.5 bicelles. C_L = 9% (w/v), q = 0.5 bicelles were simulated twice over 1 μs. The two q = 0.5 simulated bicelles had different q*-ratios, representing two different structures. SAXS profiles of the simulated bicelles were generated with CRYSOL to determine the Rg and L.

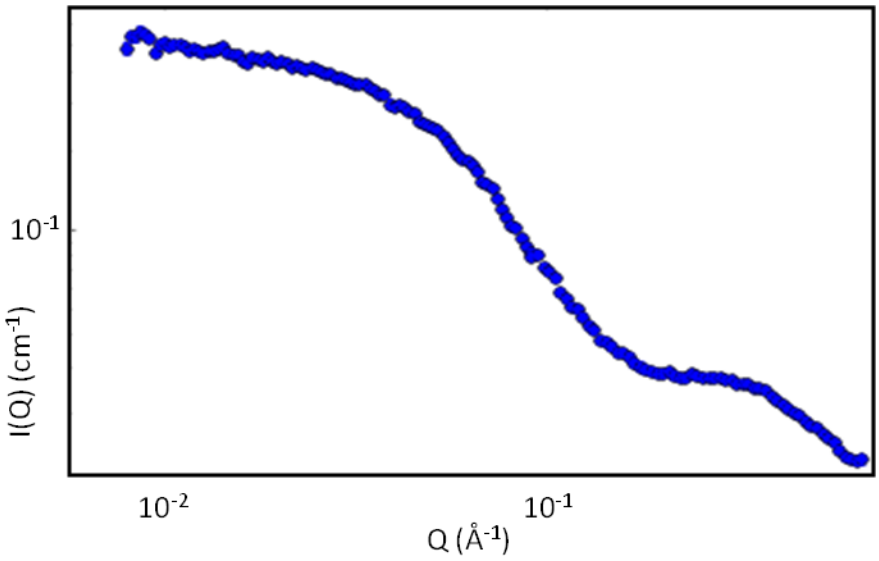

Figure 5.17. Opa proteobicelle SANS scattering profile. Neutron scattering lineshape from Opa d54-DMPC/DHPC bicelles at C_L = 1.5% at 25°C. This scattering profile is at 45% D_2O, potentially the CMP for the bicelle, representing scattering from the Opa β-barrel membrane protein.

5.6. Methods

5.6.1. Sample preparation

1,2-dihexanoyl-*sn*-glycero-3-phosphocholine (DHPC), 1,2-dimyristoyl-*sn*-glycero-3-phosphocholine (DMPC), 1,2-dimyristoyl-d54-*sn*-glycero-3-phosphocholine (d54-DMPC), and 1,2-didecanoyl-*sn*-glycero-3-phosphocholine (diC_{10}PC) were purchased from Avanti Polar Lipids. D_2O was purchased from Cambridge Isotope Labs and all other chemicals were obtained from Fisher, unless otherwise noted.

DMPC/DHPC bicelles were prepared by resuspending DMPC with sodium phosphate buffer containing DHPC to a total amphiphile concentration of 1.5% (w/v). Three lipid:detergent q-ratios of 0.3, 0.5, and 0.7 were used in these experiments. Freeze-thaw cycles and vortexing was used until the solutions were clear at room temperature. Each sample was divided in half. One half was dialyzed in H_2O phosphate buffer with 7 mM DHPC and the other half was dialyzed in D_2O phosphate buffer with 7 mM DHPC. The post-exchange buffer was collected for buffer subtraction. Titration of these two samples was used to produce the ratios of D_2O and H_2O needed for SANS contrast variation experiments. Final buffers for all samples consisted of 10 mM phosphate, pH 6.6, and the appropriate D_2O/H_2O ratio for contrast variation.

Opa proteobicelles were produced with two methods. The first method was preparing Opa proteobicelles from Opa PDCs. This involved refolding 2.25 mg denatured Opa into refolding buffer (20 mM sodium phosphate, pH 8.0, 500 mM NaCl) with FC12 detergent for 5 days, immobilizing the refolded protein onto a Co^{2+} immobilized metal ion affinity (IMAC) column, and exchanging the FC12 detergent with DHPC via washing

the column with three column volumes of wash buffer (20 mM sodium phosphate, pH 7.8, 150 mM NaCl, 20 mM imidazole) with excess DHPC, and eluting with elution buffer (20 mM sodium phosphate, pH 7.0, 150 mM NaCl, 680 mM imidazole) with DHPC. The Opa-DHPC PDC was dialyzed for 1 hour to remove excess imidazole and the DHPC concentration was determined using 1-D ^{1}H NMR. solid d54-DMPC lipid was added to Opa-DHPC bicelles to obtain a C_L of 1.5% and a q-ratio of 0.3.

Opa proteobicelles prepared from Opa proteoliposomes involved adding 4.5 mg denatured Opa to diC_{10}PC liposomes in borate buffer (20 mM sodium borate, 20 mM boric acid, 0.5 M EDTA), incubating at 37°C for 3 days, centrifuging the solution at 142,400 x g for 2 hours at 10°C, and resuspending the pellet with d54-DMPC in resuspension buffer (30 mM Tris, pH 7.3, 150 mM NaCl). The Opa protein and deuterated lipids were pulse-sonicated for 20 min with 30 s on/off cycles. The appropriate amount of DHPC was added to the Opa proteoliposomes to obtain a C_L of 1.5% and a q-ratio of 0.3.

5.6.2. SANS data collection and contrast variation

SANS data were measured on the CG-3 Bio-SANS in the High Flux Isotope Reactor facility of the Oak Ridge National Laboratory (ORNL; Oak Ridge, TN). Measurements were collected with a 1 x 1 m^2 2-D linear position-sensitive detector at a resolution of 192 x 256 pixels. The samples were measured at 6 Å neutron wavelength and sample to detector distances of 0.3 and 6 m. Data was collected at 25 and 40°C using 1 mm quartz banjo cells. Exposure time ranges from 300 to 12000 seconds based on the concentration and solvent D_2O content. The usable Q-range was 0.0009 to 0.8 $Å^{-1}$.

The contrast variation experimental data was reduced using MantidPlot data reduction software. Buffer subtraction was completed with Primus. SasView was used for all of the bicelle data fits. CRYSOL and CRYSON were used for generating SAXS and SANS profiles from the MD atomic structures.

5.7. References

1. Fitter, J., T. Gutberlet, and J. Katsaras. 2006. Neutron scattering in biology: techniques and applications. Springer, New York, NY.

2. Svergun, D. and M. Koch. 2003. Small-angle scattering studies of biological macromolecules in solution. Rep Prog Phys 66: 1735-1782.

3. Guinier, A. 1939. La diffraction des rayons X aux tres petits angles; application a l'etude de phenomenes ultramicroscopiques. Ann Phys (Paris) 12: 161-237.

4. Guinier, A. and G. Fournet. 1955. Small angle scattering of X-rays. Wiley, New York, NY.

5. Gaemers, S. and A. Bax. 2001. Morphology of three lyotropic liquid crystalline biological NMR media studied by translational diffusion anisotropy. J Am Chem Soc 123: 12343-12352.

6. Feigin, L. and D. Svergun. 1987. Structure analysis by small angle X-ray and neutron scattering. Plenum Press, New York, NY.

7. Oliver, R., J. Lipfert, D. Fox, R. Lo, S. Doniach, and L. Columbus. 2013. Dependence of micelle size and shape on detergent alkyl chain length and head group. PLoS ONE 8: e62488.

8. Glover, K., J. Whiles, G. Wu, N. Yu, R. Deems, J. Struppe, R. Stark, E. Komives, and R. Vold. 2001. Structural evaluation of phospholipid bicelles for solution-state studies of membrane associated biomolecules. Biophys J 81: 2163-2171.

9. Vold, R. and R. Prosser. 1996. Magnetically oriented phospholipid bilayered micelles for structural studies of polypeptides. Does the ideal bicelle exist? J Magn Reson B 113: 267 – 271.